

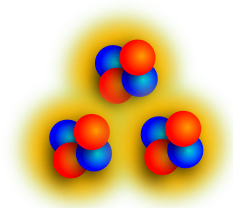


UNIVERSIDAD NACIONAL DE COLOMBIA  
DEPARTAMENTO DE FÍSICA  
FACULTAD DE CIENCIAS  
GRUPO DE FÍSICA NUCLEAR DE LA UNIVERSIDAD NACIONAL (GFNUN)

# Alpha-Transfer Reaction Technique for Nuclear Magnetic Moment Measurements

MSC THESIS

ANA MARÍA GÓMEZ LONDOÑO



**Supervisor:** Diego Alejandro Torres Galindo.  
Associate Professor

Bogotá, 2019

---



*Universidad Nacional*



Universidad Nacional de Colombia  
Departamento de Física  
Facultad de Ciencias  
Grupo de Física Nuclear de la Universidad Nacional (GFNUN)

# Alpha-Transfer Reaction Technique for Nuclear Magnetic Moment Measurements

MSC THESIS

ANA MARÍA GÓMEZ LONDOÑO

**Supervisor:** Diego Alejandro Torres Galindo.  
Associate Professor

Approved by

Date: 18/07/2019.

*(Signature)*

*(Signature)*

*(Signature)*

.....  
Neelima Govind Kelkar  
Associate Professor

.....  
Ramiro Cardona  
Associate Professor

.....  
Diego Milanes  
Associate Professor

Bogotá, 2019







Universidad Nacional de Colombia  
Departamento de Física  
Facultad de Ciencias  
Grupo de Física Nuclear de la Universidad Nacional (GFNUN)

Copyright © – All rights reserved. Ana María Gómez Londoño, 2019.

This copy of the thesis has been supplied on condition that anyone who consults it is understood to recognize that its copyright rests with its author and that no quotation from the thesis and no information derived from it may be published without the author's prior consent.

*(Signature)*

.....  
Ana María Gómez Londoño



# Abstract

---

In this work the  $\alpha$ -transfer reactions mechanism is studied as a technique to populate medium-to-low spin states in nuclei that cannot be produced with enough intensity in the present radioactive beam facilities. Uses of the  $\alpha$ -transfer population mechanism to measure  $g$  factor and lifetimes, with the Transient Field Technique and the Doppler Shift Attenuation Method respectively, are presented. Some aspects of the theoretical model to approach the understanding of the mechanism, such as the Distorted Wave Born Approximation in combination with Optical Potentials, are also presented. Experimental challenges for future uses of the  $\alpha$ -transfer technique are shown, and possible experimental campaigns are proposed with all possible combinations of stable beams that can populate radioactive nuclei.

As part of this work an experiment using the reaction  ${}^{28}_{14}\text{Si} + {}^{12}_6\text{C} \rightarrow {}^{32}_{16}\text{S} + 4\text{He} + 4\text{He}$  was approved by the Program Advisor Committee at University of Sao Paulo, and will be carry out during 2019. A segmented  $\gamma$ -Ray detector LYSO(Ce) with an array of 16  $\Delta E$ - $E$  particle detectors will be part of the detection system. In future experiments, it is expected to obtain a set of more detailed nuclear structure parameters to unveil the structure of the populated states.

## Keywords

Alpha-transfer reactions,  $g$  factor, lifetime, Transient Field Technique, Doppler Shift Attenuation Method.



## Resumen

---

En este trabajo, el mecanismo de reacciones de transferencia alfa, es estudiado como una técnica para poblar estados de espín de medios a bajos en núcleos que no pueden ser producidos con suficiente intensidad usando las herramientas experimentales actuales para producir rayos de núcleos radioactivos. El uso del poblamiento de estados radioactivos en el núcleo por medio del mecanismo de transferencia alfa, en combinación con las técnicas de Campo Transiente y Método de Atenuación por Corrimiento Doppler, para medir factores  $g$  y tiempos de vida respectivamente, es presentado. Algunos aspectos del modelo teórico usado para bosquejar el entendimiento del mecanismo de transferencia alfa, tal como la aproximación de onda distorsionada de Born en combinación con el uso de potenciales ópticos, son también presentados. Los desafíos en el uso de la técnica de transferencia alfa en futuros experimentos para la medición de factores  $g$  y tiempos de vida son mostrados junto con la proposición de unas posibles campañas experimentales que utilizan todas las posibilidades de obtener núcleos radioactivos a partir de proyectiles estables.

La fase exploratoria de estas campañas experimentales, comienza con la realización de un experimento que utiliza la reacción  ${}^{28}_{14}\text{Si} + {}^{12}_6\text{C} \longrightarrow {}^{32}_{16}\text{S} + 4\text{He} + 4\text{He}$ , el cual fue aprobado por el Comité Asesor de la Universidad de São Paulo y será llevado a cabo en el año 2019. El sistema de detección consistirá de varios detectores LYSO(Ce), los cuales constan de la unión de varios segmentos de cristales semiconductores y se encargarán del registro de la radiación gama y de un arreglo de 16 detectores  $\Delta E-E$  que registrarán las partículas emitidas durante la reacción. En futuros experimentos se espera obtener un conjunto más completo de parámetros de estructura nuclear que permitan develar la estructura de los estados poblados por la reacción.

## Palabras Clave

Reacciones de Transferencia Alfa, Factor  $g$ , Tiempo de vida, Técnica de Campo Transiente, Método de Atenuación por Corrimiento Doppler.



*To my beloved Jānis Danebergs and Jairo Gómez*





# Contents

---

Abstract	1
Abstract	3
<b>1 Introduction</b>	<b>17</b>
<b>2 Theoretical Fundamentals</b>	<b>21</b>
2.1 Structure Models of Nucleus . . . . .	22
2.1.1 The Shell Model . . . . .	22
2.1.2 Liquid-Drop model of nucleus . . . . .	24
2.2 Fundamentals of Nuclear Reactions . . . . .	33
2.2.1 Cross Section . . . . .	34
2.2.2 Optical potential . . . . .	35
2.2.3 São Paulo Potential . . . . .	37
2.3 Nuclear Magnetic Moments . . . . .	38
2.3.1 Quantum description of Magnetic Moment . . . . .	39
2.4 Larmor's Precession . . . . .	44
2.4.1 Precession Angle . . . . .	45
<b>3 Experimental techniques to measure Nuclear Magnetic Moments of short-lived excited states: description and challenges</b>	<b>49</b>
3.1 General description of precession experiments . . . . .	50
3.1.1 Hyperfine Fields . . . . .	51
3.2 Transient Field Technique . . . . .	53
3.2.1 Angular correlation function and g-factor measurement . . . . .	56
3.2.2 Life-time measurements . . . . .	59
3.3 Population of nuclear states . . . . .	65
<b>4 State of the art</b>	<b>67</b>
4.1 Basics of Alpha-transfer reactions . . . . .	68

---

4.2	The spin alignment and the angular distribution . . . . .	69
4.3	Understanding nuclear structure and reaction mechanism . . . . .	72
4.3.1	Uses in the nuclear structure characterization . . . . .	74
<b>5</b>	<b>Our experimental proposal and perspectives</b>	<b>77</b>
5.1	Proposed experiment: the reaction and the experimental layout . . . . .	78
5.1.1	Accelerators . . . . .	78
5.1.2	Ion sources . . . . .	82
5.1.3	Reaction and Detection system . . . . .	83
5.2	Future experiments in alpha transfer reactions . . . . .	88
	<b>Conclusions</b>	<b>95</b>
	<b>Appendices</b>	<b>99</b>
<b>A</b>	<b>More about g-factor</b>	<b>101</b>
A.1	Quantum mechanical formalism . . . . .	101
<b>B</b>	<b>Schmidt lines</b>	<b>105</b>
<b>C</b>	<b>Larmor Theorem</b>	<b>109</b>
<b>D</b>	<b>São Paulo Proposal</b>	<b>113</b>
<b>E</b>	<b>TRIUMF possible experiments list</b>	<b>125</b>
	<b>Acknowledgements</b>	<b>143</b>
	<b>Bibliography</b>	<b>155</b>
	<b>Abbreviations</b>	<b>157</b>

## List of Figures

---

1.1	In the chart of nuclides each point plotted represents the nuclide of a chemical element. The different colors represents the regions conformed by nuclei with an specific type of decay described in the conventions. Figure adopted from <a href="https://www.revolvy.com/page/Stable-nuclide">https://www.revolvy.com/page/Stable-nuclide</a> . . . . .	18
2.1	Shell model level scheme prediction. In the right side, some magic numbers, which are predicted from the spin-orbit interaction included by Mayer, are shown. The inclusion of the spin-orbit term, predict the magenta level scheme. . . . .	24
2.2	Representation of energy level occupation . The blue line indicates the nuclear potential for neutrons and the red one the potential for protons. The dashed line indicates the Coulomb potential. Proton and neutron with a given spin, occupy energy levels with an occupation number given by $2j + 1$ , fulling degenerate energy levels by pairs with spin up and down cancelling the total angular momentum value. Nuclear spin or total angular momentum rises from the contribution of the one unpaired nucleon. . . . .	25
2.3	Illustration of the neutron and proton potential. The liquid-drop model predicts an inner structure of the nucleus so that most of the protons are placed in the surface detached from the center due to the Coulomb repulsion. Some nucleon-nucleon type of interaction and the nuclear radius of the liquid drop model can be observed at the bottom. . . . .	26
2.4	Binding energy per nucleon prediction from the semi-empirical mass formula. The peaks in the left side are the binding energy for some even-even nuclei. The most tight binding nuclei is the $^{56}\text{Fe}$ . The left and right sides belongs to nuclei yields for fission and fusion respectively. . . . .	30
2.5	Deformed shapes for even-even nuclei predicted by the rotational model. The deformed shape (prolate or oblate) is a characteristic associated with the electric moment. . . . .	32
2.6	Cross section representation. . . . .	35
2.7	Coordinate system of two nuclei (projectile and target) with masses $A_1$ and $A_2$ . . . . .	37

2.8	Schematic representation of forces in a DC motor. In a DC motor with electric current $\mathbf{I}$ passing through two coils which are under the action of a magnetic field $\mathbf{B}$ , it produces a torque $\boldsymbol{\tau}$ perpendicular to the rotation axis. Adapted from hyperphysics. . . . .	38
2.9	Graphical representation of dipolar magnetic moment $\mu$ induced by a current loop $I$ with area $A$ . Magnetic moment is oriented perpendicular to the current loop plane in the right-hand rule direction. . . . .	39
2.10	Graphic representation of the magnetic moments of different nucleons. In (a) is shown the magnetic moment produced by the protons which are parallel to the nuclear spin $I$ . In (b) the magnetic moment has a non-parallel direction to the nuclear spin for a neutron. This difference in the magnetic moment direction is key to understand the nuclei internal structure. The determination of proton and neutron currents within the nuclei is related with the sign of the magnetic moment and with its direction with respect to nuclear spin. . . . .	42
2.11	An illustration of the nuclear spin as a vector whose magnitude is the expected value of its operator. In (a) the maximum projection of a state of spin on the axis $z$ is shown. In (b) all the possible values that $M$ can take for a value of $I = 2$ are shown, it is noteworthy that the maximum value of $M$ is found in $M = I$ . . . . .	43
2.12	Geometrical description of precession angle graphic. The magnetic field $\mathbf{B}$ vector oriented in the direction of the $z$ -axis which is the axis of rotation of $m\boldsymbol{\mu}$ and $\mathbf{I}$ . The displacement is named $\Delta\mathbf{I}$ , it corresponds to the arc length traveled in an angular change of $\Delta\theta$ . . . . .	46
3.1	Experimental techniques to measure Nuclear Magnetic Moment classified by their validity in different ranges of life times. The techniques mentioned in the figure includes: Transient Field (TF), Recoil Into Vacuum (RIV), Time Differential Recoil Into Vacuum (TDRIV), Perturbed Angular Correlation (PAC), Time Differential Perturbed Angular Distribution (TDPAD) and Nuclear Magnetic Resonance (NMR). . . . .	50
3.2	Angular distributions shapes predicted by spherical harmonics for $I = 2$ nuclear state. . . . .	50
3.3	Graph of $\tau$ against $B$ for different values of precession angle. The interaction time between the magnetic field and the spin, represented by the factor $\Delta t$ in (2.34) was replaced by the Greek letter $\tau$ . This graph is built on a logarithmic scale. . . . .	51
3.4	Graphic representation of the spin-orbit interaction of a hydrogen atom. The light blue circle represents the nucleus ( $+Ze$ ), the red circle represents the electron ( $-e$ ) and the dotted red oval represents the hyperfine interaction. . . . .	52

3.5	Graphic representation of a three-layer target. The thinnest layer (cyan) represents the target, where the nuclear reaction takes place. The middle layer (green) represents the ferromagnetic material, where a fraction of the ions, are left with only one electron; in this layer the hyperfine interaction produced by the transient field takes place. Finally, the stopper layer (brilliant blue) stops the ions that made their way through the ferromagnet. The points attached to the lines represent the ion probe and the red curve its $\gamma$ -emission radiation. . . . .	54
3.6	Typical $\gamma$ -particle detection layout for TF experiments. This arrangement is the one used for a quadrupolar transition whose x-z plane is represented by a green flower or clover leaves in the figure. Particle detector is positioned behind the target to implement inverse kinematics nuclear reactions. The clover detector is defined by the group of four Ge-detectors. . . . .	55
3.7	Graphical representation of the detection and the shift of the angular distribution of the $\gamma$ -radiation. The angular correlation function is calculated for the two different directions of transient field (see $W(\theta)plot$ ). The angular shift is produced by the nuclear magnetic moment precession (represented in the bottom) which produce a rotation in the <i>gamma</i> -distribution. . . . .	57
3.8	Schematic representation of DSAM experiment. In the left part of the figure a typical setup is shown. The incoming beam is shot against the target with a energy such that the desired excited states are populated via nuclear reaction with target ions (full stop). After the reaction, resulting ions recoil into the stopper (gray layer). A detector, positioned at an angle $\theta$ with respect to the beam axis, registers the $\gamma$ -rays produced from nuclear de-excitation with a shifted energy. A particle detector is positioned behind target to register recoil nuclei. In the right side of figure, spectrum corresponding to detection of $\gamma$ -rays in every moment of the ion motion, peaks corresponding to fully shifted (purple peak), partially shifted (peach color region) and fully stopped (cyan peak) ions while they are emitting $\gamma$ -rays are shown. . . . .	61
4.1	Graphical representation of $^{12}\text{C}$ nucleus made of three alpha clusters. . . . .	67
4.2	The Alpha transfer process in the reaction $^{96}\text{Ru} + ^{12}\text{C} \rightarrow ^{100}\text{Pd}$ , where the residual products can be two $\alpha$ -particles or a $^8\text{Be}$ nucleus. . . . .	69
4.3	Possible $\gamma$ -ray intensities distributions for a quadrupolar transition for different spin projections (top) and mix of all of the distributions for a random spin alignment in the quadrupolar transition (bottom). . . . .	70
4.4	The experimental $\gamma$ -ray angular correlations, $W(\theta)$ , for the $2_1^+ \rightarrow 0_1^+$ transitions; open circles correspond to $^{100}\text{Pd}$ and diamonds to $^{96}\text{Ru}$ . The solid and dashed lines correspond to fits to the angular correlation function for $^{100}\text{Pd}$ and $^{96}\text{Ru}$ , respectively. Figure taken from [1]. . . . .	71

4.5	$S_a$ spectroscopic parameter obtained from ( $d, {}^6\text{Li}$ ) reactions, normalized to unity at ${}^{16}\text{O}$ plotted as a function of target mass $A_T$ . Figure taken from [2]. . . . .	72
5.1	Schematic representation of a Van de Graff accelerator system. This kind of accelerators works with a pellet chain, transporting a big amount of charge to a terminal that uses the electric attraction to expel a negative ion beam found inside it to a evacuation tube inside a electrode array and afterwards shot to a target. . . . .	79
5.2	Working's schema of pelletron-tandem accelerator. This type of electrostatic accelerator is an evolution of Van de Graff acceleration system. . . . .	80
5.3	The pellet chain. In the right side the parts of the pellet chain are indicated. A picture of a pellet chain is shown in the left side. The picture of the pellet chain was adopted from <a href="https://www.slideshare.net/AnuradhaKVerma/m1-accelerators">https://www.slideshare.net/AnuradhaKVerma/m1-accelerators</a> . . . . .	81
5.4	Schematic representation of pelletron charge system. This charged system is used to accumulate a large amount of charge (up to and above 25 MV) in the dome of the accelerator. . . . .	82
5.5	MC-SNICS: Multicathode Source of Negative Ions by Cesium Sputtering schema of working. This negative ion source is specially designed for the working of the Tandem accelerator. . . . .	83
5.6	Schematic representation of the nuclear reactions to be performed in the proposed experiment. When ${}^{12}\text{C}$ is shot against a ${}^{28}\text{Si}$ target at energies around 13.13 MeV, two type of reactions should be observed. When an alpha particle is transferred to the ${}^{28}\text{Si}$ nucleus (situation illustrated at the top) a radioactive ${}^{32}\text{S}$ is produced. If the ${}^{12}\text{C}$ do not transfer, or the ${}^{28}\text{Si}$ do not capture the alpha particle, a low-lying spin state in ${}^{28}\text{Si}$ is populate via Coulomb excitation. For both reactions is expected to observe a decay from the $2^+$ spin state. . . . .	84
5.7	The detection setup of the proposed experiment. For the $\gamma$ detection, four segmented scintillator detectors composed by an array of 25 LYSO(Ce) crystals will be placed at $67^\circ$ of the beam direction. For the particle detection 16 $\Delta E$ -E photo-switch detectors will be positioned behind the target. . . . .	85
5.8	LYSO(Ce) array or segmented square LYSO(Ce) crystal available in LAFN with its dimensions. Every crystal in the array is a square of (16 x 16) mm, a total of 25 crystals will be used. The longitude of the crystals is of 50 mm. All these crystals are connected to a silicon photomultiplier. . . . .	86
5.9	LYSO(Ce) crystal pictures. In picture on the left side (a) an array of LYSO(Ce) crystals similar as the one represented in Figure 5.8 is shown. On the right picture there is a LYSO crystal joint to a SiPM forming a scintillator detector. . . . .	87

## LIST OF FIGURES

---

5.10	$\Delta E - E$ telescope or photo-switch formed by a thin and a thick scintillator array together with a photomultiplier tube. The blending of the $\Delta E - E$ array and the photomultiplier tube form a plastic scintillator detector. The photo-switch is responsible for producing the spark as the result of the interaction between the particle and the material and th photomultiplier convert the spark into a suitable electrical signal. . . . .	88
5.11	Alpha gamma angular correlations with the $^{20}\text{Ne}$ reaction for three different positions of the rectangular mask. The three curves were fitted simultaneously to the experimental points normalized to the coincident yield at $0^\circ$ of the beam direction. Figure taken from [3]. . . . .	96
5.12	Schematic representation of a circular segmented particle detector proposed to be used in the next Alpha-transfer experiments. This detector is able to distinguish the dispersed angle of the detected particle (i.e. $\theta_1, \theta_2\dots$ ). The information of the particle is registered in coincidence with a $\gamma$ -ray which comes from the radioactive nuclei produced in the ATR. With this information the particle- $\gamma$ - $\gamma$ correlation function will improve it. . . . .	98
B.1	Graphic representation of level energy occupation of even-even and odd-even nuclei.	105
B.2	Schmith lines with different spin values. . . . .	106
B.3	Superposition of the Schmidt lines and the experimental measurements of nuclear magnetic moment of some nuclei. The experimental measurements were taken from the reference [4]. . . . .	107





# List of Tables

---

2.1	Table of description of Semi-Empirical mass formula terms. Every term contains information about interaction which liquid-drop model assumes to describe nuclear structure. Information here sorted, consider the fundamental aspects of the model.	27
2.2	Predictions of the vibration forms for two values of the nuclear spin based in the vibrational model. . . . .	31
2.3	Nuclear magneton values for two different unit systems. . . . .	41
2.4	Table of $g$ factors associated with the orbital angular momentum and the spin for protons and neutrons [5]. . . . .	41
4.1	(*)These isotopes were created by two $\alpha$ -particles transfer and results were obtaining by TDRIV method in combination with DSAM ("plunger method"). (**)Lifetimes values taken from [6]. Result from first experiments to perform $g$ factor measures with $\alpha$ transfer in combination with transient field technique. . . . .	75
5.1	Table of transfer reactions. This table shows life time ( $\tau$ ) and nuclear $g$ -factors measures of even spin states with positive parity. The first column indicates and the laboratories that can produce the beams of the second column. Light violet color indicates the existence of measures of another nuclear spin states different that even nuclear spin with positive parity. Red color indicates that there is no nuclear magnetic moment measures of any spin state until 2011. The "Product"column belong to the group of nuclei that populate radioactive states after alpha-transfer reaction. . . . .	89
E.1	Table of Alpha-Transfer reactions with available beams (parent) at TRIUMF [7]. All lifetimes corresponds to ground state of the daughter nuclei. $\tau$ values were taken from [8]. . . . .	125



## Chapter 1

### Introduction

---

Nuclear physics studies present several questions with outstanding challenges for physical sciences. The chart of nuclides gives a general landscape of the main characteristic of stable and radioactive nuclei, and plays the same role as the periodic table in atomic physics. The periodic table is the most important referent to study the atoms and classify them. In nuclear physics *the chart of nuclides* (also called *the nuclear map*) is the referent in which all nuclei are sorted under parameters which define their internal structure.

The nuclear map contains a complete collection of nuclides of a real or hypothetical chemical element. Every nuclide is positioned corresponding to its number of nucleons in a  $(Z, N)$  coordinate, where  $Z$  is the number of protons and  $N$  is the number of neutrons.

The nuclear map is divided by regions conformed by groups of nuclei with specific characteristics. The black line, for example, is formed by the most stable nuclei; that is, the ones that do not decay into another nucleus with less mass. The part of the black line formed by nuclei with  $Z = N$  whose number of protons and neutrons are even are formed by alpha-particles [9]. The yellow region belongs to the nuclei whose more probable way of decaying is by emitting alpha-particles.

An alpha-particle is the nucleus,  ${}^4\text{He}$  which is made up of two protons and two neutrons, it is also called  $\alpha$ -cluster. The nuclear structure based on  $\alpha$ -clusters as the constituents of the nucleus is one of the most senior nuclear structure models. Up to day, the  $\alpha$ -cluster model has been able to explain the nuclear structure of light and heavy ions with good accuracy [9].

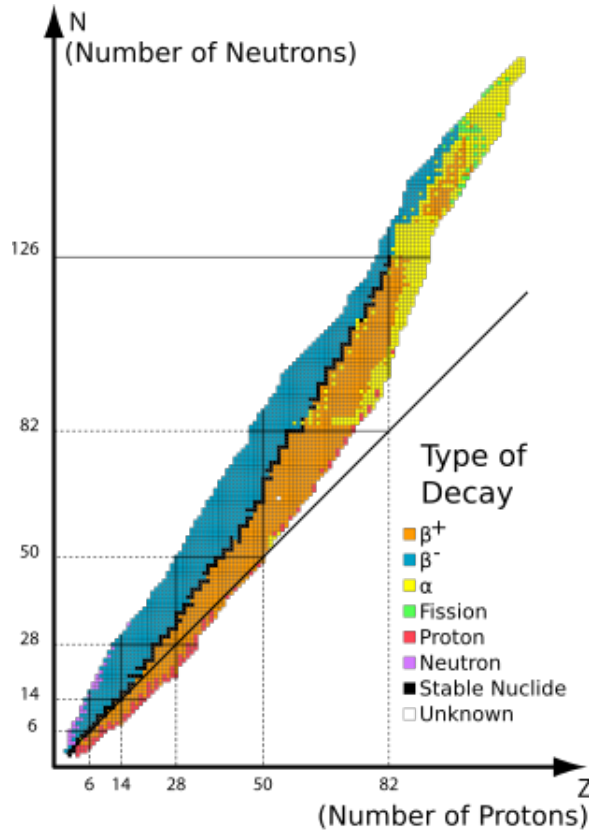


Figure 1.1: In the chart of nuclides each point plotted represents the nuclide of a chemical element. The different colors represent the regions conformed by nuclei with a specific type of decay described in the conventions. Figure adopted from <https://www.revolvy.com/page/Stable-nuclide>

The Alpha-Transfer Reactions (ATR) are a class of direct nuclear reactions which consist of the donation, or the capture of an  $\alpha$ -particle by the projectile or target. The alpha-particle transfer mechanism has been studied from the 60's to the 90's and complex theoretical descriptions of the problem were developed [10–12]. The scientists at that time were expecting that future computational facilities will allow using the theoretical description in order to make predictions about alpha transfer reactions. Nowadays, there are many unknown aspects of the reaction mechanism and several questions have to be solved to be able to retrieve a deep understanding of ATR. The nuclear structure information is closely related to the reaction mechanism [13]. Models which describe  $\alpha$ -cluster nuclei together with interaction models will be able to provide information about the reaction mechanism.

On the other hand, ATR has been used as a method to populate low-to-medium nuclear spin states. Reactions of the type  $X + {}^{12}\text{C} \rightarrow (X+\alpha) + 2\alpha$  with energies around the coulomb barrier, have been used in transient magnetic field experiments to obtain nuclear magnetic moment measurements [3, 14–21]. The great experimental advantage of  $\alpha$ -Transfer Technique is the provision of radioactive products without the need to handle a radioactive beam. This opens the possibility to study many low lying spin states in nuclei that are close to the stability line of the nuclear map with stable beams. Most of these nuclei are even numbered for protons and neutrons and present collective effects. Nevertheless,  $\alpha$ -Transfer reactions method is not the optimal to populate spin states. There is a lack of precision in the  $g$ -factor measurements obtained in experiments that use ATR as a technique to populate spin states. The problem is the resulting low spin alignment (nuclear spin without a preferable  $m$ -projection) after the states population. As a consequence of the poor spin alignment, isotropic  $\gamma$  distribution of the decay is observed. The angular correlation function tends to be flatten when the anisotropy of the  $\gamma$  radiation decreases, as a consequence the  $g$  factor uncertainty increases.

The aleatory  $m$ -projection of the spin state in nuclei populated with ATR is related with the reaction mechanism and there is a lack of knowledge regarding this aspect. Theoretical approaches to understand transfer- and pick up reactions mechanism as DWBA in combination with Optical Potential have presented a good fit to differential cross sections in heavy and light nuclei reactions [22]. However, available experimental data is not good enough. As the reaction mechanism is closely related with nuclear structure [13], future experiments of  $\alpha$ -Transfer reactions should be aimed to get more information of  ${}^{12}\text{C}$  structure. This knowledge could give an answer how to truly improve the  $g$ -factor measurement.

This work is aimed to review the state of the art of the Alpha-transfer reaction technique and its' usage to measure nuclear magnetic moment measurements. From this review, we expect to propose an experimental setup which allows to improve the angular correlation function of the gamma radiation, as well as a specific experiment that uses such setup. It is expected that future experiments will contribute not only with the  $g$ -factor measurement precision but also with a better understanding of the alpha transfer reaction mechanism. This can be achieved obtaining nuclear

---

structure information as:  $\alpha$  widths, spectroscopic factors, and wave functions as the ultimate goal, to unveil  $^{12}\text{C}$  structure.

## Chapter 2

# Theoretical Fundamentals

---

The nucleus is a finite quantum system, composed of particles of  $1/2$  spin (fermions) called nucleons, which are governed by the Pauli exclusion principle. The nucleons are confined into the nuclear radius which has an order of  $r \approx 10^{-15}$  m, they have high kinetic energies and move at relativistic velocities ( $\sim 0.32 c$  [23]). Nucleons are massive particles that are subdivided into two classes, protons and neutrons. Protons are positively charged particles, while neutrons have a zero net charge. Protons and neutrons are under the action of a potential of the atomic nucleus. The average nuclear potential can be seen as originating from a mean field which depends on the interaction of one nucleon with the remaining ones. The associated distribution of the nuclear mass and charge give us, in turn, information about the nuclear shape and, to some degree, the symmetries of the nuclear potential. The structure and ordering of atomic nuclei has been described by different models of nuclear structure, such as, the liquid drop model and the shell model.

A useful tool to study nuclear structure is via the Nuclear Magnetic Moment (NMM). The origin of NMM can be found both in the proton currents within the nucleus and the intrinsic magnetic moments of protons and neutrons. The nuclear magnetic moment value allows to predict the nucleus internal structure [24], and therein lies the importance of its measurement.

In this chapter will be presented a general description of nuclear magnetic moments together

with the Larmor's theory, which describes the magnetic moment dynamics under influence of a magnetic field. Larmor's theory presents the physical principle on which specialized experimental techniques are based for the measurement of NMM in short-lived states.

## 2.1 Structure Models of Nucleus

Nuclear structure models are the quantum mechanical description of the behaviour of nucleons (proton and neutrons) inside the atomic nucleus. There are many models which describe the nucleus, the validity of the model depends on the characteristic of the nucleus. Structure models can be classified in two big groups, single particle models and collective models. Single particle model consider that all of nuclei properties depends of only one nucleon and consider that the rest of the nucleons are coupled or paired in energy levels cancelling their contribution to the total angular momenta. On the other hand, collective models consider nucleus as a rotating hard core, and nucleons exhibiting the same behaviour. The next subsections are aimed to present the basic aspects of this two models.

### 2.1.1 The Shell Model

Nuclear shell model has similarities with Fermi gas model where the nuclear structure is described in terms of nucleons occupying energy levels in a separate potential for protons and neutrons. These energy levels are predicted by a harmonic oscillator potential. The difference between Fermi gas model and shell model consist in the prediction of the energy levels.

For the shell model, a phenomenological nuclear potential of (2.1) named *the Wood-Saxon potential*, was introduced in the Schrodinger equation to obtain the level scheme prediction. This potential depends on the distance  $r$ .

$$V(r) = -\frac{V_0}{1 + e^{(r-R)/a}}. \quad (2.1)$$



Where  $a \approx 0.65$  fermi,  $V_0 \approx 57$  MeV+corrections and  $R = 1.2A^{1/3}$  where  $A$  is the total number of nucleons. Nevertheless, the Woods-Saxon potential is complicated to solve and describes the behavior for one independent particle. A new nuclear potential called Modified harmonic oscillator was proposed. This potential is an interpolation between harmonic oscillator and square well. In addition, the shell model includes the spin-orbit interaction in the Hamiltonian, which allows the correct prediction of *the magic numbers*, the name that was given to the numbers of nucleons such that they are arranged into complete shells within the atomic nucleus. Spin-orbit interaction was proposed by Maria Goeppert Mayer in 1949 [25]. Thus, the energy level scheme predicted by shell model is as the one shown in Figure 2.1. The labels on the levels are different from the symbols for atomic case. The energy levels increase with orbital angular momentum quantum number  $\ell$ , and the  $s, p, d, f...$  symbols are used for  $\ell = 0, 1, 2, 3...$  exactly as the atomic notation. But there is really no physical analog to the principal quantum number  $n$ . The numbers associated with the level start at  $n = 1$  for the lowest level associated with a given orbital quantum number, giving such symbols as  $1g$  which could not occur in the atomic labeling scheme. The quantum number for orbital angular momentum is not limited to  $n$  as in the atomic case. The spin-orbit interaction splits energy levels predicted by the potential well including angular momentum effects. The multiplicity of the states is given by  $2j + 1$  which indicate the number of nucleons that can occupy the level. The parity of the state is  $(-1)^\ell$ .

It is worth to say that there is no a general level scheme for all nuclei, every nucleus has its own level scheme predicted by shell model and depend of its own particular characteristics. This model it is not able to predict any excited state, all nuclear measurements as total angular momentum, magnetic moment, electric moment, among others predicted from the shell model are for nuclei in their fundamental state. There are a lot of modifications of the shell model which are aimed to describe every kind of nucleus, but we are interested in showing just the basic generalities of the shell model.

As is shown in Figure 2.2 nucleons occupy level scheme with a number of occupation equal to  $2j + 1$  following the Pauli's principle. Neutron potential is deeper than proton potential for the contribution of Coulomb proton-proton repulsion to the potential. Neutron are particles whose

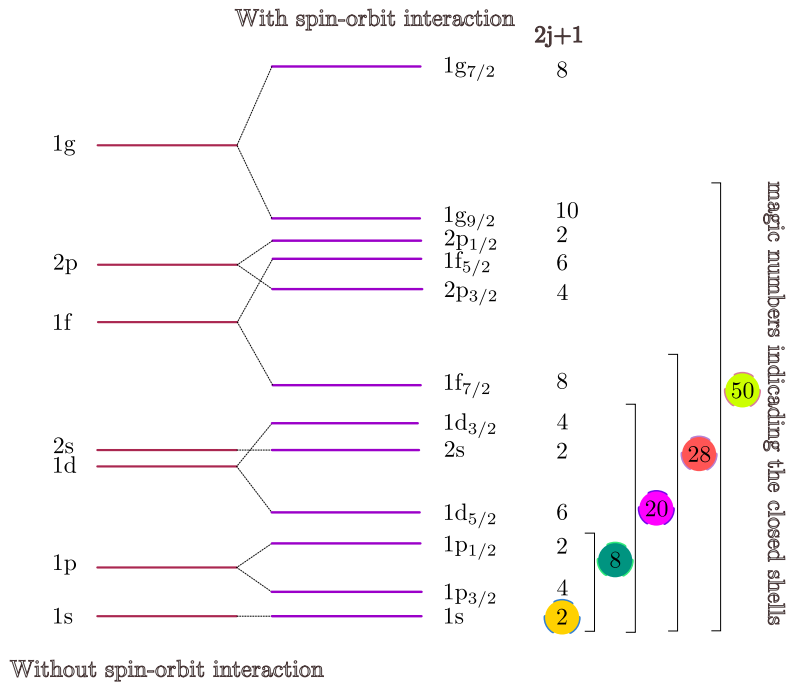


Figure 2.1: Shell model level scheme prediction. In the right side, some magic numbers, which are predicted from the spin-orbit interaction included by Mayer, are shown. The inclusion of the spin-orbit term, predict the magenta level scheme.

net total charge is equal to zero, therefore they are not affected by Coulomb effects.

Every couple of neutrons and protons has a nucleon total angular momentum contribution equal to zero leaving only the unpaired nucleon contribution left. This is an independent particle behaviour which works well to predict nuclear measurements in even-odd or odd-even nuclei. For even-even nuclei, collective are strongly observed, and another nuclear structure model is used to describe their behaviour. This model will be presented in the next subsection.

### 2.1.2 Liquid-Drop model of nucleus

It was first proposed by George Gamow and then developed by Niels Bohr and John Archibald Wheeler. Is the most simple model and describes the nucleus as a tight binding particles set, very close to each other, with a sharp border surface and a homogeneous density. The model supposes the nucleus to has a behavior similar to an incompressible liquid-drop in which nucleon would play the role of molecules in the drop. Due to the Coulomb repulsion, protons tend to reside closest

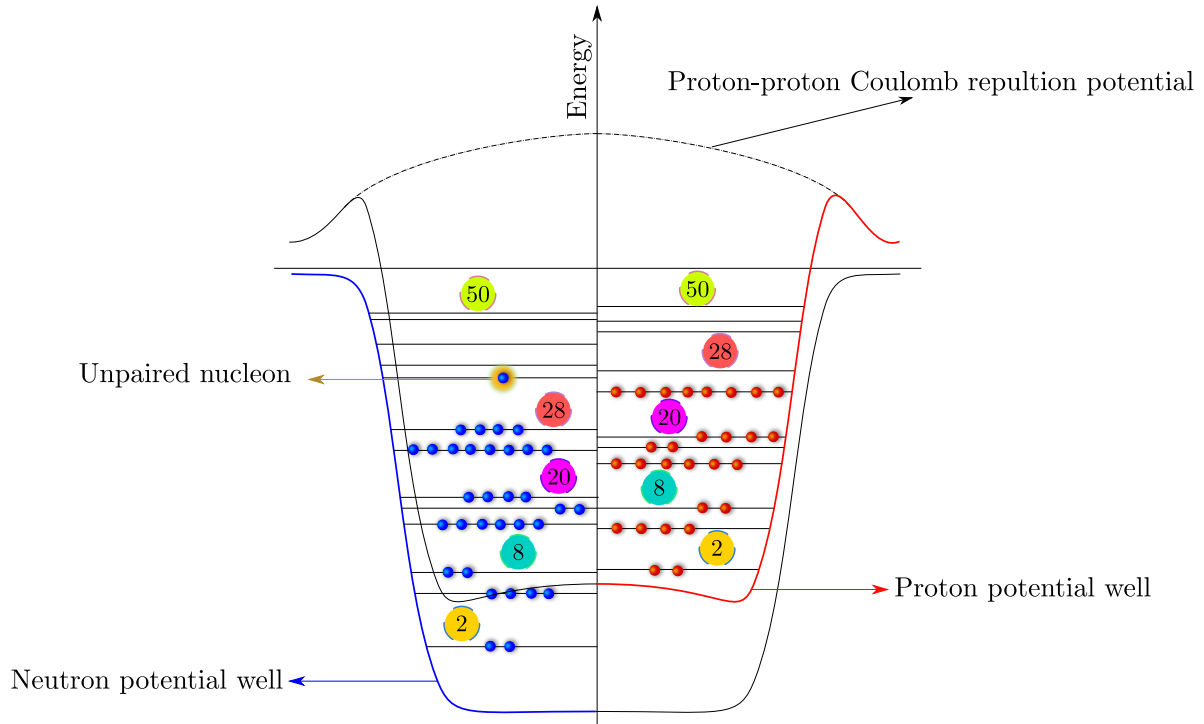


Figure 2.2: Representation of energy level occupation . The blue line indicates the nuclear potential for neutrons and the red one the potential for protons. The dashed line indicates the Coulomb potential. Proton and neutron with a given spin, occupy energy levels with an occupation number given by  $2j + 1$ , filling degenerate energy levels by pairs with spin up and down cancelling the total angular momentum value. Nuclear spin or total angular momentum rises from the contribution of the one unpaired nucleon.

to the surface. The forces on the nucleons on the surface are different from those on nucleons on the interior where they are completely surrounded by other attracting nucleons as is show in Figure 2.3. This is something similar to the surface tension as a contributor to the energy of a tiny liquid drop. In the liquid drop model, the volume of the nucleus is proportional to the mass number  $A$ , and the surface is proportional to  $A^{1/3}$ . Nucleons are under the action of five type of interactions. In Figure 2.3 are shown three of these interactions.

The Bethe-Weizsacker formula or the Semi-empirical mass formula is the relation which predict the binding energy between nucleons. The equation contains the sum of all type of interaction between nucleons assumed by the liquid drop model as it follows:

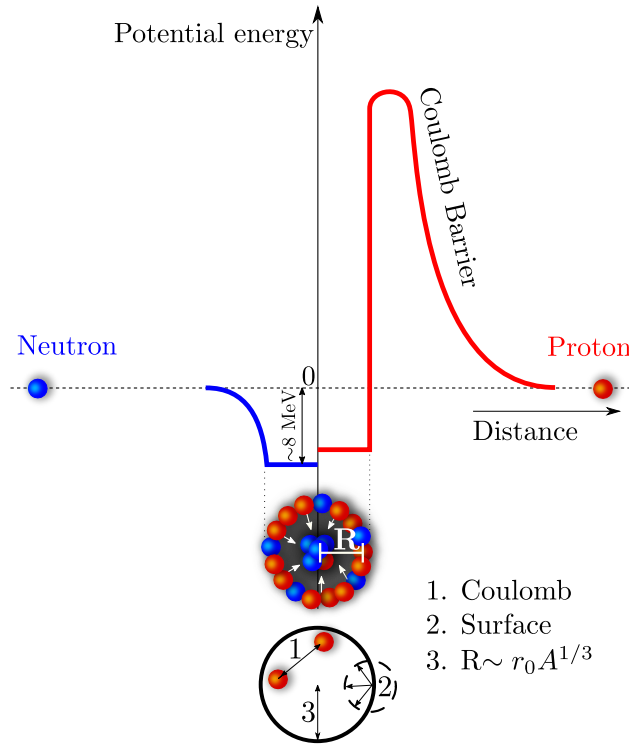
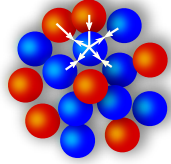
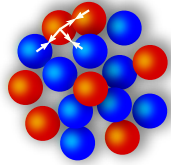


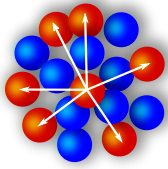
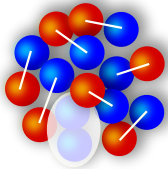
Figure 2.3: *Illustration of the neutron and proton potential. The liquid-drop model predicts an inner structure of the nucleus so that most of the protons are placed in the surface detached from the center due to the Coulomb repulsion. Some nucleon-nucleon type of interaction and the nuclear radius of the liquid drop model can be observed at the bottom.*

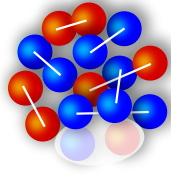
$$B(A, Z) = a_v A - a_s A^{2/3} - a_c Z \frac{Z-1}{A^{1/3}} - a_A \frac{(A-2Z)^2}{A} \pm \delta(A, Z) \quad (2.2)$$

Where  $B(A, Z)$  is the total binding energy of the nucleus,  $Z$  is the number of protons and  $A$  is the total number of nucleons. The meaning of every term of (2.2) is presented in Table 2.1 following the same order as the terms are disposed in (2.2).

Table 2.1: Table of description of Semi-Empirical mass formula terms. Every term contains information about interaction which liquid-drop model assumes to describe nuclear structure. Information here sorted, consider the fundamental aspects of the model.

Term	Description
<b>Volume</b> ( $a_v$ )	<p>Since the nucleons are interacting with the same neighbors, and the nucleus is assumed to have a homogeneous density, so the binding energy is assumed to be the same for every nucleon as well. The volume term energy is a consequence of the strong nuclear force. Then, the volume term is equivalent to <math>A</math> multiplied by a volume energy <math>a_v = 15.85</math> MeV. This energy is smaller than the binding energy of the nucleons which is of order of 40 MeV . [26]. The quantity <math>a_v</math> come from the Fermi energy concepts.</p> 
<b>Surface</b> ( $a_s$ )	<p>Notwithstanding the nucleons was assumed to have the same binding energy to calculate the contribution of the volume term, a correction has to be included. As is shown in Figure 2.3 there are nucleons some arranged in the surface. This nucleons have less surrounding neighbors and binding energy must be reduced. The surface term is then negative and proportional to the sphere area of the nucleus (of empirical radius <math>R = 1.2 \text{ fm}A^{1/3}</math>) <math>a_s A^{2/3} = 18.1 A^{2/3}</math> MeV.</p> 

<p><b>Coulomb</b> (<math>a_c</math>)</p>	<p>Coulomb term is associated to protons. As the protons have equal charge this term is negative because makes lower the binding energy between protons. Coulomb term is proportional to the proton pairs <math>2Z/R</math>. The <math>a_c</math> factor has been calculated to be equal to 0.71 MeV.</p>	
<p><b>Asymmetry</b> (<math>a_A</math>)</p>	<p>This term is complex to explain. Is based only on the Pauli exclusion principle. Neutrons and protons occupy energy levels following the exclusion principle. As energy starts to increase, nucleons would be at higher levels, increasing the total energy of the nucleus and decreasing the binding energy. Heavier nuclei commonly have more neutrons than protons. The extra neutrons provide compensation for the repulsion between protons via proton-neutron attractive forces. Nevertheless, <math>Z = N</math> nucleus is the most stable, and as neutron number is increasing in heavy nuclei, they will get more and more unstable. The asymmetry term calculates the "energy of instability" of heavy nuclei with an excess of neutron mass. The coefficient <math>a_A \sim 23.7</math> MeV.</p>	

<p style="text-align: center;"><b>Pairing</b> (<math>\delta(A, Z)</math>)</p>	<p>Pairing term represents the effects of spin-coupling. As asymmetry term is lower for nuclei with <math>Z = N</math>, an even-even nucleus is more stable due to spin-coupling between their nucleons. So <math>\delta</math> is a parameter which depends on <math>A</math> and <math>Z</math> and it represents a positive contribution for the binding energy in even-even nuclei (+12 MeV), a negative contribution in odd-odd nuclei (-12 MeV) and a null contribution in even-odd, odd-even.</p> 
-----------------------------------------------------------------------------------	----------------------------------------------------------------------------------------------------------------------------------------------------------------------------------------------------------------------------------------------------------------------------------------------------------------------------------------------------------------------------------------------------------------------------------------------------------------------------------------------------------------------------------------------------------------------------------------------

The binding energies of nucleons are in the range of millions of electron volts (MeV) compared to tens of eV for atomic electrons. For that reason, a de-excitation process dramatically more energetic for nuclei than for atoms. In an atomic transition a photon might be emitted in the range of a few electron volts, maybe in the visible light region. In a nuclear transition a more energetic photons can be emitted producing gamma-radiation with quantum energies in the order of MeV.

The binding energy curve is obtained by dividing the total nuclear binding energy by the number of nucleons  $A$ . The curve is disposed in Figure 2.4. The binding energy per nucleon increases dramatically with mass number  $A$  up to 20. For  $A < 20$  exists a peaks recurrence of nuclei whose mass number are multiples of four and they contain not only equal but also even number of protons and neutrons. Then the liquid-drop model predicts the stability of even-even nuclei. The curve becomes almost flat for mass number between 40 and 120. Beyond 120, it decreases slowly as mass number increases.

There is a maximum of binding energy per nucleon for  $A = 56$  corresponding to the iron nucleus  ${}^{56}_{26}\text{Fe}$  of 8.8 MeV, becoming it the most stable one, but in general the Fe nuclei are the most stable. The average binding energy is about 8.5 MeV for nuclei in a range of mass between 40 and 120.

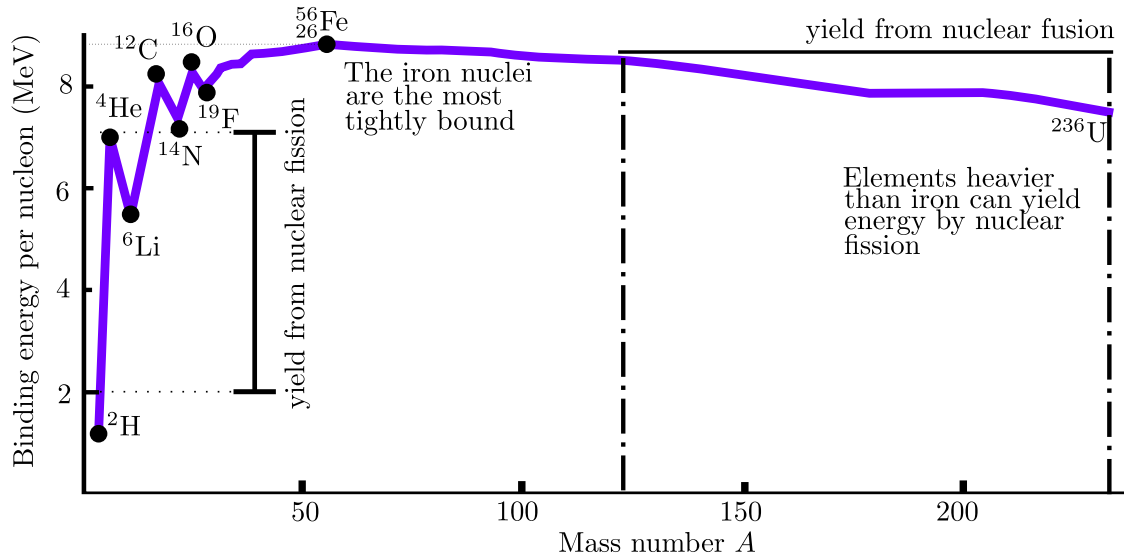


Figure 2.4: Binding energy per nucleon prediction from the semi-empirical mass formula. The peaks in the left side are the binding energy for some even-even nuclei. The most tight binding nuclei is the  $^{56}\text{Fe}$ . The left and right sides belongs to nuclei yields for fission and fusion respectively.

These nuclei are comparatively more stable and non radioactive. For masses higher than 120, the curve drops slowly, and nuclei becomes unstable and radioactive. For example, the average binding energy per nucleon uranium isotopes is about 7.6 MeV, they are radioactive and unstable. The lesser amount of binding energy for lighter and heavier nuclei explains nuclear fusion (left side of Figure 2.4) and fission (right side of Figure 2.4) respectively.

Large amount energy is liberated in a fusion process (when a lighter nucleus is fused with a heavier one), and also in the opposite, a fission process (when a heavier nucleus disintegrate into lighter nuclei).

Liquid-drop model is for the collective models of the nucleus, what shell model is for the single particle models of the nucleus. Collective models are of special interest for this work due to  $^{12}\text{C}$  nucleus, is an even-even nucleus whose nuclear structure presents a collective behaviour. In the next section we are going to show the most basic aspects of collective models for the prediction of nuclear internal states.



## Collective Models

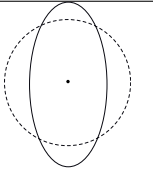
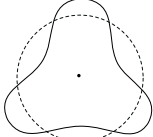
Shell model predicts all even-even nuclei to have  $I^P = 0$  in their ground state. The existence of a first excited state at one energy of 1 MeV with  $I^P = 2^+$  is a property of even-even nuclei in nearly all cases, it does not matter their level structure [27]. Such property is known as a *collective property* and it is not possible to explain it from the shell model. The collective model explains the existence of this low-lying state, considering that all nucleons belonging to a nucleus make a transition the first state *together*.

There are two general models which explains the behaviour of nucleus as a collective: the vibrational model and the rotational model, let us review some basic aspects of them.

### *The vibrational model*

The nucleus is considered as a liquid drop that vibrates with a high frequency, whose shape is in average spherical. All nucleons are vibrating such that they deform the shape of the nucleus. Every vibrational mode is characterized by  $\lambda$  and they are associated with the total angular momentum value. The corresponding states to a vibrational mode  $\lambda$  are actually eigenstates of total angular momentum  $I = \lambda$  with well defined parity  $P = (-1)^\lambda$ . In Table 2.2 are shown some of this vibrations.

Table 2.2: *Predictions of the vibration forms for two values of the nuclear spin based in the vibrational model.*

<p><b>Quadrupole vibration</b> (<math>\lambda = 2</math>): <math>I^P = 2^+</math>. Is the fundamental mode of vibrational model. The vibrations are not spherical and the nucleus oscillates between prolate and oblate shapes.</p>	
<p><b>Octupole vibration</b> (<math>\lambda = 3</math>): <math>I^P = 3^-</math>. Includes changes in the parity. Vibrations are complex in sundry axes.</p>	

Fundamental state  $I^P = 0^+$  is symmetrically spherical and there are no vibration. Vibrational model is used for even-even nuclei with  $A < 150$ .

*The rotational model*

Rotational model is applicable for the so-called deformed nuclei, these nuclei does not have a spherical equilibrium position and are far from magic numbers regions ( $150 < A < 190$ ,  $220 < A < 250$  and  $A \sim 24$ ). Deformed nuclei shape can be prolate or oblate with a rotation axis perpendicular to the symmetry axis as in Figure 2.5.

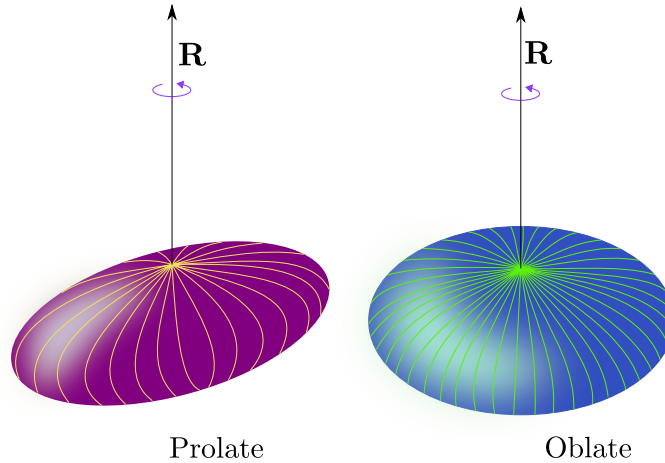


Figure 2.5: *Deformed shapes for even-even nuclei predicted by the rotational model. The deformed shape (prolate or oblate) is a characteristic associated with the electric moment.*

Only deformed nuclei can rotate collectively. It is possible to define just one moment of inertia  $J$  and the hamiltonian of even-even nuclei (with no nucleons external to the core) becomes

$$H_{rot} = \frac{\mathbf{R}^2}{2J} \quad (2.3)$$

Where  $\mathbf{R}$  is the collective angular momentum. For purely collective rotation  $\mathbf{I} = \mathbf{R}$  and it is said that the nucleus is a perfect rotor. The energy values for the perfect rotor are:

$$E_I = \frac{\hbar^2}{2J} I(I+1) \quad (2.4)$$

Where  $I^\pi = 0^+, 2^+, 4^+, 6^+ \dots$ . The sequence of states  $|I\rangle$  whose energies are defined by (2.4) are defined as a *rotational band*.

In this section, we have presented the most referenced nuclear structure models. These models are successful in understanding ground states in the most nuclei of the nuclear map. Nuclear structure is crucial for the understanding of the interaction between nuclei (nuclear reaction). Let us review some fundamental aspects of nuclear reactions.

## 2.2 Fundamentals of Nuclear Reactions

A nuclear reaction takes place when two nuclei interact. In a nuclear reaction there are a projectile, a target and products. Nuclear reactions can be classified by the outgoing products and by the mechanism type which governs the process, like this:

1. **Direct reactions:** This type of reaction refers to the ones in which projectile interacts only with the nucleons of the surface of the target. During the interaction some nucleons can be shared between target and projectile, removing or inserting them of nuclei involved in the reaction. The time needed for the interaction is typical of  $10^{-22}$  s.
2. **Compound reactions:** Contrary to the direct reactions, in compound reactions, projectile and target are completely fusion. After the reaction projectile and target become indistinguishable and together constitute the particular excited state of the compound nucleus. The compound nucleus is excited by both the kinetic energy of the projectile and by the binding nuclear energy. The time scale of compound nucleus reactions is of the order of  $10^{-18}$  s –  $10^{-16}$  s, but lifetimes as long as  $10^{-14}$  s have been also observed [28].

A broadly use notation for nuclear reaction is the follow

$$X(a,b)Y.$$

Where  $a$  is the projectile,  $X$  is the target,  $Y$  and  $b$  are the products.

An important aspect of nuclear reactions is the Coulomb barrier. In a nuclear reaction, the projectile has to overcome the Coulomb repulsion having larger energy than the Coulomb barrier

energy.

### The Coulomb barrier

Due to the coulomb repulsion between protons from the projectile and target, there is an energy which tends to separate away the nuclei of a reaction. As nuclei are getting closer this repulsion energy increases, but when nuclei are close enough the Coulomb barrier is overcome by the projectile and starts to interact with the target. The energy of the coulomb barrier is given by.

$$E_{CB} = \frac{kZ_1Z_2e^2}{r_c} \text{ with } k = 8.99 \times 10^9 \text{ Nm}^2/\text{C}^2. \quad (2.5)$$

Where  $Z_1$  and  $Z_2$  are the number of protons of the projectile and target respectively,  $e$  is the elemental charge  $1.60217653 \times 10^{-19}$  C, and  $r_c$  is the interaction radius of the nuclei.

#### 2.2.1 Cross Section

For a flux of ions  $F$  that are being shot against a target of area  $A$  with a number  $n$  of scattering centers as in Figure 2.6, there is a number of scattering events expected in a solid angle  $d\Omega$  whose direction is deviated on an angle  $\theta$  with respect of the beam axis. The number of scattering events with respect to the solid angle per unit time is called the differential cross section. Is one of the most important parameters in the study of nuclear reactions, and can be expressed as it follows.

$$\frac{d\sigma}{d\Omega} = \frac{\text{Number of reactions}}{\Delta t \text{ per scattering center through } d\Omega \text{ in } (\theta)F}$$

Then

$$\frac{d\sigma}{d\Omega} = \frac{N}{N_0 n x \Delta\Omega}. \quad (2.6)$$

Where

- $N$  - Number of particles registered by the detector.
- $N_0$  - Total number of particles falling on the target.
- $n = \rho N_A / M$  - Number of nuclei per unit volume on the target thickness (scattering centers).
- $x$  - is the target thickness.
- $\Delta\Omega$  - the solid angle which could be determined from the system configuration.

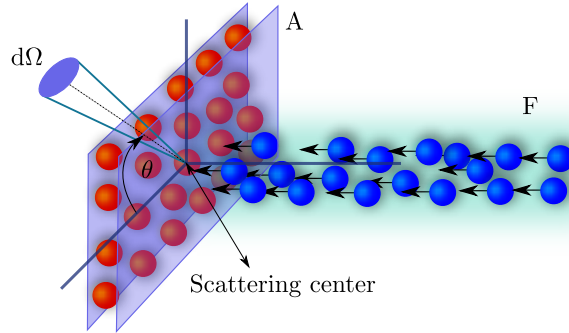


Figure 2.6: *Cross section representation.*

The total cross section  $\sigma$  is then defined as

$$\sigma = \int \frac{d\sigma}{d\Omega} d\Omega. \quad (2.7)$$

Roughly speaking  $\omega$  is a measure of the probability that the reaction happens. Total cross section has dimensions of area per nucleus and its unit is the barn ( $1 \text{ b} = 100 \text{ fm}^2$ ).

### 2.2.2 Optical potential

The optical potential comes from the analysis of an elastic scattering process by partial waves [29]. The analysis is made in the description of the time evolution of the states associated to a particle scattered by a potential. The state of the scattered particle is represented by a *wave packet*, whose time evolution is obtained if it is expressed as a superposition of stationary states. Those stationary states are the associated solutions of the Schrodinger equation of the system and have a well-defined energy  $E$ . Thus, the total wave function  $\psi(\mathbf{r})$  it is expressed as a superposition of

a plane incident wave with a scattered spherical wave. This total wave function can be written asymptotically as

$$\psi(\mathbf{r}) \Rightarrow e^{i\mathbf{k}\cdot\mathbf{r}} + f(\Omega)\frac{e^{ikr}}{r} \text{ for } r \Rightarrow \infty. \quad (2.8)$$

Where  $f(\Omega)$  is the total scattering amplitude which depends on the angle of the scattered waves,  $r$  is the distance to the potential,  $k$  is the wave number and the term  $\frac{e^{ikr}}{r}$  is the spherically outgoing wave. The information about the potential is contained in the scattering amplitude (or nuclear phase shift which defines it).

The plane wave packet has a plane wave expansion as it follows.

$$e^{ikz} = \sum_{\ell=0}^{\infty} (2\ell + 1) i^{\ell} j_{\ell}(kr) P_{\ell}(\cos \theta). \quad (2.9)$$

The scattering amplitude is related with differential cross section this way

$$\frac{d\sigma}{d\Omega} = |f(\Omega)|^2. \quad (2.10)$$

The simplest form of the optical potential

$$V_N(r) = Uf(r) + iWg(r). \quad (2.11)$$

Where  $U$  and  $W$  are the depths of the real and imaginary parts, and  $f(r)$  and  $g(r)$  their radial form factors.

That is so called to make an analogy with the refraction index in optics, where adding an imaginary part accounts for the processes in which light is absorbed by a medium.

The optical potential has successfully predict the cross section of many reactions and it is broadly referenced and used to understand nuclear reactions [30].

### 2.2.3 São Paulo Potential

The São Paulo Potential (SPP) is a model based on a double-folding potential with an additional factor. The SPP potential attempts to describe the mean nuclear potential of two interacting nuclei [31] and has the form

$$V_{\text{SPP}}(\mathbf{R}, E_{\text{rel}}) = V_{\text{Fold}}(\mathbf{R})e^{-4v^2/c}. \quad (2.12)$$

Where  $c$  is the speed of the light,  $v$  is the speed of relative motion between nuclei,  $\mathbf{R}$  is the relative coordinate between the center of mass of the projectile and the target (see Figure 2.7).

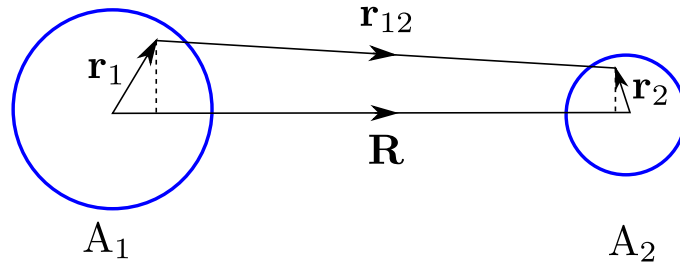


Figure 2.7: Coordinate system of two nuclei (projectile and target) with masses  $A_1$  and  $A_2$ .

$V_{\text{fold}}$  is the double folding potential given by

$$V_{\text{Fold}}(\mathbf{R}) = V_0 \int d\mathbf{r}_1 \int d\mathbf{r}_2 \rho_1(\mathbf{r}_1) \rho_2(\mathbf{r}_2) \delta(\mathbf{r}_{12} = \mathbf{R} + \mathbf{r}_2 - \mathbf{r}_1). \quad (2.13)$$

Where the  $\rho_i$  parameter represents the distributions of the nuclei center of mass at the ground state of the  $i$ -nucleus, they are called *density distribution* and their values are obtained from shell model. The parameter  $V_0 = -456 \text{ MeVfm}^3$ .

The São Paulo potential has described heavy-ion reaction successfully in a broad energy rank [32]. The SPP has the advantage of depends only on the distance between the nuclei, energy and the relative velocity between the nuclei.

One of the perspectives of this work is to use the SPP potential to study alpha-transfer reactions.

In this section we have review the fundamental aspects of nuclear reactions. To enter to the main part of this work, the next section is aimed to present different aspects of the nuclear magnetic moment.

## 2.3 Nuclear Magnetic Moments

To explain softly the meaning of magnetic moment, let's remember the action of the torque in a DC motor with a coil moving around an axis (see Figure 2.8). When electrical current  $\mathbf{I}$  pass through the coil with a longitude  $L$  and width  $W$  under the action of a magnetic field  $\mathbf{B}$ , it produces a magnetic force  $\mathbf{F}$  (Lorentz force) perpendicular to the axis of rotation and  $\mathbf{F}$  produces a torque which turns the DC motor.

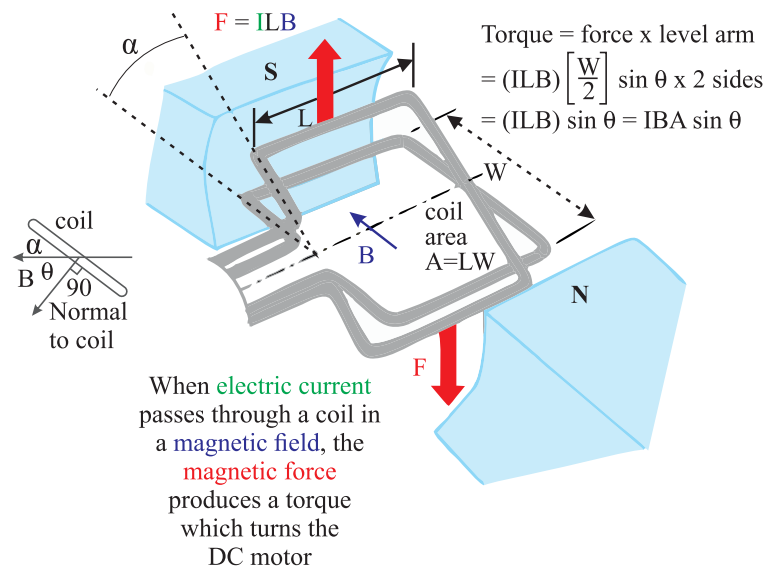


Figure 2.8: Schematic representation of forces in a DC motor. In a DC motor with electric current  $\mathbf{I}$  passing through two coils which are under the action of a magnetic field  $\mathbf{B}$ , it produces a torque  $\tau$  perpendicular to the rotation axis. Adapted from hyperphysics.

As it follows in the inferior-left part of Figure 2.8, torque is proportional to  $\mathbf{I}$  and  $\mathbf{B}$  magnitudes multiplied by area  $A$  of the coil, multiplied by sin of the angle between direction of magnetic field and normal to coil  $\theta$ .



$$\tau = IBA \sin \theta. \quad (2.14)$$

Torque on a DC motor is related to the characteristic of the coil. They are basically: the area  $A$  and the current-carrying  $I$ . Now, in general, this characteristics on any current loop can be summarized on its Magnetic Moment  $\mu$  as it follows,

$$\mu = IA. \quad (2.15)$$

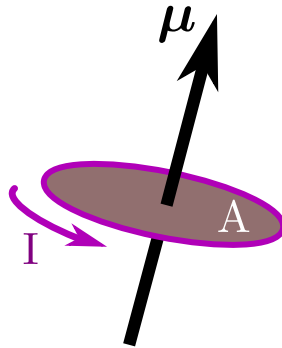


Figure 2.9: Graphical representation of dipolar magnetic moment  $\mu$  induced by a current loop  $I$  with area  $A$ . Magnetic moment is oriented perpendicular to the current loop plane in the right-hand rule direction.

The magnetic moment is a vector quantity with direction perpendicular to the current loop.

### 2.3.1 Quantum description of Magnetic Moment

Consider a charged particle  $+q$  and mass  $m$  moving along a perfectly circular loop of radius  $r$  at a velocity  $v$ , as shown in Figure 2.9, produces an electric current

$$I = \frac{qv}{2\pi r}, \quad (2.16)$$

therefore, the magnitude of (2.15) becomes:

$$\begin{aligned}
 \mu &= \frac{qva}{2\pi r} & (2.17) \\
 &= \frac{q}{2\pi r} \pi r^2 v \\
 &= \frac{qrv}{2}.
 \end{aligned}$$

Adding a factor  $m/m$  (where  $m$  corresponds to the mass of the charged particle) in (2.17) and taking into account that the magnitude of the angular momentum is given by  $|\ell| = mvr$ , we have:

$$\mu = \frac{qmv r}{2m} \Rightarrow \frac{q\ell}{2m}, \quad (2.18)$$

finally, taking the corresponding vector magnitudes, the dipole magnetic moment is given by:

$$\boldsymbol{\mu} = \frac{q}{2m} \boldsymbol{\ell}. \quad (2.19)$$

In nuclear physics, nuclear spin  $\mathbf{I} = \boldsymbol{\ell} + \mathbf{S}$  is the equivalent to the total angular momentum  $\mathbf{J}$ . Then, the mathematical relationship for the magnetic moment of one nucleon is,

$$\boldsymbol{\mu} = g \frac{e\hbar}{2m_N} \mathbf{I}. \quad (2.20)$$

Where the  $g$  factor is a dimensionless correction value which has a quantum mechanical prediction (see Appendix A for more details),  $m_N$  and  $e$  are the mass of the nucleon and the proton charge respectively. It is convenient to introduce the so called **nuclear magneton**. This term refers to the magnetic unit for the nuclear magnetic moment, which obeys the relationship

$$\mu_N = \frac{e\hbar}{2m_N}.$$

The approximate values of the nuclear magneton are arranged in Table 2.3.

SI	CGS
$5.05078353(11) \times 10^{27}$ Joules/Tesla	$3.1524512550(15) \times 10^{-8}$ eV/Tesla

Table 2.3: *Nuclear magneton values for two different unit systems.*

The nuclear magnetic moment is the sum of the individual magnetic moments of each nucleon that composes the nucleus

$$\boldsymbol{\mu} = \sum_{i=1}^A \boldsymbol{\mu}_i. \quad (2.21)$$

Where  $A$  is the total number of protons and neutrons. The expression (2.21), can be decomposed into;

$$\boldsymbol{\mu} = \sum_{i=1}^Z \boldsymbol{\mu}_i + \sum_{j=1}^N \boldsymbol{\mu}_j. \quad (2.22)$$

Where  $Z$  and  $N$ , are the total number of protons and neutrons respectively. Nuclear magnetic moment has a contribution of each proton and neutron inside the nucleus. As nucleons have independent contribution to the total angular momenta, they have a different  $g$  factor value for protons and neutrons. The respective values of  $g$  factor are arranged in the Table 2.4. The sign of the factor  $g$ , indicates if the magnetic moment is parallel (positive) or nonparallel (negative) to the total angular momentum. It is important to remark that we will mainly mention  $g$  factor value along this document, but it is very easy to migrate from magnetic moment value to  $g$  factor with the relation (2.20).

Nucleon	$g_{\ell}$	$g_s$
p	1	+5.5858
n	0	-3.8263

Table 2.4: *Table of  $g$  factors associated with the orbital angular momentum and the spin for protons and neutrons [5].*

The magnetic moment does not have the same direction as the total angular momentum. In concordance with Table 2.4, the different values of the  $g$  factor, will cause the magnetic moment

vector to point to a different direction than  $\mathbf{I}$ , as shown in Figure 2.10.

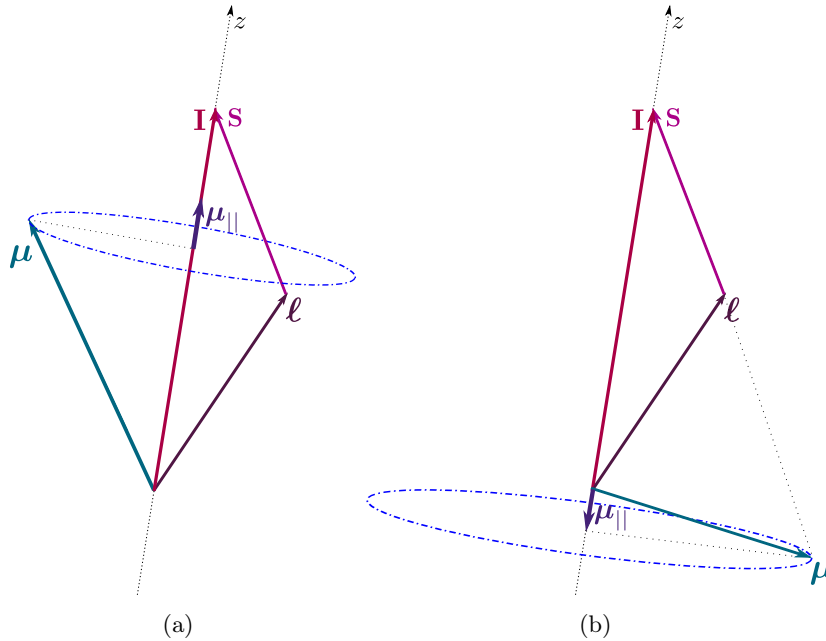


Figure 2.10: *Graphic representation of the magnetic moments of different nucleons. In (a) is shown the magnetic moment produced by the protons which are parallel to the nuclear spin  $I$ . In (b) the magnetic moment has a non-parallel direction to the nuclear spin for a neutron. This difference in the magnetic moment direction is key to understand the nuclei internal structure. The determination of proton and neutron currents within the nuclei is related with the sign of the magnetic moment and with its direction with respect to nuclear spin.*

The expected value of  $|\mathbf{I}\rangle$  is defined as its maximum projection on the  $z$  axis as is shown in Figure 2.11. This projection corresponds to the maximum value of the magnetic quantum number  $M$ , that is, when  $M = I$  [33]. The expected value of the nuclear spin, then follows the relationship

$$M = \max I_z. \quad (2.23)$$

The expected value of an arbitrary operator  $\hat{O}$  in the maximum projection on the axis  $z$ , fulfills the relation,

$$\langle \hat{O} \rangle = \langle M = I | \hat{O} | M' = I \rangle. \quad (2.24)$$

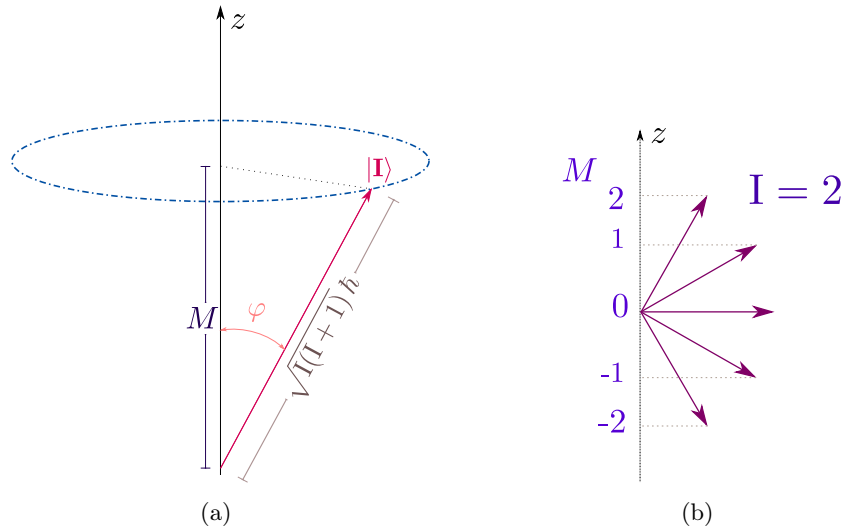


Figure 2.11: An illustration of the nuclear spin as a vector whose magnitude is the expected value of its operator. In (a) the maximum projection of a state of spin on the axis  $z$  is shown. In (b) all the possible values that  $M$  can take for a value of  $I = 2$  are shown, it is noteworthy that the maximum value of  $M$  is found in  $M = I$ .

Where the action of  $\langle \hat{O} \rangle$  makes the state  $|M' = I\rangle$  to become into a state of the same basis as  $\langle M = I|$ .

According with (2.24)

$$\mu = \langle M = I | \hat{\boldsymbol{\mu}} | M' = I \rangle, \quad (2.25)$$

Thus the magnetic moment has the value of its maximum projection.

$$\mu = \max \mu_z. \quad (2.26)$$

For even-even nuclei the nuclear magnetic moment is equal to zero at ground states. There are some exceptions including odd-odd nuclei, however they are present only in very few cases and therefore not considered in this work. A large number of nuclei have  $g$ -factor values close to  $+0.5$  ( $g \approx Z/A$ ), because of the collective effects that dominates the vast majority of atomic nuclei. A prediction of the  $g$ -factor value in the case of collective effects is described in the next subsection.

*The  $g$  factor prediction for collective nuclei*

When nucleus has collective effects, the  $g$  factor is no longer governed by the equation (A.7) and is governed by [34]:

$$g = g_\pi \frac{N_\pi}{N_\pi + N_\nu} + g_\nu \frac{N_\nu}{N_\nu + N_\pi}, \quad (2.27)$$

$N_\pi$  is the number of proton bosons and  $N_\nu$  the number of neutron bosons,  $g_\nu$  and  $g_\pi$  are the  $g$  factors associated with each term. It can be considered an inert nucleus for which the intrinsic spin of the nucleons is coupled and is zero, therefore  $g_\pi = 1$  and  $g_\nu = 0$ , thus;

$$g = \frac{N_\pi}{N_\pi + N_\nu} = \frac{Z}{A}. \quad (2.28)$$

Besides the fact that neutron is an uncharged particle it has a magnetic moment different to zero, which is attributed to its internal structure formed by three quarks. Furthermore, its intrinsic magnetic moment *is negative* which means that the magnetic moment of the neutron tends to precess counterclockwise in the direction of the magnetic field. This behaviour is fundamental for the study of the structure of the atomic nucleus, the opposite signs in the intrinsic  $g$  factors of the proton and the neutron open the possibility to determine if the wave function of a nuclear state is dominated by protons or neutrons. Most of nuclei have a positive  $g$  factor, due to the double contribution of both the orbital part and the spin part of protons.

In this section we have presented some aspects of nuclear magnetic moment, in the next section we are going to present its dynamic under a magnetic field.

## 2.4 Larmor's Precession

According with (2.14) and (2.15) and considering the vector product magnitude relationship, torque is related with magnetic moment this way

$$\boldsymbol{\tau} = \boldsymbol{\mu} \times \mathbf{B}, \quad (2.29)$$

(2.29) is called Larmor's theorem (see Appendix C for more information), this torque tends to line up the magnetic moment with the magnetic field  $\mathbf{B}$ , so this represents its lowest energy configuration [35]. The potential energy associated with the magnetic moment is,

$$U(\theta) = -\boldsymbol{\mu} \cdot \mathbf{B}. \quad (2.30)$$

Where  $U(\theta)$  is a parameter which depends on the angle, since if energy associated to  $\boldsymbol{\mu}$  is higher, magnetic moment vector will be less aligned with  $\mathbf{B}$  and vice-versa.

Torque produces a translation of the magnetic moment and the spin forcing them to rotate around the direction of the magnetic field, this movement is known as *Larmor precession*.

### 2.4.1 Precession Angle

The precession angle is the name given to the length of the arc traveled by the magnetic moment and the spin when subjected to a magnetic field. Its mathematical deduction is described bellow.

Starting from (2.29), it is known that the magnitude of the torque vector is given by,

$$|\boldsymbol{\tau}| = B \mu \sin \varphi. \quad (2.31)$$

Where  $\varphi$  is an angle formed by the two vectors  $\boldsymbol{\mu}$  and  $\mathbf{B}$  as Figure 2.12.

Torque can also be expressed as the rate of change between the spin and the orbital angular moment, taking into account the measure of the arc length due to the change of position of the spin, we have:

$$|\boldsymbol{\tau}| = \frac{\Delta I}{\Delta t} = \frac{\Delta \theta I \sin \varphi}{\Delta t} = B \mu \sin \varphi. \quad (2.32)$$

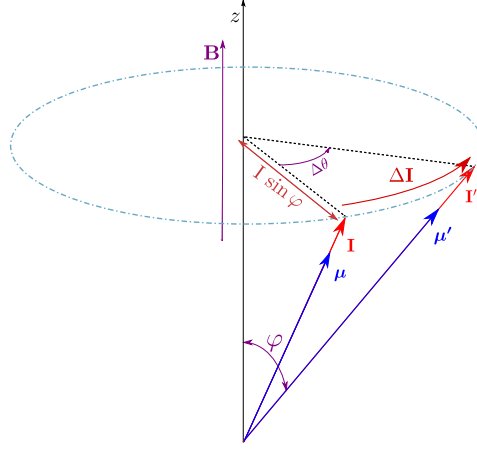


Figure 2.12: *Geometrical description of precession angle graphic. The magnetic field  $\mathbf{B}$  vector oriented in the direction of the  $z$ -axis which is the axis of rotation of  $\mathbf{m}\mathbf{u}$  and  $\mathbf{I}$ . The displacement is named  $\Delta\mathbf{I}$ , it corresponds to the arc length traveled in an angular change of  $\Delta\theta$ .*

Applying this formalism to the case of the nucleus and returning to what has already been shown in the previous section, we know that the magnitude of the nuclear magnetic moment is given by,

$$\mu = \frac{ge}{2m_p} I,$$

therefore,

$$|\tau| = \frac{\Delta I}{\Delta t} = \frac{\Delta\theta I \sin\varphi}{\Delta t} = \frac{ge}{2m_p} I B \sin\varphi. \quad (2.33)$$

Clearly  $\Delta\theta$  is equivalent to

$$\begin{aligned} \Delta\theta &= \frac{ge}{2m_p} B \Delta t. \\ \therefore \Delta\theta &= \frac{g\mu_N}{\hbar} B \Delta t. \end{aligned} \quad (2.34)$$

This effect of precession have been widely used in the nuclear magnetic moments measuring of short-lived spin states. In the next chapter, we will present experimental techniques based on



Larmor precession, the relation with the angular distribution of gamma rays and their challenges.



## Chapter 3

# Experimental techniques to measure Nuclear Magnetic Moments of short-lived excited states: description and challenges

---

During the last 100 years  $\gamma$ -spectroscopy experiments have been carried out using elegant and innovative techniques. They have been used to collect measurements of electric moments, charge radii,  $g$ -factor measurements, among others. The result, in the most of the cases, were only obtained after overcoming challenging technology limitations. Techniques aimed to obtain magnetic and electric moments measurements have been performed for specific lifetimes ranges of nuclear states. Each method can be classified according to its time range effectiveness, as Figure 3.1 shows.

Techniques as Transient Field (TF), have allowed measuring the  $g$  factor in nuclear states with life-times of few picoseconds or less [36]. Less recent techniques as Recoil Into Vacuum (RIV) have been used to obtain  $g$ -factor measurements as well, although they show more limitations in comparison with TF. Such techniques exploit the principle of precession by submitting excited nucleus under the action of strong hyperfine fields.

This chapter is aimed to present the experimental techniques used to measure NMM in very short-lived states. We describe the transient field technique, showing the experimental performance

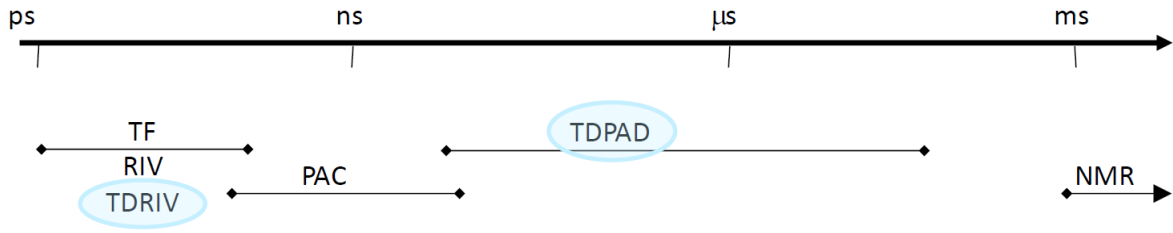


Figure 3.1: *Experimental techniques to measure Nuclear Magnetic Moment classified by their validity in different ranges of life times. The techniques mentioned in the figure includes: Transient Field (TF), Recoil Into Vacuum (RIV), Time Differential Recoil Into Vacuum (TDRIV), Perturbed Angular Correlation (PAC), Time Differential Perturbed Angular Distribution (TDPAD) and Nuclear Magnetic Resonance (NMR).*

targets, accelerators, ion sources, magnets, detector arrays and while giving a general description of data analysis to introduce the main challenge: the use of radioactive and no radioactive beams to populate nuclear states, which is the central point of this work. In addition, an explanation of how the Transient field technique can be used to obtain lifetime measurements will be made.

### 3.1 General description of precession experiments

Intensity and angular distribution of radiation emitted from nuclei are predicted by quantum radiation theory. Depending on the nuclear spin projections, the angular distribution of the gamma radiation of the decay will present the shapes shown in Figure 3.2

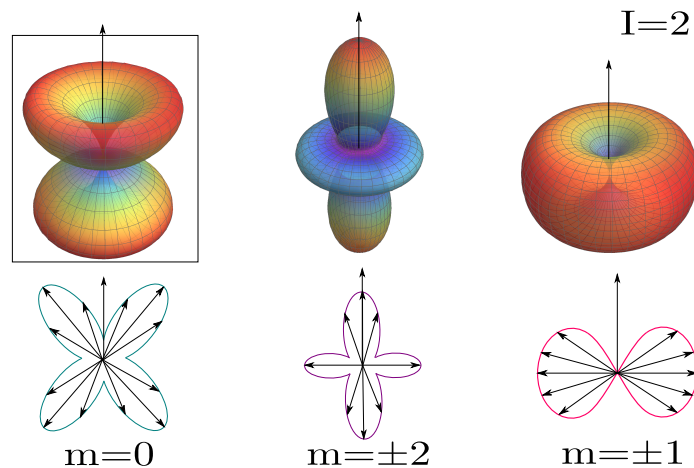


Figure 3.2: *Angular distributions shapes predicted by spherical harmonics for  $I = 2$  nuclear state.*

In  $\gamma$ -spectroscopy experiments the information of nucleus is obtained through the detection of gamma radiation. Precession effects in the angular distribution of the emitted radiation are used to estimate the value and sign of  $g$ -factor measurements. The Magnetic field intensity to produce this precession depends on the interaction time, which is limited by how long lived the nuclear state is. According to equation (2.34), the relationship between interaction time and magnetic field strength for different values of  $\Delta\theta$  and taking  $g = 1$  the Figure 3.3 is obtained.

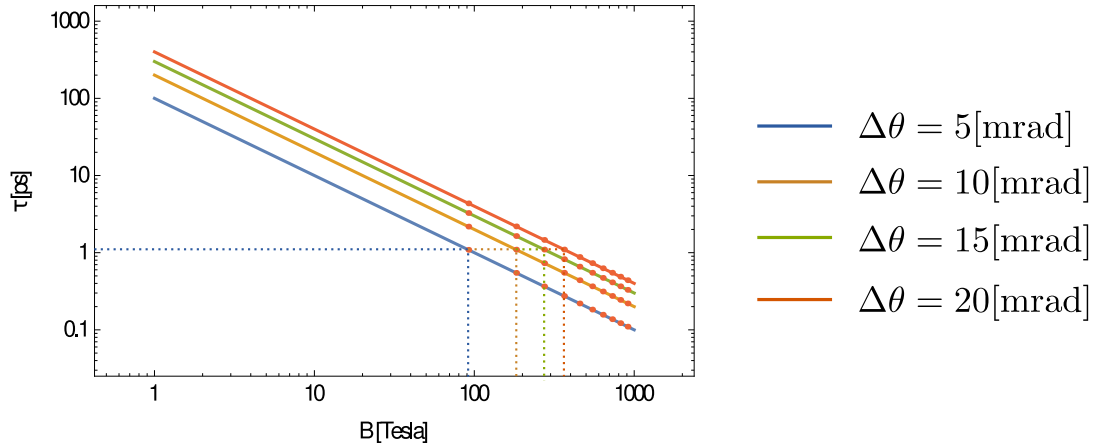


Figure 3.3: Graph of  $\tau$  against  $B$  for different values of precession angle. The interaction time between the magnetic field and the spin, represented by the factor  $\Delta t$  in (2.34) was replaced by the Greek letter  $\tau$ . This graph is built on a logarithmic scale.

From Figure 3.3 it can be conclude that huge magnetic fields are needed to produce a small precession of the magnetic moment for short lived nuclear states. Magnetic fields with these strengths can not be produced with current technology, only hyperfine fields reach such intensities therefore experimental techniques have to be aimed to produce them.

### 3.1.1 Hyperfine Fields

Magnetic hyperfine fields are generated by hyperfine interaction between the nucleus and a inner-shell electron. In experiments to measure nuclear magnetic moments of short-lived excited states, hyperfine fields in experimental setups attempting to measure  $g$  factor can be generated by recoiling in ferromagnetic solids or foil (TF) or recoiling into vacuum (RIV). In TF experiments, when ions recoil beyond the target and get through in the ferromagnetic foil they can lose some or even

all their electrons depending on the recoil velocity [37]. After implantation into the foil, unpaired electrons from foil can be trapped by the nucleus, when only one is trapped by nuclear field the hyperfine interaction occurs and transient magnetic field takes place. The situation is illustrated in Figure 3.4.

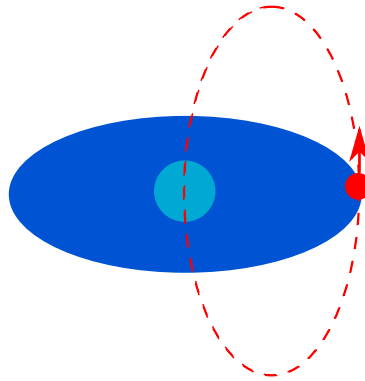


Figure 3.4: *Graphic representation of the spin-orbit interaction of a hydrogen atom. The light blue circle represents the nucleus ( $+Ze$ ), the red circle represents the electron ( $-e$ ) and the dotted red oval represents the hyperfine interaction.*

Something similar occurs with ions recoiling into vacuum, as they start to recoil beyond the target after the nuclear reaction, they lose all their electrons and becomes h-like ions (with just one electron) hyperfine interaction takes place generating a free-ion hyperfine field.

For TF and RIV techniques, measuring the hyperfine field is needed for the g-factor estimation. Calculations of transient fields could be made from first principles (Hartree-Fock) for the transient field case, but charge state distributions of ions moving in solid ferromagnetic hosts are required, and they are still unknown [38]. Parametrizations have been performed for the TF measurement. Although, we will not go deep into this subject, it is worth to recommend a good explanation available in [39]. For the RIV technique there have also been challenges for hyperfine field calculations because of the electron configuration.

In the next section, details of TF technique will be presented.

## 3.2 Transient Field Technique

Transient field (TF) experiments have consistently been used to measure  $g$ -factor of low-to-medium spin states of heavy and light nuclei with life time in the order of picoseconds (cite Rutgers articles). This section is aimed to present a basic notion of this method to obtain  $g$ -factor measurements.

TF technique is based on a three layer target (see Figure 3.5). In the first layer (called objective) the nuclear reaction takes place. Objectives are generally constructed from sputtering deposition of carbon on ferromagnetic layer. They have a typical thickness of  $0.5\text{mg}/\text{cm}^2$  (less than  $1\ \mu\text{m}$ ). In this layer nuclei are excited and ejected with a certain recoil velocity towards the ferromagnetic layer. Recoil velocities have a magnitude of around  $0.06\ c$ , which is not a considerable fraction of light speed. The second layer, is made by a ferromagnetic solid, generally iron or gadolinium, with a typical thickness of  $5\ \mu\text{m}$ . In ferromagnetic layer hyperfine interaction between nuclei and electrons from host takes place while producing the transient field. In this layer, ions start to slow down as well. Subsequently, the nuclei lead to the third layer (*stopper*) which is usually a copper material with thickness between  $6 - 10\ \mu\text{m}$  and in this layer the nuclei are completely stopped.

The target is exposed to an external magnetic field produced by a cooled magnet (with a liquid nitrogen cooled or He-cooled Closed-Cycle Cryocooler design), this magnet has two pole tips which enclose the target at the top and bottom sides so the pole axis lays perpendicular to the beam axis. The ferromagnetic layer becomes polarized when the the magnet provides a magnetic field of  $0.06\ \text{T}$ . The external magnetic field direction (purple arrow in Figure 3.5) is changed periodically in time intervals shorter than the beam pulse. This change induces he inversion of the ferromagnetic inner field direction (black arrow), which in turn induces the inversion of the hyperfine field direction (red arrow), finally producing an inversion in the precession movement of magnetic moment. Both the magnet and the target are located inside a vacuum chamber

Beam production and population of nuclear states in TF experiments have two ways to be performed; the first, coulomb excitation, involves radioactive beams to produce radioactive products and to populate low spin states via elastic scattering reactions, and the second, Alpha Transfer

Reaction, involves a non radioactive beam to produce radioactive products and to populate low-to-medium spin states. We will give more details about this two ways to options by the end of this chapter to introduce the central point of this work.

In TF experiments, inverse kinematic nuclear reactions are suitable given that heavy nuclei are involved. It results convenient to accelerate heavy particles because it is more feasible that light particles get enough kinetic energy from the reaction, to recoil through ferromagnetic host and stopper layers and finally reach the particle detector. In the recoiling process nuclei have certain probability to decay by gamma ray emission.

In transient field experiments usually low lying spin states are populated. Generally the  $I = 2$  spin state with  $M = 0$  projection is populated.

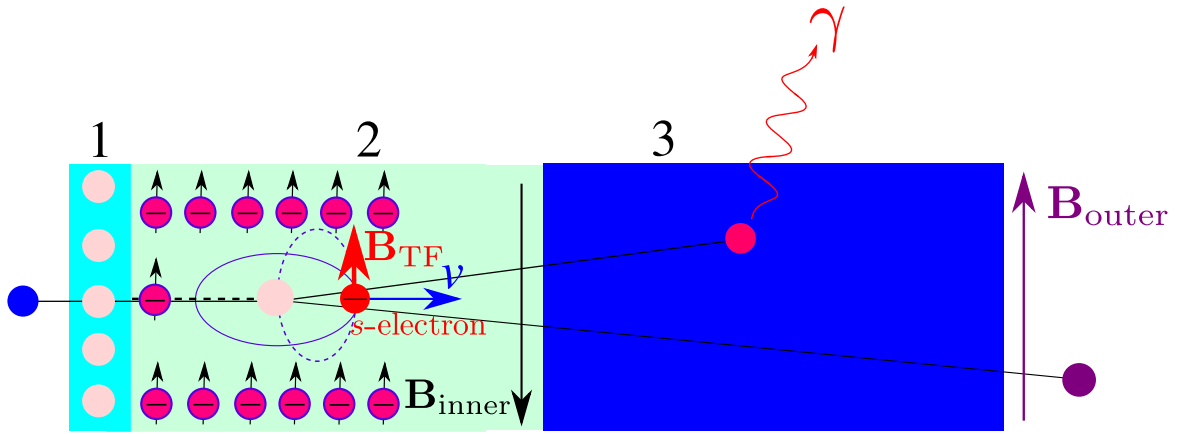


Figure 3.5: *Graphic representation of a three-layer target. The thinnest layer (cyan) represents the target, where the nuclear reaction takes place. The middle layer (green) represents the ferromagnetic material, where a fraction of the ions, are left with only one electron; in this layer the hyperfine interaction produced by the transient field takes place. Finally, the stopper layer (brilliant blue) stops the ions that made their way through the ferromagnet. The points attached to the lines represent the ion probe and the red curve its  $\gamma$ -emission radiation.*

TF experiments need a detection system which should be able to record both, recoil particles and gamma rays. Different  $\gamma$ -detection systems have been used, from clover to gammasphere arrays, with scintillator detectors (as NaI or BaF) or semiconductor detectors as High Purity Germanium (HP-Ge). For most experiments, clover detectors are preferable for their high efficiency result of the junction of 4 High Purity Germanium detectors [40]. Multi-detectors arrays, as gammasphere,



do not add considerable sensitivity. A large amount of detectors occupy insensitive angles and detectors out of plane see a diminished anisotropy of the angular correlation [36]. Clover detector is a junction of four HP-Ge detectors arranged in a clover leaves like shape. A typical clover detector layout (see Figure 3.6) involves 16 HP Ge-detectors. Detector arrangement is crucial for  $\gamma$  detection. Positions of the detectors are chosen so to record the small magnetic moment rotation, while defined angles at which the slope of the angular correlation is large and the intensity of  $\gamma$ -rays is not too low. When spin alignment is high in a quadrupolar decay, the highest probability of emission is at  $67^\circ$  degrees of the beam direction.

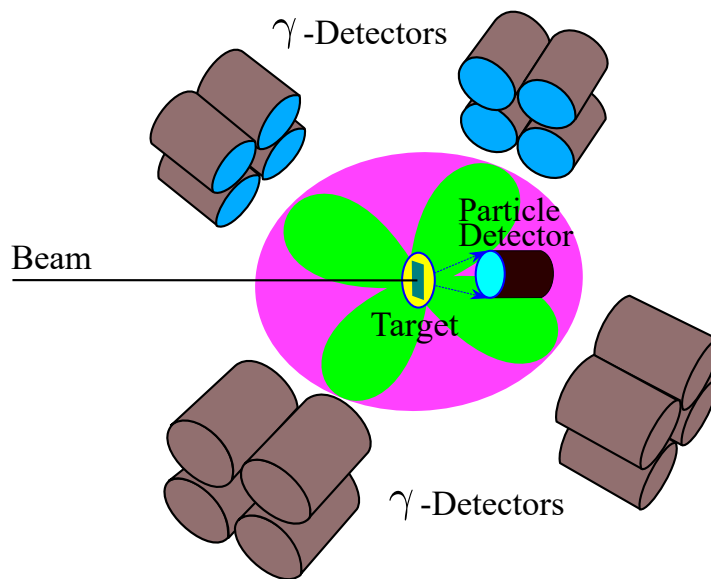


Figure 3.6: Typical  $\gamma$ -particle detection layout for TF experiments. This arrangement is the one used for a quadrupolar transition whose  $x$ - $z$  plane is represented by a green flower or clover leaves in the figure. Particle detector is positioned behind the target to implement inverse kinematics nuclear reactions. The clover detector is defined by the group of four Ge-detectors.

Particle detection is important for reaction products selection. For example, scattered particles at  $180^\circ$  degrees have a special interest since they are related with the interaction type, that is, they give information about excitation functions making possible to know if there was a superficial or inner interaction. Particle detector position depends on the kinematics, of the reaction. For inverse kinematic an annular Si-surface-barrier particle detector located behind the target facing the beam, is typically used to detect the recoiled particles. For direct kinematics nuclear reactions, the detector is placed facing of the target. A thin beam stopper is placed on the particle detector

behind or forward (depending on kinematics) the target to avoid any particle from the beam reach to the detector. Furthermore, particle detection cone is placed out of the scattered particles range. Only  $\gamma$ -rays in coincidence with backscattered particles are considered in the data analysis.

In the next section, the mechanism to measure the slight precession by means of the angular correlation of gamma radiation will be explained.

### 3.2.1 Angular correlation function and g-factor measurement

The theory of the angular distribution of  $\gamma$ -rays has been systematically developed from nuclear spectroscopy theory, both the formulas of angular distribution, and the transition probability corresponding to gamma emission with wave vector  $\mathbf{k}$  and a polarization  $\epsilon$  between to states, they are deduced using the time-dependent perturbation theory [41].

When the reaction takes place and nuclei reach excited states, the orientation of spins follows a definite distribution. The **spin alignment** is a term that refers to the largest probability of population for a specific quantum magnetic number (just one of all possible projections), which means that after the reaction most of nuclei will show an anisotropic angular distribution of gamma radiation with a well defined shape (Figure 3.2).

The spins of the excited nuclei can be aligned by the reaction, as is the case of Coulomb excitation reactions, with the first layer of the target. This alignment is perpendicular to the direction of the beam.

The angular correlation function of gamma radiation is described by

$$W(\theta) = 1 + \sum_{k \text{ par}} A_k \cdot P_k(\cos \theta), \quad (3.1)$$

where  $P_k$  are the Legendre polynomials and  $A_k$  are coefficients that depend on the geometry of the experimental array and the detection efficiency [42].

The direction of the transient field follows the direction of the polarization field of the alternating

polarization ferromagnetic layer (*up-down*). This situation is illustrated in Figure 3.7. The measurement of the precession is directly proportional to the rate of the change of the  $\gamma$  ray decays; and these, in turn, have a different value according to the polarity of the field. The decay change ratios for opposite polarities are calculated by the pairs of detectors arranged at opposite angles. For the detector **i** and the detector **j**, the decay rate is [42]:

$$\rho_{i,j} = \sqrt{\frac{\epsilon_i \uparrow \epsilon_j \downarrow}{\epsilon_i \downarrow \epsilon_j \uparrow}} \quad (3.2)$$

Where  $\epsilon_i \uparrow$  and  $\epsilon_j \downarrow$  are the change ratios measured by each detector with different polarities (*up-down*).

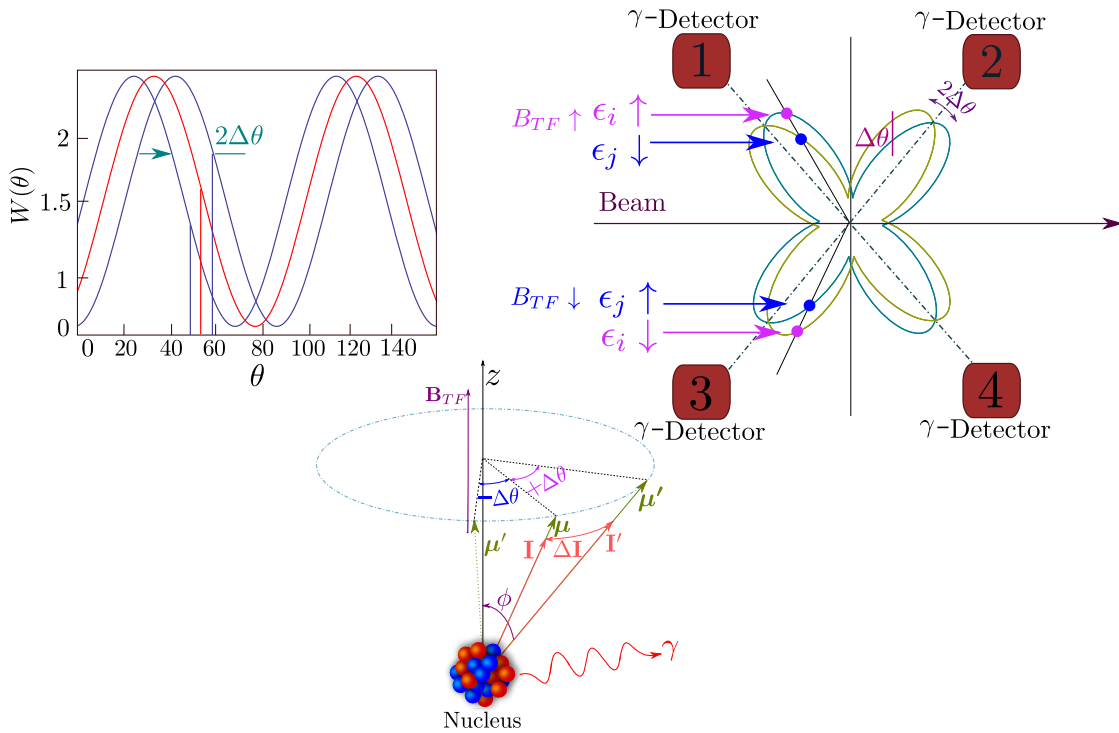


Figure 3.7: Graphical representation of the detection and the shift of the angular distribution of the  $\gamma$ -radiation. The angular correlation function is calculated for the two different directions of transient field (see  $W(\theta)$  plot). The angular shift is produced by the nuclear magnetic moment precession (represented in the bottom) which produce a rotation in the gamma-distribution.

In this way, the change rate of change of all the detectors is equal to the rate of change between the detectors **i**, **j** arranged at opposite angles and can be defined as:

$$f = \frac{\rho - 1}{\rho + 1}. \quad (3.3)$$

And the logarithmic slope parameter is given by:

$$S(\theta) = \frac{1}{W(\theta)} \frac{dW(\theta)}{d\theta}. \quad (3.4)$$

Finally,  $\Delta\theta$  will be the ratio between (3.3) and (3.4),

$$\Delta\theta = \frac{f}{S(\theta)}. \quad (3.5)$$

Following the formalism presented in section 2.4.1 and taking into account the action of transient magnetic field, (2.34) becomes an integral equation

$$\Delta\theta = \frac{g\mu_N}{\hbar} \int_{t_{in}}^{t_{out}} B[v(t)] e^{-\frac{t}{\tau}} dt, \quad (3.6)$$

where  $t_{in}$  and  $t_{out}$  corresponds to the times when the ion enters and leaves, respectively the ferromagnetic layer<sup>1</sup>,  $B[v(t)]$  is the transient magnetic field which depends on the recoiling velocity of the ion and  $\tau$  is the life-time of the excited state that appears in the exponential attenuation factor of the transient field. This equation is called integral of the precession, its sign can vary depending on the orientation of the precession, that is, if the precession has an clockwise orientation, precession integral will have a negative value, otherwise it will have a positive value.

#### *Recoil Into Vacuum (RIV)*

RIV is another experimental technique to obtain  $g$ -factor measurements of low spin nuclear states with lifetimes in the order of picoseconds. This technique works with hyperfine fields as well, but in contrast to TF the ions produced in the reaction are recoiled into vacuum instead on the ferromagnetic solid. Hyperfine field is produced by hyperfine interaction between the inner shell

---

<sup>1</sup>remember transient field appears for the interaction with ion and ferromagnetic electrons

electron spin and the nuclear magnetic moment. In a typical RIV experiment, the target layout consists of a thin first layer where reaction takes place, free space instead of the ferromagnet and a stopper. This stopper can be movable. As the ion is flying across the vacuum, detected gamma radiation is being attenuated,  $g$ -factor measurement is obtained from attenuation functions as well as lifetime measurements. One of the limitations of RIV technique is that the direction of the precession can not be determined, therefore the  $g$  factor sign can not be known and a TF experiment is required to obtain it.

In the next section, methods to obtain lifetime measurements in TF and RIV experiments, will be presented.

### 3.2.2 Life-time measurements

Experimental setup for  $g$ -factor measurements that include hyperfine fields are commonly performed in combination with Doppler Shift measurements to obtain life-time measurements. In this section we will explain the general aspects of this technique.

#### Doppler Shift Measurements (DSM) of Nuclear lifetimes

Doppler shift principle has been used as a tool to measure lifetimes of nuclear states in the order of few picoseconds or less. This method is based on the detection of emitted  $\gamma$ -rays by nuclei in a de-excitation process, while they move. The detection of  $\gamma$ -rays will be affected by Doppler effect and a energy shifted will observed. The Doppler Shift effect is utilized in different methods to obtain lifetime measurements. In Transient Field experiments, Doppler Shift Attenuation Method (DSAM) is widely used. In this section we are going to present DSAM. In addition, we briefly mention the plunger method which is used in combination with the RIV technique to measure the  $g$ -factor and lifetimes of short-lived nuclear states.

The working principle of DSAM is illustrated in Figure 3.8. When projectiles are shot against the target with a certain energy, part of this energy will be transferred as kinetic energy to the excited ions produced during the collision. In case the excited ions have sufficient kinetic energy ,it will

be able to recoil beyond the first layer and travel into the stopper. The ions have the possibility to decay while they are moving and the gamma radiation from the de-excitation is affected by Doppler effect, and the energy observed  $E_\gamma^{\text{obs}}$  by detector at laboratory frame is given by:

$$E_\gamma^{\text{obs}} = E_\gamma^0 \frac{\sqrt{1 - (\beta(t))^2}}{1 - \beta(t) \cos \theta} \stackrel{v \ll c}{\approx} E_\gamma^0 (1 + \beta(t) \cos \theta) \quad (3.7)$$

$$\therefore \Delta E = E_\gamma^0 \beta(t) \cos \theta,$$

where  $E_\gamma^0$  is the energy of  $\gamma$ -ray emitted by the ion at rest,  $\beta(t) = |\mathbf{v}(t)|/c$  with  $\mathbf{v}(t)$  the velocity distribution of ions,  $c$  the the speed of light and  $\theta$  the angle defined by the beam axis and the direction of emitted  $\gamma$ -ray. Right side of (3.7) results after first order Taylor approximation for velocities considerable smaller than  $c$ . Last line of (3.7) results of grouping term  $E_\gamma^{\text{obs}} - E_\gamma^0 = \Delta E$  which represent the energy shift.

A typical spectrum of a DSAM experiment is shown on the right side of Figure 3.8, as ion travels across the stopper its velocity decreases and the shifted energy of  $\gamma$ -rays is attenuated. This process will produce a spectrum with two different energies of  $\gamma$ -rays, both associated to the same transition and has a shape similar to a elephant silhouette. The energy spectrum in Figure 3.8 of detected  $\gamma$ -ray is composed by ions in three different stages. When ion is just entering into the stopper (fully shifted) the most energetic (purple peak) is created. The less energetic peak (cyan) corresponds to  $\gamma$ -emission by ions at the rest (fully stopped) and the contribution of ions which are traveling across the stopper (partially shifted) are plotted on the peach colored part of the spectrum. Lifetime measurement is extracted from the attenuation factor which is proportional to the energy shift.

To explain the obtaining of the life time, consider an ensemble of  $N_0$  nuclei prepared at  $t = 0$  in an excited state with mean lifetime  $\tau$ . Assume these nuclei have an initial velocity  $\vec{v}_0$  with a well defined magnitude and direction, and that they decay by  $\gamma$  ray emission with unshifted energy  $E_0$ . If nuclei are recoiling into a solid, it will take at most a few picoseconds to stop them. As nuclei are slowed down, their rate of decay is given by

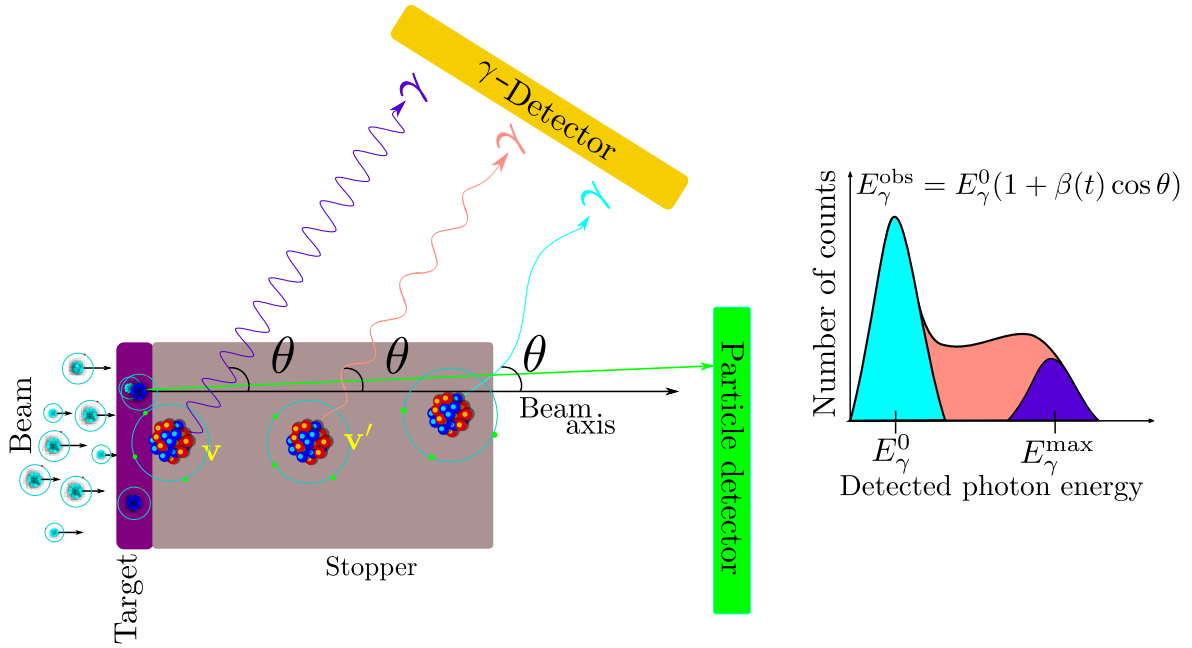


Figure 3.8: Schematic representation of DSAM experiment. In the left part of the figure a typical setup is shown. The incoming beam is shot against the target with a energy such that the desired excited states are populated via nuclear reaction with target ions (full stop). After the reaction, resulting ions recoil into the stopper (gray layer). A detector, positioned at an angle  $\theta$  with respect to the beam axis, registers the  $\gamma$ -rays produced from nuclear de-excitation with a shifted energy. A particle detector is positioned behind target to register recoil nuclei. In the right side of figure, spectrum corresponding to detection of  $\gamma$ -rays in every moment of the ion motion, peaks corresponding to fully shifted (purple peak), partially shifted (peach color region) and fully stopped (cyan peak) ions while they are emitting  $\gamma$ -rays are shown.

$$\frac{dN(t)}{dt} = -\frac{N_0}{\tau} e^{-\frac{t}{\tau}}, \quad (3.8)$$

where  $N(t)$  is the number of nuclei that have not decayed at time  $t$ . If nuclei preserve the same direction after crossing the whole stopper, the Doppler shift can be obtained as follows: the fraction of nuclei decaying between  $t$  and  $(t + dt)$  is given by (3.8), the Doppler shift associated with decay is given by (3.7). Finally, the average Doppler shift is obtained by multiplying (3.8) times the energy shift (3.7) and integrating over time until the last decay (infinity)

$$\Delta E = \frac{E_0 \cos \theta}{c\tau} \int_0^\infty v(t) e^{-\frac{t}{\tau}} dt. \quad (3.9)$$

The maximum energy shift reached when  $|\mathbf{v}(t)| = v_0$ , since  $v_0$  is the maximum ion speed, so

$$\Delta E_{\max} = \frac{v_0}{c} E_0 \cos \theta. \quad (3.10)$$

The ratio  $\Delta E/\Delta E_{\max}$  is called *attenuation factor* and is given by

$$F(\tau) = \frac{1}{v_0 \tau} \int_0^{\infty} v(t) e^{-\frac{t}{\tau}} dt. \quad (3.11)$$

The attenuation factor  $F(\tau)$  relates lifetime  $\tau$  with attenuated Doppler shift through nuclei velocities. Slowing down time is the standard time to which lifetime is compared. Equation (3.11) has a limited usage due to restrictions on the initial velocity distribution and subsequent slowing-down characteristics. In practice, nuclear reactions might not produce monoenergetic and unidirectional recoiling nuclei and modifications of  $F(\tau)$  are necessary, normally by averaging over the initial velocity distribution. In addition, the assumption that nuclei travel in straight lines while they are recoiling is valid only in special cases. When the nuclei does not travel in straight line it is necessary to include a detailed description of energy loss for ions moving in a stopping medium [43].

There are different manner in which nuclei loses energy when they are crossing solid materials. Electronic stopping for example, is a energy loss mechanism in which energy is transferred to the atomic electrons of the stopping material via ionization and excitation. If ions travel with velocities shorted than a small fruition of the velocity of light, electronic stopping power or energy loss per unit path length is directly proportional to ion velocity;

$$\begin{aligned} \frac{dE}{dx} &= -kv \\ \frac{d(1/2mv^2)}{dx} &= -kv \\ \frac{1}{2}m \frac{2vd(v)}{dx} &= -kv \\ \therefore \frac{dv}{dx} &= -\frac{k}{m} \end{aligned} \quad (3.12)$$



Where  $dE$  is the kinetic energy lost per unit path length  $dx$  by an ion of mass  $m$  moving at velocity  $v$ , and  $k$  is a constant of proportionality. Hence

$$\frac{dv}{dt} \frac{dt}{dx} = -\frac{k}{m},$$

taking into account that,

$$\frac{dt}{dx} = \frac{1}{v}.$$

Then

$$\frac{dv}{dt} = -\frac{k}{m}v. \quad (3.13)$$

Last differential equation has the solution,

$$v(t) = v_0 e^{-\frac{t}{\alpha}}. \quad (3.14)$$

where  $\alpha$  is the characteristic slowing-down time equivalent to  $m/k$  and  $v_0 = v(t = 0)$ . If (3.14) is inserted to (3.11), the attenuation factor becomes,

$$F(\tau) = \frac{\alpha}{\alpha + \tau}. \quad (3.15)$$

Nevertheless, (3.15) is valid only when ions lose energy due to electronic stopping, if any other kind of ion-solid interaction is present then, significant modifications in the velocity distribution expression and the attenuation factor function are needed [43]. In general, an ion losses energy by both electronic stopping and nuclear scattering processes. Depending on the magnitude of its initial velocity, different models of stopping power can be used. In TF-experiments, recoil velocities do not reach a considerable fraction of the velocity of the light (from 6% of  $c$  onwards).

Bethe formula with charge distribution corrections for  $Z > 26$  nuclei is used. There are different methods to obtain  $\tau$  measurements. Desired state of the method depends on the experimental conditions (methods to excite the given state, stopping material or detector geometry). If the stopping power is known, the lifetime of the observed state can be extracted [43]. In general, Doppler shift methods use the fact that the decay law is given by  $e^{-t/\tau}$  and (3.15) is a good starting point. There are two main variants of Doppler shift measurements: the first evaluates the shift in the centroid of  $\gamma$ -ray energy distribution observed at two angles and compares it with the maximum shift energy obtaining the measure of attenuation, and the second makes a comparison of the  $\gamma$ -rays observed at a single angle, when they recoil into two different stopping materials (or vacuum). In the case of vacuum, a plunger can be used, this method is briefly described below.

#### *Plunger Method*

The plunger method is used to measure lifetimes shorter than tens of picoseconds or even in the order of femtoseconds. From the mechanical point of view, the design looks like a syringe: a movable tube inside a tube. The setup consists of the target and stopper previously explained although now they are separate. The target is placed on the fixed face of the syringe (where the needle would be) and the stopper is placed on the plunger behind the target. The projectiles are shot and the excited ions recoil in the space between target and stopper. The whole assembly is within a vacuum chamber. During this process, ions can decay while they are traveling at a given velocity with respect to the surface of the plunger. When they reach the plunger, they brake abruptly until stopping. In that case, the decay occurs at rest. Comparison of the intensities of the "in flight" and "at rest" peak intensities is made as a function of the distance between the target and the plunger inner surface. This intensity-to-distance analysis differs from the intensity-to-time by the velocity factor, whose measurement is necessary to determine the lifetime of any state. The methodology of this experiment is summarized as: measure the "in flight" and "at rest" intensities for a certain distance, that is, take data during, for example, one hour (the mean lifetime of the state and the intensity of the accelerator beam determine that time). Save the data, change target-plunger distance. Regain intensities for an hour and so on. The comparison of the intensities emitted in flight and emitted at rest allows to calculate the life time of the nuclei.

### 3.3 Population of nuclear states

Population of nuclear states is completed by the nuclear reaction. In TF-experiments two types of nuclear reactions are used to populate spin states, in the first, a radioactive beam is needed, which allows a very good spin alignment. In the second, there is no radioactive beam, what represents an experimental advantage due to the difficulty of a radioactive beam production, however spin alignment is poor.

#### *Coulomb excitation*

In Coulomb excitation (Coulex) the spin alignment is very high, for example, the  $m = 0$  projection is strongly observed for a quadrupolar transition induced with this mechanism. With this method, the mass of the involved nuclei remains equal after and before the reaction. In  $\alpha$ -transfer reactions, a new nucleus is created and populated after the reaction. Then, the spin projections are not equally probable.

#### *Alpha Transfer reactions*

Alpha-transfer reactions can populate low-to-medium spin states without radioactive beams. Nevertheless, this mechanism has limitations, whereas Coulomb excitation (Coulex) uses only electrostatic repulsion to populate spin states; in alpha-transfer process more than only electrostatic forces are involved. The spin alignment term refers to a preferential total angular momentum projection of the populated excited state; for example, in an Coulex populated excited state, there is one preferable projection  $m$  of the nuclear spin, whereas for the alpha-transfer case, there is no preferential  $m$  projection.

Another problem in the alpha transfer population mechanism is related to the level of the excited states and feeding corrections [36]. While in Coulex the populated energy levels can be predicted, in alpha-transfer there is uncertainty in which of the possible levels will be populated and a higher spin states of the expected are achieved. The theoretical understanding of the population mechanism could explain why this happen.

Despite the problems, alpha-transfer reactions have been utilized in the measurement of nuclear magnetic moments. In the next section the use of alpha-transfer population mechanism in combination with another experimental techniques for the obtaining of this measurement will be explained.

## Chapter 4

### State of the art

---

Alpha particles are made of two protons and two neutrons in a highly symmetrical nuclear arrangement with a total angular momentum of  $J = 0$  (they are bosons), parity  $\pi = +$ , and isospin  $T = 0$ . The alpha particle does not have excited states below 20 MeV, its binding energy has a value of 28.3 MeV [44] and it has a positive charge of value  $2e$ . Alpha decay processes occur in heavy nuclei such as  $^{238}\text{U}$  which decays through the reaction  $^{238}\text{U} \rightarrow ^{234}\text{Th} + \alpha$ , the theoretical description of this decay was formulated by Gamow in 1928 [45]. The high stability of alpha particles makes them suitable for the description of some nuclei  $\alpha$ -clusters [46].

The  $^{12}\text{C}$  isotope is a good example of an  $\alpha$ -clusterized nucleus. Its description as a junction of three alpha particles (see Figure 4.1) is the most successful model to explain its nuclear structure [47].

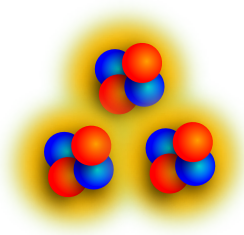


Figure 4.1: *Graphical representation of  $^{12}\text{C}$  nucleus made of three alpha clusters.*

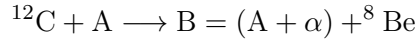
The transient field experiments have been used  $^{12}\text{C}$  as a target or projectile. The pick up of the  $\alpha$ -particle is strongly observed in a range of energies near to the Coulomb barrier. This allows the

possibility to produce new nuclei in excited states, and to study radioactive species.

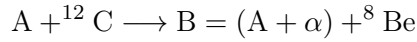
The population of excited states in radioactive nuclei is another interesting point to consider when studying the alpha transfer process. In this chapter, a review of the state of the art theory and recent experimental results of alpha-transfer process are presented.

## 4.1 Basics of Alpha-transfer reactions

Alpha-transfer reactions (ATR) are a kind of heavy ion reactions in which the projectile or target capture an alpha particle from the other nucleus involved in the reaction, and creates a new isotope. The reaction can populate medium-to-low spin states of the new isotope. Generally alpha transfer reactions involve  $^{12}\text{C}$  nuclei because of their alpha-cluster inner structure. They can be used either as a target or projectile as it follows:



In direct kinematics, or



In inverse Kinematics.

A specific example of an  $\alpha$ -transfer process is the nuclear reaction  ${}^{96}\text{Re} + {}^{12}\text{C} \rightarrow {}^{100}\text{Pd} + 2\alpha$ , illustrated in the Figure 4.2

After the collision, the radioactive states in the formed nucleus are populated and a  ${}^8\text{Be}$  nucleus or two alpha particles can be produced as residual products.

The Coulomb barrier in alpha transfer reactions is calculated with the formula:

$$V_c = 1.109(A_1 + A_2)[Z_1 Z_2 / A_2(A_1^{1/3} + A_2^{1/3})] \text{ [MeV]}. \quad (4.1)$$

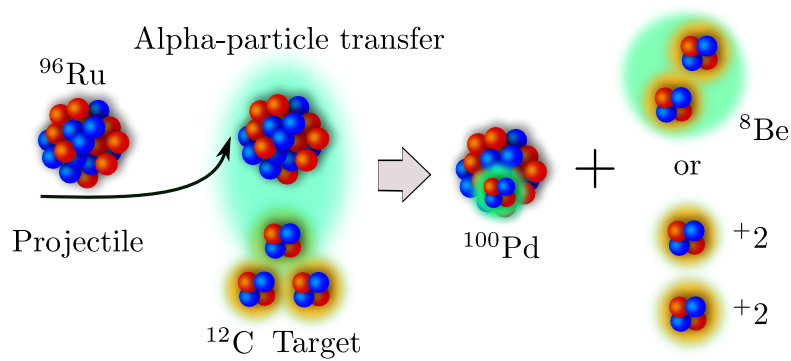


Figure 4.2: The Alpha transfer process in the reaction  $^{96}\text{Ru} + ^{12}\text{C} \rightarrow ^{100}\text{Pd}$ , where the residual products can be two  $\alpha$ -particles or a  $^8\text{Be}$  nucleus.

Where  $A_1$  and  $Z_1$  are the number of nucleons and protons of the projectile respectively and  $A_2$  and  $Z_2$  are the number of nucleons and protons of the target respectively.

In ATR the final product is formed during the reaction. As the radioactive nuclei is formed in the process, the spin alignment is low. In the next subsection the experimental problems associated with the spin alignment will be explained.

## 4.2 The spin alignment and the angular distribution

The major problem with the low spin alignment in  $\alpha$ -transfer reactions is that there is not a well defined angular distribution (anisotropic) for random nuclear spin projections. Instead a *mix* of possible  $\gamma$ -radiation (isotropic) is observed instead.

Alpha-transfer commonly populates the  $2^+$  states (quadrupolar transitions) of the produced nucleus. Three possible configurations of spin projections for a quadrupolar transition are shown in the top of Figure 4.3. In Coulex experiments, the beam is prepared to populate  $2^+$  levels with a defined  $m = 0$  projection and as a result, a high spin alignment is obtained with a well defined anisotropic distribution of the gamma rays. Contrary, with ATR, the beam is prepared only for obtaining the radioactive nucleus and the subsequent spin state population is poorly aligned. It implicates that their  $m$  projections are something specific of the nature of the population mechanism of the reaction and it does not depend on the experimental setup. Then, the three possible

$m$  projections are contributing on the angular distribution of the gamma radiation, and the sum of the spherical harmonics that describe their shape is approximately a sphere or a circle in a 2-dim plane.

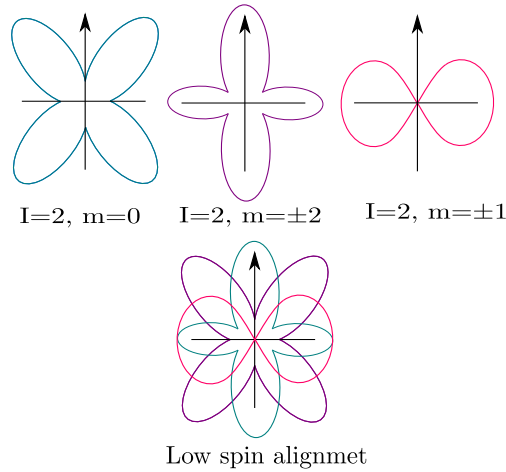


Figure 4.3: Possible  $\gamma$ -ray intensities distributions for a quadrupolar transition for different spin projections (top) and mix of all of the distributions for a random spin alignment in the quadrupolar transition (bottom).

When the photon associated with the gamma distribution reach the detector it has an energy that gives information about the nuclear transition. By interacting with the atoms of the detector (through Compton or photoelectric effects or forming a pair production) the energy of this photon is transferred, amplified and registered as a count. Many photons produced in the reaction reach the detector and an energy peak is formed by the counts. This peak is positioned in a channel which corresponds to a determined energy. The ratio between the number of counts in a full-energy peak by the number of photons that are actually emitted by the decay is called the efficiency of the detector.

In the TF experiments which uses the ATR technique to populate spin states, the efficiency changes when magnetic field change its orientation. The angular correlation functions ( $W(\theta)$ ), which are obtained from the efficiency in a specific direction of the magnetic field, present an angular shift ( $\Delta\theta$ ) between them. The origin of this shift is the precession of the magnetic moment.

The angular correlation function for a well shaped anisotropic gamma distribution is a well defined



curve. When there is a mix between different gamma radiation distributions, the photons associated to all gamma distributions reach the detector and the angular correlation function becomes flat. Therefore, the uncertainty of  $\Delta\theta$  measurement and the subsequent  $g$  factor measurement increases.

Let us see Figure 4.4, where the angular correlation function for the quadrupolar radiation of  $^{100}\text{Pd}$  is shown. This angular correlation function corresponds to the quadrupolar radiation of  $^{100}\text{Pd}$ . The ion was obtained and excited by an  $\alpha$ -transfer reaction.

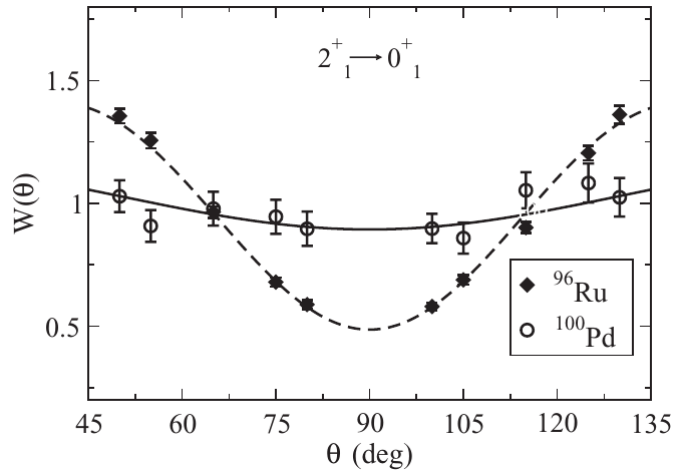


Figure 4.4: The experimental  $\gamma$ -ray angular correlations,  $W(\theta)$ , for the  $2_1^+ \rightarrow 0_1^+$  transitions; open circles correspond to  $^{100}\text{Pd}$  and diamonds to  $^{96}\text{Ru}$ . The solid and dashed lines correspond to fits to the angular correlation function for  $^{100}\text{Pd}$  and  $^{96}\text{Ru}$ , respectively. Figure taken from [1].

It is easy to notice the difference between the angular correlation for the  $^{96}\text{Ru}$  which was excited with Coulex and the one obtained for the  $^{100}\text{Pd}$ , produced and excited by an ATR.

Experimental investigation with the aim to obtain angular correlation functions of ATR is required to solve this problem. Theoretical understanding of the population mechanism is also needed to improve the correlation function.

In the next section the state of the art of the role of the ATR in the nuclear structure characterization of medium-to-low spin states via magnetic and electric moments measurements will be presented. As an added value a short review of the theoretical and experimental attempts to understand the reaction mechanism was made.

### 4.3 Understanding nuclear structure and reaction mechanism

From early times of nuclear physics research,  $\alpha$ -particles have been of particular interest because of their relation with nuclear structure. In 1929 a simple model of the nuclei was proposed by G. Gamow. This model consist in a nucleus formed by alpha particles, very similar to a water-drop held together by surface tension [48]. This was the first proposal where the nucleus structure was described in terms of  $\alpha$ -particles. Afterwards, in 1938, Hafstad and Teller extended the theory of the nuclei composed only by alpha particles to cases where in addition a single neutron or proton is present in the nucleus. They also proposed a model in which light nuclei is based on  $\alpha$ -particle structure [49] and in 1955, Morinaga made a description of the  $4n$ -type light nuclei energy levels structure based on experimental and theoretical results.

Alpha-transfer reactions have been used as a tool to understand different aspects of the nuclear structure. Michigan group -with a very notable production- carried out the first big alpha-transfer experiment ever performed. They worked with the  $(d, {}^6\text{Li})$  reaction using even-even nuclei in a range of masses between  ${}^{12}\text{C}$  to  ${}^{238}\text{U}$  as targets. By shooting deuteron beams with a strong intensity in energies around 35 MeV and detecting the resulting 6-Lithium nuclei at the angle corresponding to the maximum cross section of the reaction, they obtained data of the  $\alpha$ -particle picked-up from the targets.

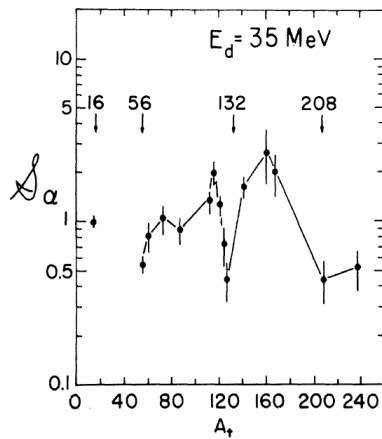


Figure 4.5:  $S_\alpha$  spectroscopic parameter obtained from  $(d, {}^6\text{Li})$  reactions, normalized to unity at  ${}^{16}\text{O}$  plotted as a function of target mass  $A_T$ . Figure taken from [2].

Using distorted wave theory, they made calculations for alpha pick up in the reaction and found a factor  $S_\alpha$  that represents the probability of finding an  $\alpha$ -particle in the target nucleus for each reaction and plotted it as a function of mass Figure 4.5. Fluctuations can be observed in Figure 4.5. In 1975, Hodgson made an interpretation of these fluctuations, performed using shell model. Targets in a closed shell have less probability to "donate" an alpha particle to the deuteron, whereas open shells present a maximum in the probably to donate an alpha particle instead.

Alpha transfer reaction mechanism is closely related with nuclear structure, thus, a more advanced knowledge about clustered  $^{12}\text{C}$  nucleus is needed to close up to the reaction mechanism knowledge and viceversa. A lot of theories have been created to understand the reaction mechanism. There are two kind of results that are possible to obtain: a weakly bound  $\alpha$ -particle tie to radioactive isotope core, or find compound effects on the radioactive isotope after the particle transfer. Therefore, theoretical descriptions of reaction mechanism can be classified in two big groups; the ones that attempt to describe the transference mechanism whose result is a weakly bound  $\alpha$ -particle orbiting around a core in the produced nucleus and the ones that try describing the mechanism that produces compound effects. DWBA (Distorted Wave Born Approximation) theory has been thoroughly used to describe reaction mechanism that produces weakly bound effects. Many theories have been used to describe reaction driving to compound effects, however we will allow us to highlight DWBA theory because of the good accuracy results it has been able to obtain in the description of differential cross section of alpha transfer reactions [22, 50].

Theories as DWBA, work in conjunction with: a model of nuclear potential and an interaction model. In general, theoretical physicists have predicted on the reaction mechanism using DWBA in combination with the optical potential.

The interaction models are the ones which define the manner in which nucleons of the target and projectile interact. Four main interaction models are worth to be mentioned:

- $JJ$  shell model.
- $SU(3)$  model.
- The pairing vibrational model.

- The linear combination of nuclear orbitals model.

The last model has been obtained interesting results for the  $^{32}\text{S}$  nucleus [51]. This subject is crucial for the study of the results of the experiment that we proposed, but is not the focus of this work.

In this subsection we have reviewed what are the principal models for the theoretical descriptions of ATR. In the next section the state of the art of the experiments which have used ATR technique to measure nuclear magnetic moments will be presented.

### 4.3.1 Uses in the nuclear structure characterization

The simultaneous measurement of  $g$ -factors and mean life times have enabled the possibility to study the nuclear structure characterization of low lying nuclear spin states of radioactive nuclei ( $I = 2_1^+, I = 4_1^+$  and  $I = 6_1^+$ ). Alpha transfer reactions have been used as a tool in front of the difficulty to obtain radioactive nuclei from radioactive beams. The earliest experiment to use  $\alpha$ -transfer reactions in order to measure  $g$ -factors was the one performed by Horstman et. al in 1975 [3]. They worked with the reactions  $^{12}\text{C}(^{16}\text{O},\alpha)^{24}\text{Mg}$  and  $^{12}\text{C}(^{12}\text{C},\alpha)^{20}\text{Ne}$  obtaining  $g$ -factors and mean lives values for  $I^\pi = 2_1^+$  states (see table 4.1). These values were obtaining from recoil-distance measurements using the time differential recoil into vacuum technique. In 2003, 28 years later, the next experiment using alpha transfer reactions to produce radioactive isotopes, by Sheickle et. al. They measured  $g$ -factors and lifetimes of the  $2_1^+$  and  $4_1^+$  states in  $^{44}\text{Ti}$  for the first time, in that way contributing to the  $N = Z$  nuclei studies. Improving the prediction of the simple rotational model ( $g = Z/A$ ), they could explain very well the  $g$ -factor, by a full  $fp$  shell model calculation using the FPD6 effective  $NN$  interaction, as well as the deduced  $B(E2)$  value [15]. Two years later, Leske et. al. made the first  $g$ -factor measurement of radioactive  $^{68}\text{Ge}$  in  $2_1^+$  state and the first lifetime measurement of the  $2_3^+$  state. Lifetimes of  $2_1^+$ ,  $2_2^+$  and  $4_1^+$  were remeasured resulting a disagreement value for the  $2_2^+$  state in comparison with the previous measurements. According with Leske, alpha transfer method is a suitable candidate to replace Coulomb excitation to populate low lying spin levels of radioactive species. Discussion presented

by Leske mentions that feeding corrections are despicable for the low contamination on  $2_1^+ \rightarrow 0_1^+$  decay [17], any discussion about spin alignment was presented. Thus, more experiments of alpha transfer reactions have been developed until 2016. All of given results from all experiments are presented in Table 4.1.

Beam	Nucleus	$I_i^\pi$	$g$ factor	$\tau$ [ps]	Ref
$^{12}\text{C}$	$^{20}\text{Ne}^{(*)}$	$2_1^+$	0.54(4)	0.8(2)	[3]
$^{16}\text{O}$	$^{24}\text{Mg}^{(*)}$	$2_1^+$	0.51(2)	2.09(13)	[3]
$^{32}\text{S}$	$^{36}\text{Ar}$	$2_1^+$	+ 0.24(12)	0.65(2)	[14]
$^{34}\text{S}$	$^{38}\text{Ar}$	$2_1^+$ and $2_2^+$	+ 0.52(18) and +1.1(11)	0.71(3) and 0.068(8)	[14]
$^{40}\text{Ca}$	$^{44}\text{Ti}$	$2_1^+$	+ 0.52(15)	3.97(28)	[15]
$^{48}\text{Ca}$	$^{52}\text{Ti}$	$2_1^+$ and $4_1^+$	+0.83(19) and +0.46(15)	5.2(2) and 4.8(6)	[16]
$^{64}\text{Zr}$	$^{68}\text{Ge}$	$2_1^+$	+ 0.55(14)	2.9(2)	[17]
$^{78}\text{Kr}$	$^{82}\text{Sr}$	$2_1^+$ and $4_1^+$	+0.44(19) and +0.53(39)	-	[18]
$^{86}\text{Kr}$	$^{90}\text{Sr}$	$2_1^+$ and $4_1^+$	+0.12(11) and +0.02(17)	-	[18]
$^{84}\text{Sr}$	$^{88}\text{Zr}$	$2_1^+$ and $4_1^+$	+0.30(11) and +0.65(18)	3.6(4) and 2.2(2)	[19]
$^{96}\text{Ru}$	$^{100}\text{Pd}$	$2_1^+$ and $4_1^+$	+0.12(11) and +0.02(17)	9.0(4)** and 3.6(3)**	[20]
$^{106}\text{Cd}$	$^{110}\text{Sn}$	$2_1^+$ and $4_1^+$	+0.29(11) and +0.05(14)	0.81(10) and unknown	[21]

Table 4.1: *(\*) These isotopes were created by two  $\alpha$ -particles transfer and results were obtaining by TDRIV method in combination with DSAM ("plunger method"). (\*\*) Life-times values taken from [6]. Result from first experiments to perform  $g$  factor measures with  $\alpha$  transfer in combination with transient field technique.*

In general, in all TF experiments arranged in the Table 4.1 a considerable improve in the angular correlation function was not proposed or performed. Due to this reason this work is aimed to open the door to a detailed investigation of alpha-transfer reactions that provides a deep understanding about experimental and theoretical aspects of the reaction mechanism. The improvement of the angular correlation function is the first step to follow. Through a modern experimental setup it is expected to obtain more information about the gamma-radiation distribution as well as the subsequent particles in the reaction. From the particle- $\gamma$  coincidence method, important information about excitation functions must be obtained. In the next chapter, the first experimental proposal of a campaign of alpha transfer reaction is presented.



## Chapter 5

### Our experimental proposal and perspectives

---

As a part of this work, an experimental proposal was presented to Laboratório Aberto de Física Nuclear (LAFN) of São Paulo University, Brazil. The proposal has been accepted and scheduled to be carried out in 2019. The entire document of the proposal is shown in Appendix D. This experiment is just the door of entrance to an experimental campaign for measuring off nuclear magnetic and electric moments of short-lived radioactive states in nuclei close to stability line. In this chapter will be described the facilities of LAFN and their main working principles. A complete list of nuclei whose radioactive states can be populated with stable beams via alpha-transfer reactions is presented in this chapter. Most of these nuclei present collective effects. Such list contains the most update information about electric moments (life times) and magnetic moments ( $g$  factor) measurements of low lying states of nuclei we are interested in. Obtained measurements will allow the unveiling nuclear structure of nuclei that present collective effects. However, it is worth saying that the experimental campaign is also aimed to study Alpha-transfer reactions themselves.

As mentioned in previous chapter, there is a lack of information about Alpha-Transfer reaction mechanism. Theoretical approaches to understanding transfer and pick up reactions mechanism as DWBA in combination with Optical Potential have presented a good fit to differential cross sections in heavy and light nuclei reactions but available experimental data is not good enough. In the future experiments, it expects to obtain nuclear structure information as  $\alpha$  widths, spectroscopic

factors, and wave functions as the ultimate goal, to unveil  $^{12}\text{C}$  structure.

## 5.1 Proposed experiment: the reaction and the experimental layout

This section is divided into three parts, the first is aimed to show the acceleration system and ion source available in LAFN, that will be used in the proposed experiment. In the second section a description of detection array which is subdivided between the gamma detection and the particle detection together with the choice of nuclear reaction will be shown, and by last, the third part contains the perspectives of future experiments in alpha-transfer reactions.

### 5.1.1 Accelerators

Accelerators are differentiated by their working physics principles, cyclotrons, for example, uses big magnets to accelerate beam particles, and electrostatic accelerators use high voltage terminals to accelerate ions. In LAFN, there is an electrostatic accelerator type tandem which works with a pellet charge system. Tandem accelerators work as a junction of two Van de Graff accelerators whose work mechanism will be discussed then.

#### Van de Graaff accelerator

Van de Graaff accelerator is a type of electrostatic accelerator, that uses the huge voltage that Van de Graaff generator can achieve to accelerated charged particles. The main elements of this type of accelerator are showing in 5.1.

The charge system working principle of this accelerator is based on triboelectric effect, which consist in a contact electrification of two materials (one of them predisposed to donate electrons and the another to receive electrons). A rubber belt turns around two rollers made of materials triboelectrically different to the rubber, an electric charge supply spray positive charge using a



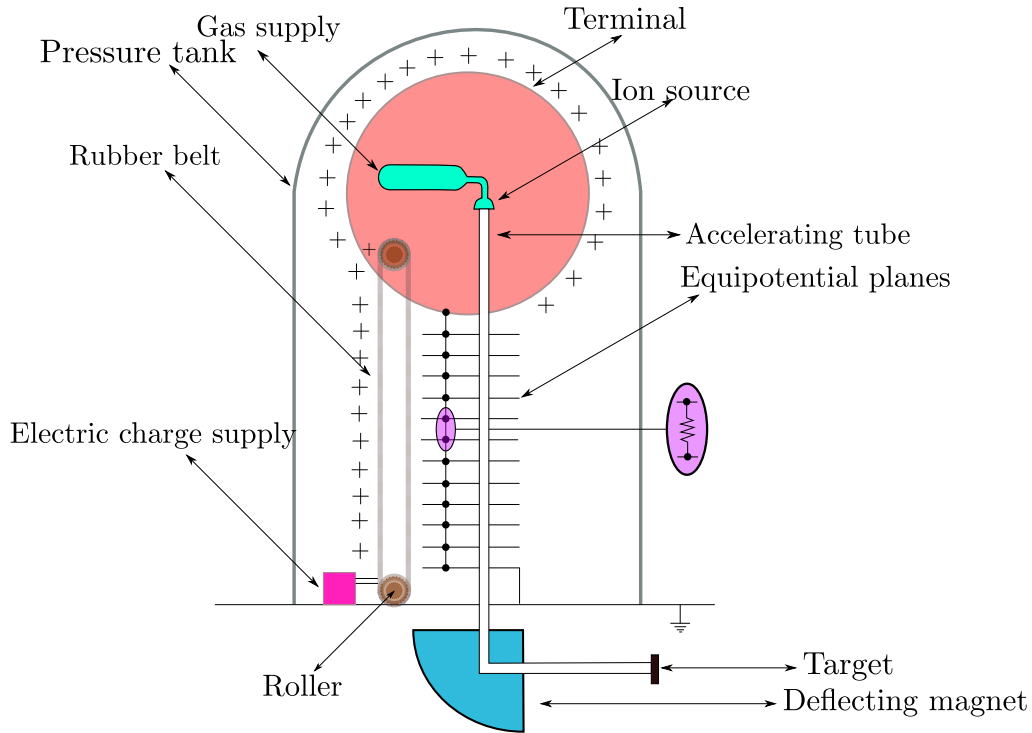


Figure 5.1: Schematic representation of a Van de Graaff accelerator system. This kind of accelerators works with a pellet chain, transporting a big amount of charge to a terminal that uses the electric attraction to expel a negative ion beam found inside it to a evacuation tube inside a electrode array and afterwards shot to a target.

voltage of 20-30 kV, which is transported to the dome by the rubber belt. The pressure tank contains a gas that avoid the possible corona discharges of the dome and helps to maintain the huge amount of charge and the subsequently the high voltage related by:

$$V = \frac{Q}{C}, \quad (5.1)$$

where  $V$  is the voltage due to the dome and  $C$  is its capacitance; in an accelerator system placed in air, voltages can up to a few MV, for inert gases like nitrogen at 15 atm, voltage of up to 12 MV can be obtained.

Positive ions are produced in the ion source; they are repelled by the positive charge distribution at the dome and conduced though the acceleration tube, this tube is positioned onto equipotential planes attached by resistances using to distribute the terminal voltage uniformly and avoid the

lose of kinetic energy which is directly related with the voltage following the relation:

$$qV = \frac{1}{2}mv^2, \quad (5.2)$$

where  $q$  is the charge,  $m$  is the mass and  $v$  is the velocity of the accelerated particle. Finally, the particle is deflected by a magnet towards the target.

An evolution of the Van de Graaff acceleration system is the tandem accelerator which can be viewed as the junction of two Van de Graaff accelerators and actually produces twice as much energy than Van de Graaff. This accelerator will be reviewed in the next section.

### Pelletron-Tandem accelerator

The pelletron tandem accelerator is a junction of two Van de Graaff accelerators with a charged system based on pellets. The particularity of this accelerator is that the negative ion source can be convert to a positive ion source by a stripper. Tandem's schema is shown in Figure 5.2.

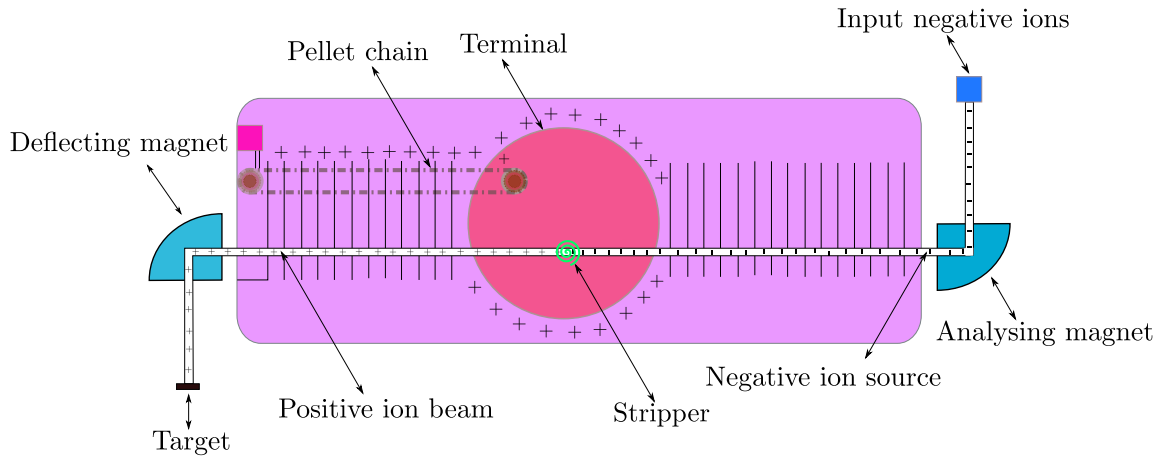


Figure 5.2: Working's schema of pelletron-tandem accelerator. This type of electrostatic accelerator is an evolution of Van de Graff acceleration system.

An input negative ion source is the first phase of the beam; the entering ions are sorted by the analyzing magnet, only allowing to pass the ions of interest. The negative ions are accelerating towards the positively charged terminal through an array of intermediate electrodes. Inside the

terminal a stripper *cuts* the electrons of the negative ion beam and the ions becomes positive. The positive ion beam is now instead repelled from the terminal and conduced into another array of intermediate electrodes, finally, a deflecting magnet send the beam to the target.

*The pellet charge system*

The pellet chains are made of an stainless steel cylinder (pellet) and connected by insulating nylon links in order to keep the charge in the pellet (see Figure 5.3).

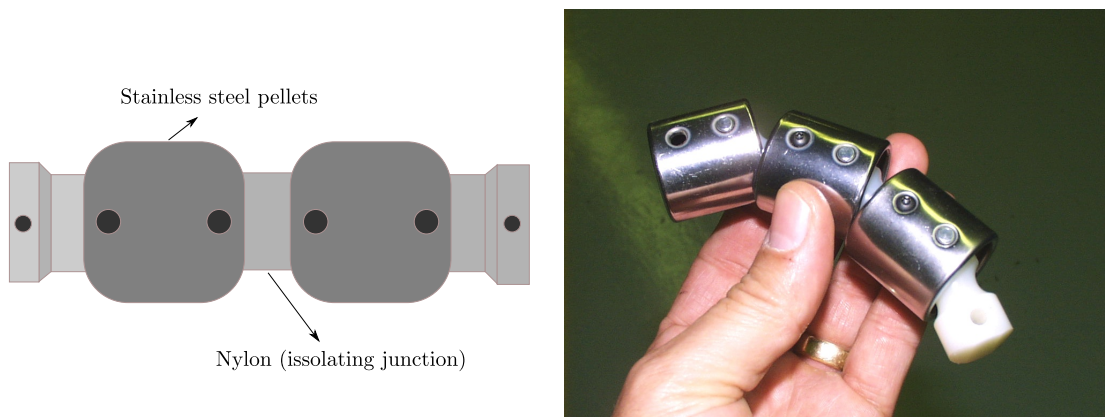


Figure 5.3: *The pellet chain. In the right side the parts of the pellet chain are indicated. A picture of a pellet chain is shown in the left side. The picture of the pellet chain was adopted from <https://www.slideshare.net/AnuradhaKVerma/m1-accelerators>.*

For a positive terminal (Single Ended) Pelletron, the negatively-charged inductor electrode pushes electrons off the pellets while they are in contact with the grounded drive pulley. Since the pellets are still inside the inductor field as they leave the pulley, they retain a net positive charge. The chain then transports this charge to the high-voltage terminal, where the reverse process occurs. When it reaches the terminal, the chain passes through a negatively-biased suppressor electrode, which prevents arcing as the pellets make contact with the terminal pulley. As the pellets leave the suppressor, charge flows smoothly onto the terminal pulley, giving the terminal a net positive charge.

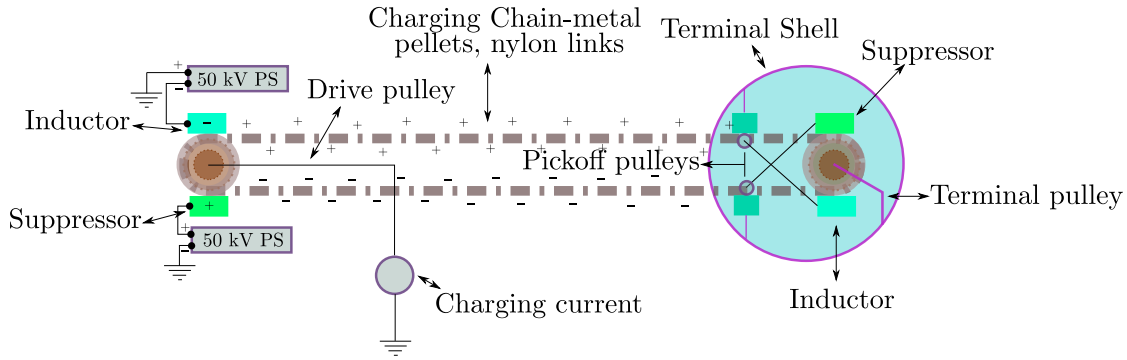


Figure 5.4: Schematic representation of pelletron charge system. This charged system is used to accumulate a large amount of charge (up to and above 25 MV) in the dome of the accelerator.

### Sao Paulo Pelletron Accelerator

The pelletron tandem accelerator in the Laboratório Aberto de Física Nuclear in São Paulo, Brazil, is a Tandem electrostatic machine, built by the National Electrostatic Corporation (NEC) and acquired by the University of São Paulo and installed at the Institute of Physics of USP in 1972. The name *pelletron* originates from an innovative process introduced by NEC which consists in the transportation of the charge by *pellets*. This accelerator works with a voltage of 8 MV and has a negative ion source to accelerate different stable ions. The working mechanism of the ion source is described below.

#### 5.1.2 Ion sources

Pelletron accelerators have a Multicathode Source of Negative Ions by Cesium Sputtering (MC-SNICS) as an ion source, acquired from NEC can produce negative ion beams of virtually all chemical elements or molecules.

Beam generation is done by cesium ion bombardment and subsequent spraying of a small amount of compacted material in a special crucible forming a tablet (cathode). The cesium vapor rises from the reservoir to the ionization chamber. Part of the cesium condenses on the front surface of the cathode and another part of the cesium is ionized by the hot surface of the ionizer. The ionizer produces a primary cesium beam that strikes the cooling surface of the sample. Cesium, positively

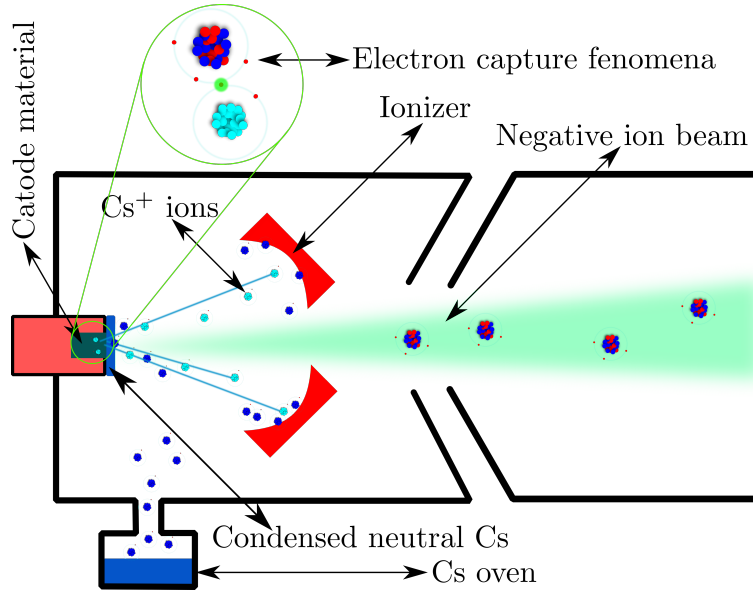


Figure 5.5: *MC-SNICS: Multicathode Source of Negative Ions by Cesium Sputtering* schema of working. This negative ion source is specially designed for the working of the Tandem accelerator.

ionized, accelerates to the cathode by bombarding particles of the tablet (cathodic spray) under the condensed cesium layer. The cathode particles, in turn, are expelled due to impact with the positive ion, traversing the cesium layer of the surface of the pellet and forming negative ions by capturing weakly bound cesium electrons.

The beams generated at this source have an energy of 5 KeV and are extracted by a potential of extraction of 20 KV. The energy of the beam after extraction is 25 KeV. The ion source is mounted on an electrically isolated structure to which a voltage of -80KV is applied to pre-accelerate the beam so that it can be injected into the accelerator. This pre-acceleration is done in the pre-acceleration tube. The beam energy after this acceleration is 105 KeV. With this, we conclude the review of the acceleration setup to produce the nuclear reaction. In the next section, the features of the reaction, and the detection system will be presented.

### 5.1.3 Reaction and Detection system

Reaction that is described in Figure 5.6, was proposed to be performed in LAFN.

In the experiment is expected to observe following spin states  $2^+$ ,  $4^+$  and  $6^+$ .

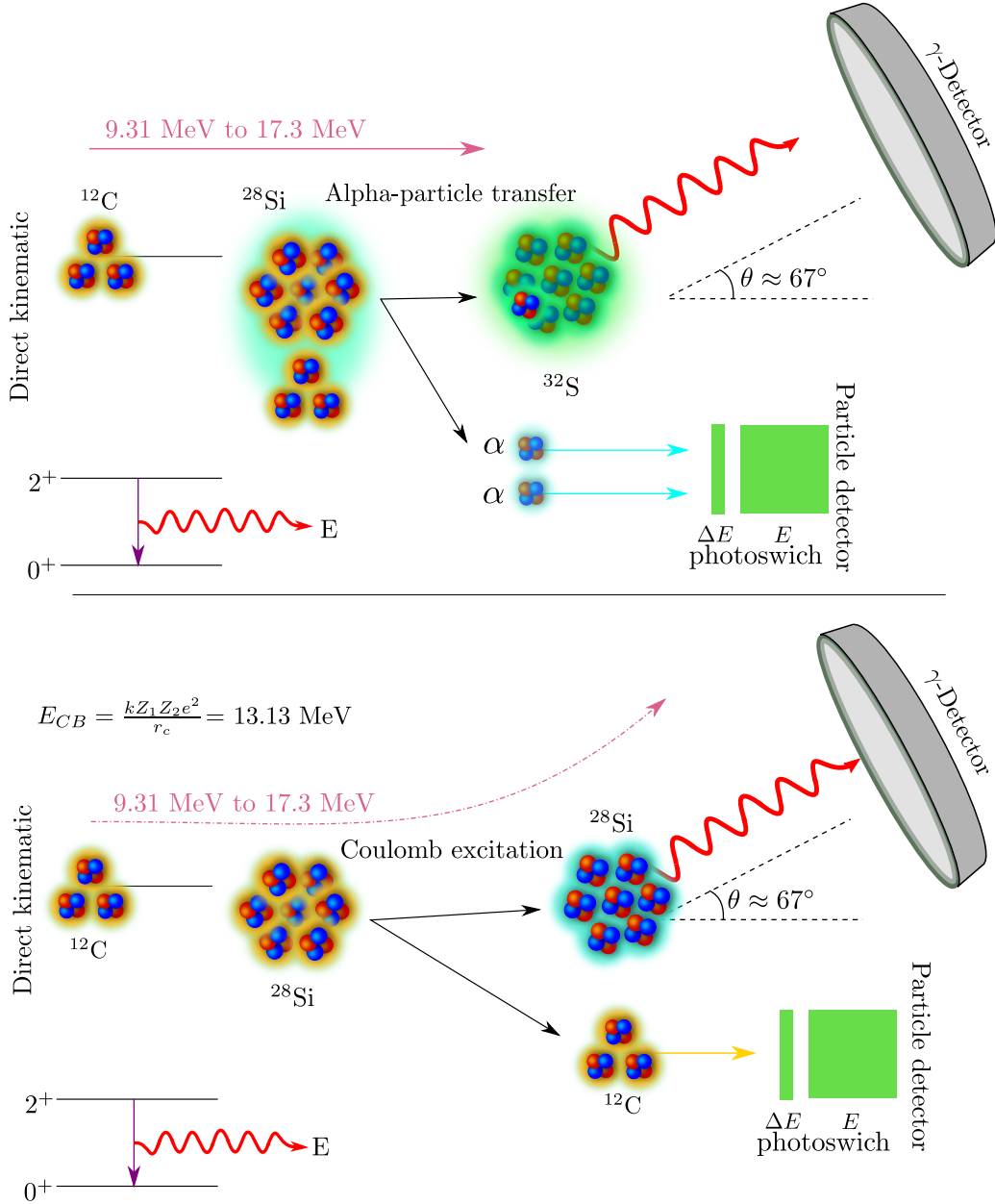


Figure 5.6: Schematic representation of the nuclear reactions to be performed in the proposed experiment. When  $^{12}\text{C}$  is shot against a  $^{28}\text{Si}$  target at energies around 13.13 MeV, two type of reactions should be observed. When an alpha particle is transferred to the  $^{28}\text{Si}$  nucleus (situation illustrated at the top) a radioactive  $^{32}\text{S}$  is produced. If the  $^{12}\text{C}$  do not transfer, or the  $^{28}\text{Si}$  do not capture the alpha particle, a low-lying spin state in  $^{28}\text{Si}$  is populate via Coulomb excitation. For both reactions is expected to observe a decay from the  $2^+$  spin state.

Alpha-transfer reaction and coulomb excitation can occurs in the experiment for beam energies around 13.13 MeV. The specific selected range is between 9.31 MeV to 17.3 MeV. Details about

data registration are disposed in D.

Detection layout is similar to the one described in Chapter 3. The disposition of detectors are shown in Figure 5.7. Gamma-ray detection system will consist of a LYSO(Ce) crystals arrangement. The goal of this experiment is to obtain a detailed particle- $\gamma$  angular correlation, that means, only detected gamma rays in coincidence with detected particles will be take into account. An array of 16  $\Delta E - E$  telescopes will be used to detect particles after the reaction. Four LYSO(Ce) scintillator crystals will be placed at approx  $67^\circ$  to the beam direction as is shown in Figure 5.7.

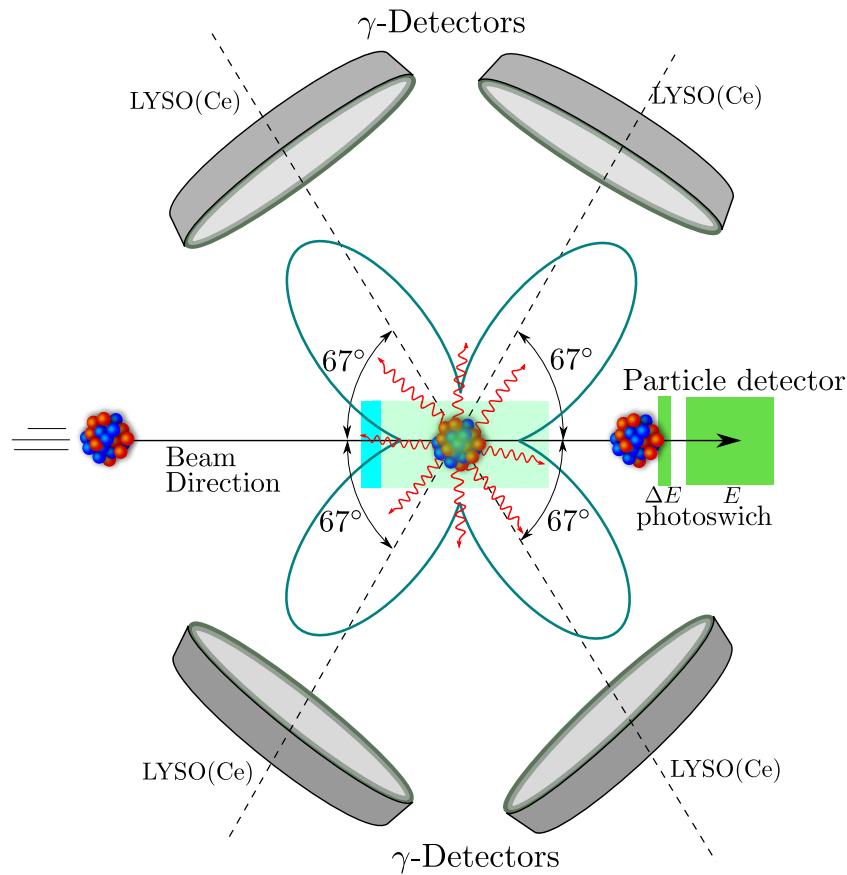


Figure 5.7: The detection setup of the proposed experiment. For the  $\gamma$  detection, four segmented scintillator detectors composed by an array of 25 LYSO(Ce) crystals will be placed at  $67^\circ$  of the beam direction. For the particle detection 16  $\Delta E$ - $E$  photo-switch detectors will be positioned behind the target.

Both,  $\gamma$  and particle detection systems are based on scintillator detectors. Scintillators detector are constructed by liquid, solid or gas materials. These materials are capable to produce sparks of

light, when they are exposed to ionizing radiation. They convert part of the kinetic energy of an incident particle into light. Below are some important aspects of the detectors that will be used in the experiment.

### Cerium-doped Lutetium Yttrium Orthosilicate $\text{LYSO}(\text{Ce})$ Scintillator $\gamma$ -ray detector

Lutetium Yttrium Orthosilicate is an inorganic chemical compound which is broadly used as a scintillator crystal, whose chemical formula is  $\text{Lu}_2\text{SiO}_5$ .  $\text{LYSO}$  is a relatively new ideal generation of a scintillator crystal, it has the advantages of high light output and density, quick decay time, adequate energy resolution and low cost. Crystal contains the element lutetium which is composed by two isotopes:  $^{175}\text{Lu}$  (stable) present in a percentage of 97,41% and  $^{176}\text{Lu}$  (beta emitter) present in a percentage of 2,59%, it decays with half-life of  $3,78 \times 10^{10}$  years. Due to the content of Lutetium, the crystal  $\text{LYSO}$  appears to be weakly radioactive. In the experiment a  $\text{LYSO}$  crystal array doped with cerium is coupled to a Silicon Photomultiplier (SiPM) to obtain a gamma radiation detector. The result is a square segmented particle detector as is shown in Figure 5.8. The segmentation on the detector will be very useful to discriminate angles of  $\gamma$ -detection which is very important for angular correlation function calculation.

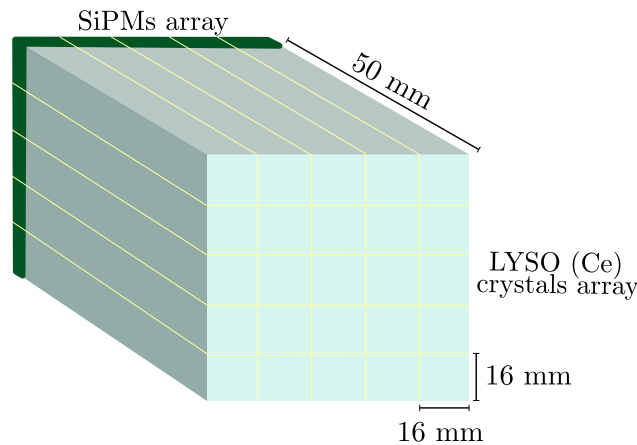


Figure 5.8:  $\text{LYSO}(\text{Ce})$  array or segmented square  $\text{LYSO}(\text{Ce})$  crystal available in LAFN with its dimensions. Every crystal in the array is a square of  $(16 \times 16)$  mm, a total of 25 crystals will be used. The longitude of the crystals is of 50 mm. All these crystals are connected to a silicon photomultiplier.

It is worth to say that  $\text{LYSO}$  crystals which will be used in the experiment are doped with Cerium



atoms. By the addition of Cerium the detector presents semiconductor properties. In Figure 5.9 are disposed two real pictures of the LYSO(Ce) crystals.

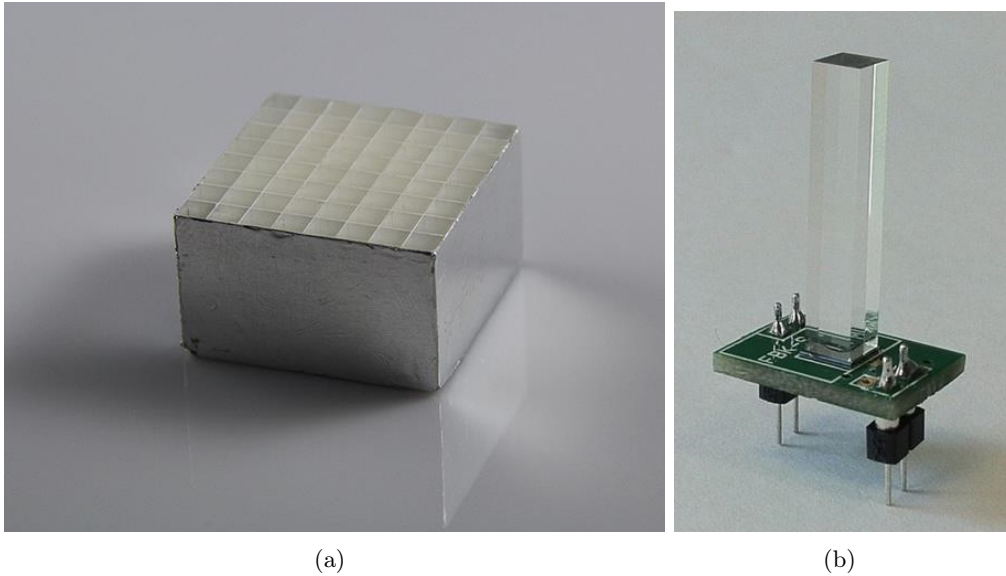


Figure 5.9: *LYSO(Ce) crystal pictures. In picture on the left side (a) an array of LYSO(Ce) crystals similar as the one represented in Figure 5.8 is shown. On the right picture there is a LYSO crystal joint to a SiPM forming a scintillator detector.*

In the next subsection it will be presented the particle detector together with a explanation of the photomultiplier function in the plastic detectors.

### **$\Delta E - E$ photo-switch**

The  $\Delta E - E$  telescope or photo-switch detector it is basically the blending of two scintillators of different thickness and a photomultiplier as is shown in Figure 5.10. The thin and thick scintillators array is close to a photomultiplier tube as LYSO(Ce) crystal. The function of this photomultiplier is to amplify the signal produced by the spark after the interaction between ionizing radiation and the detector. When spark is produced the photons interact with a photocatode which converts the interaction into an electrical signal. A focusing electrode conduce the electrical signal into an array of dynodes and anodes. As the signal ricochet in the array of dynodes and anodes is being amplified. By last, the amplified signal is deposited in connector pines and collected in the data acquisition system. All elements mentioned to amplify the signal are inside a vacuum tube.

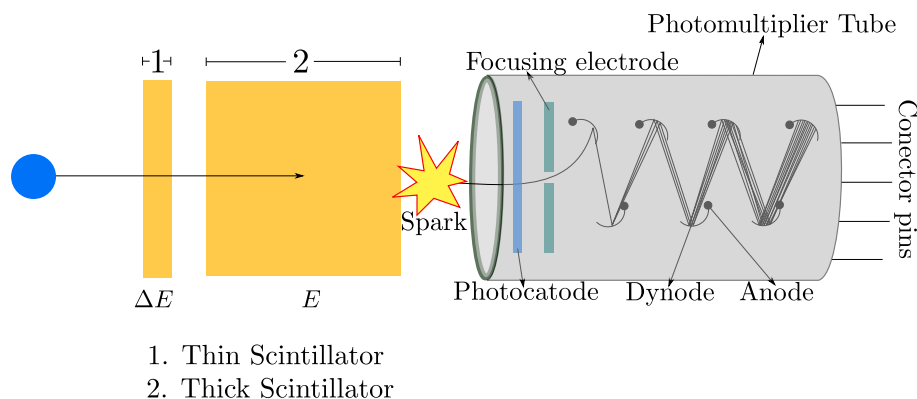


Figure 5.10:  $\Delta E - E$  telescope or photo-switch formed by a thin and a thick scintillator array together with a photomultiplier tube. The blending of the  $\Delta E - E$  array and the photomultiplier tube form a plastic scintillator detector. The photo-switch is responsible for producing the spark as the result of the interaction between the particle and the material and the photomultiplier convert the spark into a suitable electrical signal.

When the charged particle reaches the thin layer it loses energy, the residual energy of the particle is lost due to the interaction with the thin layer. This allows discerning between different types of charged particles and their energies. The layers have dimensions of 0.01 millimeters for the  $\Delta E$  layer and of 10 millimeters for the  $E$  layer. The decay time of the pulse produced by the interaction is of 2.4 ns for  $\Delta E$  and 264 ns for  $E$  layer. With this detector it is possible to distinguish the detected particle by analyzing the loss energy by Bethe-Block equation.

With this detector we finalize the description of the experimental tools which will be used in the experiment. In the next section we are going to present the future experiments as the perspectives of this first one.

## 5.2 Future experiments in alpha transfer reactions

The proposal presented to São Paulo is aimed to start a research program to study  $\alpha$ -transfer reactions, from obtaining particle- $\gamma$  correlation with nuclear reactions which involves  $n \alpha$  nuclei-like systems. Nuclear reactions with  $^{16}\text{O}$ ,  $^{20}\text{Ca}$  and  $^{24}\text{Mg}$  are thought to be next experiments in LAFN. However, the proposal of the experimental campaign of magnetic and electric moments measurements is much more comprehensive. As a result of this work, a complete recompilation

of all radioactive nuclei that can be produced from an alpha-transfer reaction with a stable beam is presented in Table 5.1. The beams needed to produce these nuclei with an alpha transfer reaction are presented together with laboratories capable to accelerate such projectiles. This table contains all the lifetimes and  $g$ -factor measurements of low lying spin states that have been made in the nuclei we are interested in produce by alpha-transfer reactions. A first approach to the TRIUMF lab have been established and in the Appendix E is disposed a list with all possible alpha transfer reactions that can be perform with their beam facilities. In these future experiments is expected to considerable improve particle- $\gamma$  correlation in order to reduce uncertainty on  $g$ -factor measurements as well as obtain structure information to understand better the reaction mechanism in alpha-transfer.

Table 5.1: *Table of transfer reactions. This table shows life time ( $\tau$ ) and nuclear  $g$ -factors measures of even spin states with positive parity. The first column indicates and the laboratories that can produce the beams of the second column. Light violet color indicates the existence of measures of another nuclear spin states different that even nuclear spin with positive parity. Red color indicates that there is no nuclear magnetic moment measures of any spin state until 2011. The "Product" column belong to the group of nuclei that populate radioactive states after alpha-transfer reaction.*

Lab	Beam	Product	$I^\pi$	$\tau$ and $T_{1/2}(\text{gs})$	$g$	Ref.
Bk/Jy	${}^3_2\text{He}$	${}^7_4\text{Be}$	$3/2^-_{\text{gs}}$	53.22(6) d		[52]
A&M/Jy/Lg/IU	${}^{14}_7\text{N}$	${}^{18}_9\text{F}$	$1^+_{\text{gs}}$	109.77(5) d		[52]
Lg	${}^{33}_{16}\text{S}$	${}^{37}_{18}\text{Ar}$	$3/2^+_{\text{gs}}$	35.04(4) d		[52]
-	${}^{39}_{19}\text{K}$	${}^{43}_{21}\text{Sc}$	$7/2^-_{\text{gs}}$	3.891(12) h		[52]
-	${}^{40}_{19}\text{K}$	${}^{44}_{21}\text{Sc}$	$2^+_{\text{gs}}$	3.97(4) h	$\mu=+2.505(3) \mu_N$	[52, 53]
			$4^+$	4.52(27) ns	+0.90(12)	[54]
			$6^+$	84.55(14) h	+0.635(1)	[53]
Lg/Jy/IU/Ar	${}^{40}_{20}\text{Ca}$	${}^{44}_{22}\text{Ti}$	$0^+_{\text{gs}}$	59.1(3) y		[52]
			$2^+$	3.97(28) ps	+0.52(15)	[15]
IUAC	${}^{45}_{21}\text{Sc}$	${}^{49}_{23}\text{V}$	$7/2^-_{\text{gs}}$	330(15) d		[52]

## 5.2 Future experiments in alpha transfer reactions

Lg	$^{48}_{20}\text{Ca}$	$^{52}_{22}\text{Ti}$	$0_{\text{gs}}^+$	1.7(1) m		[52]
			$2^+$	5.2(2) ps	+0.84(19)	[14]
			$4^+$	4.8(6) ps	+0.46(15)	[14]
-	$^{47}_{22}\text{Ti}$	$^{51}_{24}\text{Cr}$	$7/2_{\text{gs}}^-$	27.7025(24) d		[52]
IUAC/Bk	$^{50}_{23}\text{V}$	$^{54}_{25}\text{Mn}$	$3_{\text{gs}}^+$	312.20(20) d		[52]
-	$^{61}_{28}\text{Ni}$	$^{65}_{30}\text{Zn}$	$7/2_{\text{gs}}^-$	243.93(9) d		[52]
Lg/A&M/Jy/IU	$^{63}_{29}\text{Cu}$	$^{67}_{31}\text{Ga}$	$3/2_{\text{gs}}^-$	3.2617(5) d		[52]
Ar/IU/Jy/Lg	$^{64}_{30}\text{Zn}$	$^{68}_{32}\text{Ge}$	$0_{\text{gs}}^+$	270.93(13) d		[52]
			$2^+$	3.1(2) ps	+0.55(14)	[55]
			$8_1^+$	1.5(3) ps	+0.10(4)	[17]
			$8_2^+$	0.7(3,2) ps	-0.28(13)	[17]
Lg	$^{69}_{31}\text{Ga}$	$^{73}_{33}\text{As}$	$3/2_{\text{gs}}^-$	80.30(6) d		[52]
Lg	$^{77}_{34}\text{Se}$	$^{81}_{36}\text{Kr}$	$7/2_{\text{gs}}^+$	$2.29 \times 10^5(11)$ y		[52]
Lg/Ar	$^{79}_{35}\text{Br}$	$^{83}_{37}\text{Rb}$	$5/2_{\text{gs}}^-$	86.2(1) d		[52]
Jy	$^{84}_{38}\text{Sr}$	$^{88}_{40}\text{Zr}$	$0_{\text{gs}}^+$	83.4(3) d		[52]
			$2^+$	3.6(4) ps	+0.30(11)	[56]
			$4^+$	2.2(2) ps	+0.65(18)	[56]
			$8^+$	1.90(36) $\mu\text{s}$	-0.22(2)	U*
Bk	$^{86}_{36}\text{Kr}$	$^{90}_{38}\text{Sr}$	$0_{\text{gs}}^+$	28.90(3) y		[52]
			$2^+$	10.09(2) ps	-0.12(11)*	[57, 58]
			$4^+$	17.31(2) ps	-0.02(17)*	[57, 58]
-	$^{87}_{37}\text{Rb}$	$^{91}_{39}\text{Y}$	$1/2_{\text{gs}}^-$	58.51(6) d		[52]
-	$^{93}_{41}\text{Nb}$	$^{97}_{43}\text{Tc}$	$1/2_{\text{gs}}^-$	$4.21 \times 10^6(16)$ y		[52]
-	$^{105}_{46}\text{Pd}$	$^{109}_{48}\text{Cd}$	$5/2_{\text{gs}}^+$	461.4(12) d		[52]

IUAC/Bk/Ar/L	$^{107}_{47}\text{Ag}$	$^{111}_{49}\text{In}$	$9/2^+_{\text{gs}}$	2.8047(4) d		[52]
Lg	$^{99}_{44}\text{Ru}$	$^{103}_{46}\text{Pd}$	$5/2^+$	16.991(19) d		[52]
Lg	$^{96}_{44}\text{Ru}$	$^{100}_{46}\text{Pd}$	$0^+_{\text{gs}}$	3.63(9) d		[52]
			$2^+$	6.23(4) ps	+0.39(18)	[1,20]
			$4^+$	2.49(3) ps	+0.45(14)	[1,20]
			$6^+$	2.56(5) ps	+1.47(87)	[1,20]
-	$^{106}_{48}\text{Cd}$	$^{110}_{50}\text{Sn}$	$0^+_{\text{gs}}$	4.11(10) h		[52]
			$2^+$	0.56(10) ps	+0.29(11)	[21]
			$4^+$	unknown	+0.05(14) ps	[21]
			$6^+$	5.61(4)	+0.01(19)	[21]
-	$^{112}_{50}\text{Sn}$	$^{116}_{52}\text{Te}$	$0^+_{\text{gs}}$	2.49(4) h		[52]
-	$^{114}_{50}\text{Sn}$	$^{119}_{52}\text{Te}$	$1/2^+_{\text{gs}}$	16.05(5) h		[52]
-	$^{117}_{50}\text{Sn}$	$^{121}_{52}\text{Te}$	$1/2^+_{\text{gs}}$	19.17(4) d		[52]
-	$^{113}_{53}\text{In}$	$^{117}_{51}\text{Sb}$	$5/2^+_{\text{gs}}$	2.80(1) h		[52]
-	$^{115}_{53}\text{In}$	$^{119}_{51}\text{Sb}$	$5/2^+_{\text{gs}}$	38.19(22) h		[52]
-	$^{121}_{51}\text{Sb}$	$^{125}_{53}\text{I}$	$5/2^+_{\text{gs}}$	59.407(10) h		[52]
Bk	$^{124}_{54}\text{Xe}$	$^{128}_{56}\text{Ba}$	$0^+_{\text{gs}}$	2.43(5) d		[52]
-	$^{123}_{52}\text{Te}$	$^{127}_{24}\text{Xe}$	$1/2^+_{\text{gs}}$	36.346(3) d		[52]
Lg/IUAC/Jy	$^{127}_{53}\text{I}$	$^{131}_{55}\text{Cs}$	$5/2^+_{\text{gs}}$	9.689(16) d		[52]
A&M	$^{129}_{54}\text{Xe}$	$^{133}_{56}\text{Ba}$	$1/2^+_{\text{gs}}$	10.551(11) y		[52]
Jy/Bk	$^{136}_{54}\text{Xe}$	$^{140}_{56}\text{Ba}$	$0^+_{\text{gs}}$	12.7527(23) d		[52]
-	$^{137}_{56}\text{Ba}$	$^{141}_{58}\text{Ce}$	$7/2^+_{\text{gs}}$	24.84(17) s		[52]
-	$^{138}_{57}\text{La}$	$^{142}_{59}\text{Pr}$	$2^-_{\text{gs}}$	19.12(4) h		[52]
-	$^{139}_{57}\text{La}$	$^{143}_{59}\text{Pr}$	$7/2^+_{\text{gs}}$	13.57(2) d		[52]
A&M	$^{141}_{59}\text{Pr}$	$^{145}_{61}\text{Pm}$	$5/2^+_{\text{gs}}$	17.7(4) y		[52]

-	$^{142}\text{Nd}$	$^{146}_{62}\text{Sm}$	$0_{\text{gs}}^+$	$10.3 \times 10^7(5)$ y		[52]
-	$^{147}_{62}\text{Sm}$	$^{151}_{64}\text{Gd}$	$7/2_{\text{gs}}^+$	123.9(10) d		[52]
-	$^{149}_{62}\text{Sm}$	$^{153}_{64}\text{Gd}$	$3/2_{\text{gs}}^-$	240.4(10) d		[52]
-	$^{151}_{63}\text{Eu}$	$^{155}_{65}\text{Tb}$	$3/2_{\text{gs}}^+$	5.32(6) d		[52]
-	$^{153}_{63}\text{Eu}$	$^{157}_{65}\text{Tb}$	$3/2_{\text{gs}}^+$	71(7) y		[52]
-	$^{155}_{64}\text{Gd}$	$^{159}_{66}\text{Dy}$	$3/2_{\text{gs}}^-$	144.4(2) d		[52]
Bk	$^{159}_{65}\text{Tb}$	$^{163}_{67}\text{Ho}$	$7/2_{\text{gs}}^-$	4570(25) y		[52]
-	$^{161}_{66}\text{Dy}$	$^{165}_{68}\text{Er}$	$5/2_{\text{gs}}^-$	10.36(4) h		[52]
-	$^{162}_{63}\text{Er}$	$^{166}_{70}\text{Yb}$	$0_{\text{gs}}^+$	56.7(1) h		[52]
-	$^{168}_{70}\text{Yb}$	$^{172}_{72}\text{Hf}$	$0_{\text{gs}}^+$	1.87(3) y		[52]
			$2^+$	2.23(14) ns	+0.25(5)	[59, 60]
			(6+)	6.92(5) ns	+0.92(10)	[61]
			(8-)	235.10(4) ns	+0.982(8)	[61]
-	$^{169}_{69}\text{Tm}$	$^{173}_{71}\text{Lu}$	$7/2_{\text{gs}}^+$	1.37(1) y		[52]
-	$^{171}_{70}\text{Yb}$	$^{175}_{72}\text{Hf}$	$5/2_{\text{gs}}^{(-)}$	70(2) d		[52]
-	$^{174}_{72}\text{Hf}$	$^{178}_{74}\text{W}$	$0_{\text{gs}}^+$	21.6(3) D		[52]
-	$^{175}_{71}\text{Lu}$	$^{179}_{73}\text{Ta}$	$7/2_{\text{gs}}^+$	1.82(3) Y		[52]
-	$^{177}_{72}\text{Hf}$	$^{181}_{74}\text{W}$	$9/2_{\text{gs}}^+$	121.2(2) d		[52]
-	$^{180}_{73}\text{Ta}$	$^{184}_{75}\text{Re}$	$0_{\text{gs}}^+$	35.4(7) d		[52]
			$8^+$	243.81(11) d	(+)0.36(13)	[62]/ [63]
-	$^{185}_{75}\text{Re}$	$^{189}_{77}\text{Ir}$	$3/2_{\text{gs}}^+$	13.2(1) d		[52]
-	$^{187}_{76}\text{Os}$	$^{191}_{78}\text{Pt}$	$3/2_{\text{gs}}^-$	2.83(3) d		[52]
-	$^{189}_{76}\text{Os}$	$^{193}_{78}\text{Pt}$	$1/2_{\text{gs}}^-$	50(6) y		[52]
			$0_{\text{gs}}^+$	444(77) y		[52]
-	$^{190}_{78}\text{Pt}$	$^{194}_{80}\text{Hg}$				

			10 <sup>+</sup>	4.18(72) ns	-0.24(4)*	[64]
			12 <sup>+</sup>	11.68(72) ns	-0.24(4)*	[64]
-	<sup>191</sup> <sub>77</sub> Ir	<sup>195</sup> <sub>79</sub> Au	3/2 <sup>+</sup> <sub>gs</sub>	186.01(6) d		[52]
-	<sup>196</sup> <sub>80</sub> Hg	<sup>200</sup> <sub>82</sub> Pb	0 <sup>+</sup> <sub>gs</sub>	21.5(4) h		[52]
			12 <sup>+</sup>	291.42(72) ns	-0.1557(6)	[65]
Lg/A&M/Jy/IU	<sup>197</sup> <sub>79</sub> Au	<sup>201</sup> <sub>81</sub> Tl	7/2 <sup>+</sup> <sub>gs</sub>	3.0421(17) d		[52]
-	<sup>198</sup> <sub>80</sub> Hg	<sup>202</sup> <sub>82</sub> Pb	0 <sup>+</sup> <sub>gs</sub>	52.5×10 <sup>3</sup> y		[52]
			4 <sup>+</sup>	2.84(28) ns	+0.002(4)	[66]
-	<sup>199</sup> <sub>80</sub> Hg	<sup>203</sup> <sub>82</sub> Pb	5/2 <sup>-</sup> <sub>gs</sub>	51.92(3) h		[52]
-	<sup>201</sup> <sub>80</sub> Hg	<sup>205</sup> <sub>82</sub> Pb	5/2 <sup>-</sup> <sub>gs</sub>	1.73×10 <sup>7</sup> (7) y		[52]
-	<sup>203</sup> <sub>81</sub> Tl	<sup>207</sup> <sub>83</sub> Bi	9/2 <sup>-</sup> <sub>gs</sub>	31.55(4) y		[52]
-	<sup>204</sup> <sub>82</sub> Pb	<sup>208</sup> <sub>84</sub> Po	0 <sup>+</sup> <sub>gs</sub>	2.898(2) y		[52]
			6 <sup>+</sup>	6.20(14) ns	+0.88(1)	[67] [52]
			8 <sup>+</sup>	504.94(28) ns	+0.919(1)	[68]
-	<sup>206</sup> <sub>82</sub> Pb	<sup>210</sup> <sub>84</sub> Po	0 <sup>+</sup> <sub>gs</sub>	138.376(2) d		[52]
			6 <sup>+</sup>	61.45(14) ns	+0.908(2)	[68]
			8 <sup>+</sup>	138.49(20) ns	+0.908(2)	[68]
-	<sup>207</sup> <sub>82</sub> Pb	<sup>211</sup> <sub>84</sub> Po	9/2 <sup>-</sup> <sub>gs</sub>	0.516(3) s		[52]
Jy/IUAC/Ar	<sup>208</sup> <sub>82</sub> Pb	<sup>212</sup> <sub>84</sub> Po	0 <sup>+</sup> <sub>gs</sub>	44.6(4) m		[52]
Ar	<sup>209</sup> <sub>82</sub> Bi	<sup>213</sup> <sub>85</sub> At	9/2 <sup>-</sup> <sub>gs</sub>	125(6) ns		[52]
-	<sup>232</sup> <sub>90</sub> Th	<sup>236</sup> <sub>92</sub> U	0 <sup>+</sup> <sub>gs</sub>	2.342×10 <sup>7</sup> (4) y		[52]
-	<sup>234</sup> <sub>92</sub> U	<sup>238</sup> <sub>94</sub> Pu	0 <sup>+</sup> <sub>gs</sub>	87.7(1) y		[52]
-	<sup>235</sup> <sub>92</sub> U	<sup>239</sup> <sub>94</sub> Pu	1/2 <sup>+</sup> <sub>gs</sub>	24110(30) y		[52]
Ar	<sup>238</sup> <sub>92</sub> U	<sup>242</sup> <sub>94</sub> Pu	0 <sup>+</sup> <sub>gs</sub>	3.75×10 <sup>5</sup> (33) y		[52]





## Conclusions

---

Hyperfine field techniques have used alpha transfer reactions as a tool to populate medium-to-low nuclear spin states in 9 experiments (see Table 4.1). From these experiments it was obtained a total of 19  $g$ -factor and 14 lifetime measurements of the  $2_1^+$ ,  $2_2^+$  and  $4_1^+$  spin states. Such  $g$ -factor values present an uncertainty considerable larger than the ones measured in Coulex-populated excited states [20]. The reason is the low level spin alignment, which is strongly observed after the population of the nuclear states with  $\alpha$ -transfer reactions. As it was discussed in Chapter 4, the anisotropy of the gamma distribution of the de-excitation process is directly related to the spin alignment level.

In 8 of the 9 mentioned experiments, Transient Field technique in combination with Doppler Shift Attenuation Method was used in the  $g$  factor and lifetime measurements obtaining. The remaining experiment used the Time Differential Recoil Into Vacuum technique combined with Recoil Doppler Shift Method and it was the first in using alpha transfer reactions to populate spin states. This experiment was carried out by Horstman, et al. They calculated a relatively small uncertainty in the  $g$ -factor measurement. They proposed a vertical slit with an aperture of  $45^\circ$  in front of the particle detector (see Figure 5.11) to maximize the improvement on the angular correlation function shape, which becomes flatten when anisotropy in the gamma-ray distribution decreases. In general, the alpha-transfer reactions experiments in which have been combined the TF and DSAM techniques have obtained uncertainties between 30% and 40% larger than the ones obtained from experiments in where Coulex was used as a population method [20].

The TF technique is more suitable than the RIV method due to its capability to resolve the  $g$

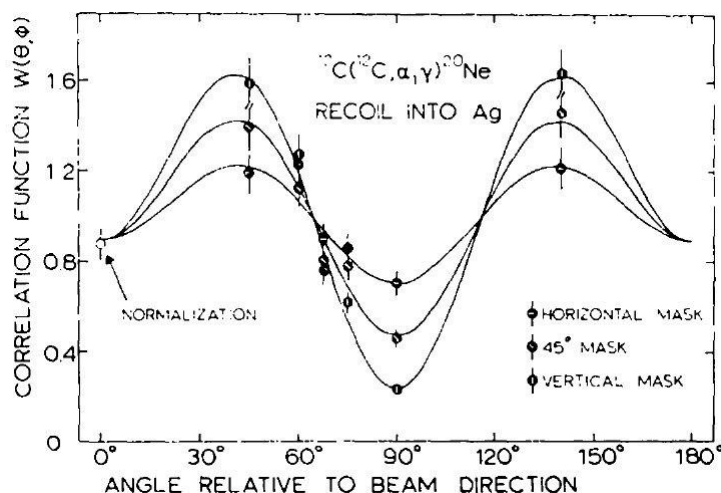


Figure 5.11: Alpha gamma angular correlations with the  $^{20}\text{Ne}$  reaction for three different positions of the rectangular mask. The three curves were fitted simultaneously to the experimental points normalized to the coincident yield at  $0^\circ$  of the beam direction. Figure taken from [3].

factor sign of short-lived ( $\sim\text{ps}$ ) excited states. Recent RIV experiments with modern setups have produced highly accurate  $g$ -factor measurements [69], however, TF technique is still indispensable to obtain the  $g$  factor sign, which is needed to tell about the protons or neutron domination in the nuclear wave function [70].

The vertical slit was kept in use as a method to obtain better angular correlation measurements. Nevertheless, the slit cannot be considered as a solution to the angular correlation function [36]. Up to this point, Coulex performs better than Alpha-transfer reaction technique as population mechanism. More experimental improvements have to be made in order to obtain precise enough  $g$ -factor measurements using the ATR technique.

On the other hand, knowledge about  $\alpha$ -transfer reaction mechanism and  $^{12}\text{C}$  structure is still being scarce [36]. Theoretical approaches to understand transfer and pick up reaction mechanism, such as DWBA in combination with Optical Potential, have presented a good fit to the experimental data of the differential cross sections in heavy and light nuclei reactions [13]. Interaction models as Linear combination of nuclear orbitals, the SU3 model and the JJ-shell model, have been used as a tool to study the reaction mechanism [71–74]. The population mechanism of the nuclear states is crucial for understanding the random distribution of the  $M$  projections. Recent studies on  $^{32}\text{S}$

suggest that alpha particle of  $^{12}\text{C}$  is transferred to the  $^{28}\text{Si}$  by tunneling through its potential [51]. Experimental data from Alpha-transfer reactions as well as theoretical studies are necessary to understand the reaction mechanism and  $^{12}\text{C}$  nuclear structure. Future experiments of alpha-transfer reactions should be aimed to discuss the angular correlation function. The usage of particle- $\gamma$ - $\gamma$  coincidence will allow to obtain more information about the reaction mechanism and re-evaluate the obtained values of magnetic and electric moments. The quality of the particle- $\gamma$ - $\gamma$  correlation function can be considerably improved by using a segmented particle detector, which enables the identification of the dispersion angle of the detected particles. Due to lack of knowledge about how the states are populated in ATR, the low spin alignment can not be reduced. Nevertheless, the flatness in the correlation function can be improved using a detector as the one shown in the Figure 5.12. This and the segmented  $\gamma$ -detectors represent a proposal for future experiments.

A campaign of  $\alpha$ -Transfer reaction experiments is proposed with all the possible combinations of a stable beam, which together with an  $\alpha$ -particle can provide a radioactive product. The first experiment of this campaign uses the reaction  $^{28}\text{Si}(^{12}\text{C}, ^4\text{He})^{32}\text{S}$  to determine the particle- $\gamma$ - $\gamma$  angular correlation function from a quadrupolar emission. The experiment is going to include an array of 16  $\Delta E - E$  particle detectors positioned behind the target, along with 4 arrays of 25 LYSO(Ce) crystals connected to a silicon photomultiplier to form a segmented  $\gamma$ -ray. The detector will be positioned at  $67^\circ$ , corresponding to the angle with the largest probability of quadrupolar emission. The SPP is the best option to study the reaction mechanism due to its good performance in the interpretation of heavy ion reactions with  $\alpha$ -cluster systems [32]. The DWBA is proposed as the method to calculate SPP with the program FRESCO [75].

The experiment suggested in this thesis is the first in a series of  $\alpha$ -transfer experiments. The final goal is a better understanding of the alpha-transfer reaction mechanism and the possibility to improve  $g$ -factor measurements of many nuclei in their low-lying spin states.

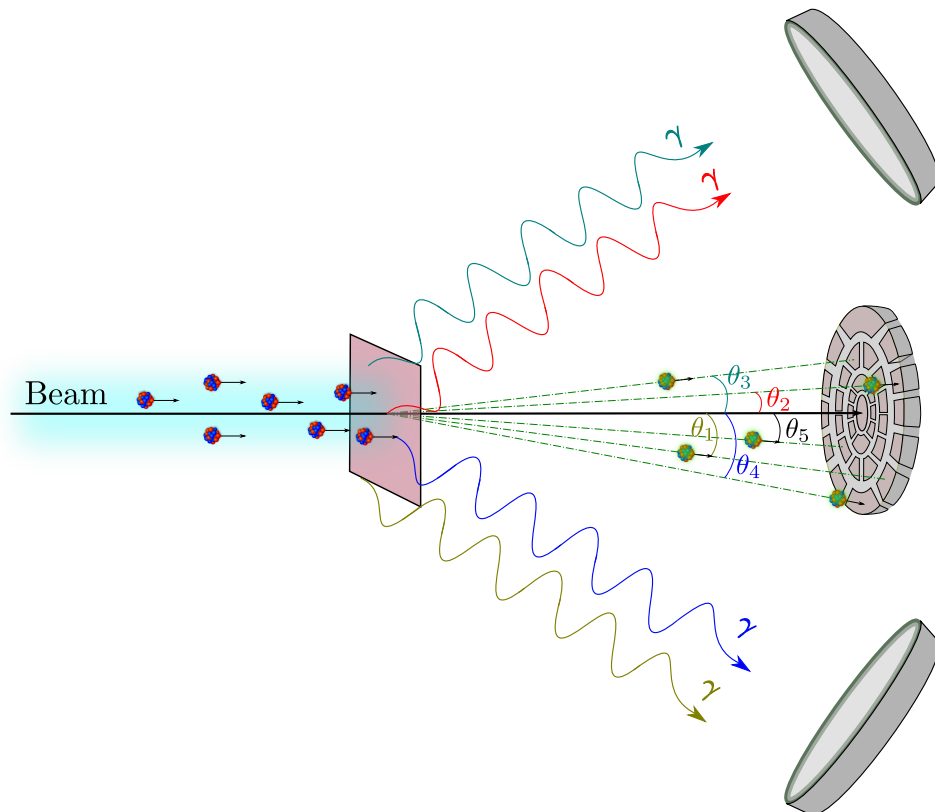


Figure 5.12: Schematic representation of a circular segmented particle detector proposed to be used in the next Alpha-transfer experiments. This detector is able to distinguish the dispersed angle of the detected particle (i.e.  $\theta_1, \theta_2 \dots$ ). The information of the particle is registered in coincidence with a  $\gamma$ -ray which comes from the radioactive nuclei produced in the ATR. With this information the particle- $\gamma$ - $\gamma$  correlation function will improve it.

# Appendices

---



## Appendix **A**

### More about g-factor

---

#### A.1 Quantum mechanical formalism

The quantum mechanical formalism of  $g$  factor will be developed in this section. As an additional detail, dependence between magnetic moment and nuclear spin will be presented as well.

As shown in Chapter 2, when the magnetic moment is displayed as a vector, it does not point in the direction of angular momentum. However, due to the Wigner-Eckart theorem, the expected value of the magnetic moment is roughly in the direction of  $\mathbf{I}$ . The factor  $g$  can be determined using this theorem and following the rules of nuclear spin selection [33].

Taking into account (2.25),

$$\langle \mathbf{I}, I_z | \boldsymbol{\mu} | \mathbf{I}, I_z' \rangle = g_I \mu_N \langle \mathbf{I}, I_z | \mathbf{I} | \mathbf{I}, I_z' \rangle. \quad (\text{A.1})$$

Adding a factor  $\langle \mathbf{I}, I_z' | \mathbf{I} | \mathbf{I}, I_z \rangle$ ,

$$\begin{aligned}
& \langle \mathbf{I}, I_z | \boldsymbol{\mu} | \mathbf{I}, I_{z'} \rangle \cdot \langle \mathbf{I}, I_{z'} | \mathbf{I} | \mathbf{I}, I_z \rangle = g_I \mu_N \langle \mathbf{I}, I_z | \mathbf{I} | \mathbf{I}, I_{z'} \rangle \cdot \langle \mathbf{I}, I_{z'} | \mathbf{I} | \mathbf{I}, I_z \rangle \quad (\text{A.2}) \\
\therefore \sum_{I_{z'}} \langle \mathbf{I}, I_z | \boldsymbol{\mu} | \mathbf{I}, I_{z'} \rangle \cdot \underbrace{\langle \mathbf{I}, I_{z'} | \mathbf{I} | \mathbf{I}, I_z \rangle}_{\text{Matriz identidad}} &= \sum_{I_{z'}} g_I \mu_N \langle \mathbf{I}, I_z | \mathbf{I} | \mathbf{I}, I_{z'} \rangle \cdot \underbrace{\langle \mathbf{I}, I_{z'} | \mathbf{I} | \mathbf{I}, I_z \rangle}_{\text{Matriz identidad}} \\
&\implies \langle \mathbf{I}, I_z | \boldsymbol{\mu} \cdot \mathbf{I} | \mathbf{I}, I_{z'} \rangle = g_I \mu_N \langle \mathbf{I}, I_z | \mathbf{I} \cdot \mathbf{I} | \mathbf{I}, I_{z'} \rangle \\
&\therefore g_I = \frac{\langle \mathbf{I}, I_z | g_L \boldsymbol{\ell} \cdot \mathbf{I} + g_S \mathbf{S} \cdot \mathbf{I} | \mathbf{I}, I_{z'} \rangle}{\langle \mathbf{I}, I_z | \mathbf{I} \cdot \mathbf{I} | \mathbf{I}, I_{z'} \rangle \mu_N}.
\end{aligned}$$

Where

$$\begin{aligned}
\mathbf{S} &= \mathbf{I} - \boldsymbol{\ell} \quad (\text{A.3}) \\
\boldsymbol{\ell} &= \mathbf{I} - \mathbf{S},
\end{aligned}$$

and

$$\begin{aligned}
\mathbf{S} \cdot \mathbf{S} = S^2 &= I^2 + \ell^2 - 2\mathbf{I} \cdot \boldsymbol{\ell} \quad (\text{A.4}) \\
\boldsymbol{\ell} \cdot \boldsymbol{\ell} = \ell^2 &= I^2 + S^2 - 2\mathbf{I} \cdot \mathbf{S},
\end{aligned}$$

therefore

$$\begin{aligned}
\boldsymbol{\ell} \cdot \mathbf{I} &= \frac{1}{2}(I^2 + \ell^2 - S^2) \quad (\text{A.5}) \\
\mathbf{S} \cdot \mathbf{I} &= \frac{1}{2}(I^2 + S^2 - \ell^2).
\end{aligned}$$

Thus, last line of (A.2) is



$$g_{\mathbf{I}} = \frac{g_{\ell}[\mathbf{I}(\mathbf{I} + 1) + \ell(\ell + 1) - \mathbf{S}(\mathbf{S} + 1)] + g_{\mathbf{S}}[\mathbf{I}(\mathbf{I} + 1) + \mathbf{S}(\mathbf{S} + 1) - \ell(\ell + 1)]}{2\mathbf{I}(\mathbf{I} + 1)}. \quad (\text{A.6})$$

Nucleons are fermions with spin  $\mathbf{S} = 1/2$  and nuclear spin  $|\ell - \frac{1}{2}| < \mathbf{I} < |\ell + \frac{1}{2}|$ , thus (A.6) becomes

$$g_{\mathbf{I}} = g_{\ell} \pm \frac{g_{\mathbf{S}} - g_{\ell}}{2\ell + 1}. \quad (\text{A.7})$$

Then, with (A.7)  $g$  factor for each nucleon can be write. Recalling the  $g_{\ell}$  and  $g_{\mathbf{S}}$  values disposed in Table 2.4,

$$g_{\text{Protón}} = 1 \pm \frac{5.59 - 1}{2\ell + 1}, \quad (\text{A.8})$$

then

$$g_{\text{Protón}} = \begin{cases} 1 + \frac{4.59}{2\mathbf{I}} & \text{si } \mathbf{I} = \ell + 1/2 \\ 1 - \frac{4.59}{2(\mathbf{I}+1)} & \text{si } \mathbf{I} = \ell - 1/2 \end{cases} \quad (\text{A.9})$$

and

$$\boldsymbol{\mu}_{\text{Protón}} = g_{\text{Protón}} \cdot \mathbf{I} = \begin{cases} \mathbf{I} + 2.3 & \text{si } \mathbf{I} = \ell + 1/2 \\ \mathbf{I} - \frac{2.3}{1+1/\mathbf{I}} & \text{if } \mathbf{I} = \ell - 1/2 \end{cases}, \quad (\text{A.10})$$

for proton, and

$$g_{\text{Neutrón}} = 0 \pm \frac{-3.83}{2\ell + 1}, \quad (\text{A.11})$$

therefore

$$g_{\text{Neutrón}} = \begin{cases} \frac{3.83}{2I} & \text{if } I = \ell + 1/2 \\ \frac{3.83}{2(I+1)} & \text{if } I = \ell - 1/2 \end{cases}, \quad (\text{A.12})$$

and

$$\boldsymbol{\mu}_{\text{Neutrón}} = g_{\text{Neutrón}} \cdot \mathbf{I} = \begin{cases} -1.92 & \text{if } I = \ell + 1/2 \\ \frac{1.92}{I+1/I} & \text{if } I = \ell - 1/2 \end{cases}, \quad (\text{A.13})$$

for neutron.

## Appendix **B**

### Schmidt lines

After developing the previous formalism, a new question can be formulated; What will be the value of  $\mu$  for different nuclear states? [33]. Assuming that the nucleus is a Fermi gas where the nucleons are subjected to a potential (*independent particle model*), the value of the nuclear magnetic moment for different nuclear states *in odd nuclei whose nucleon does not Paired is found in a well-defined orbital* is described by the *Schmidt lines*. Observe Figure B.1.

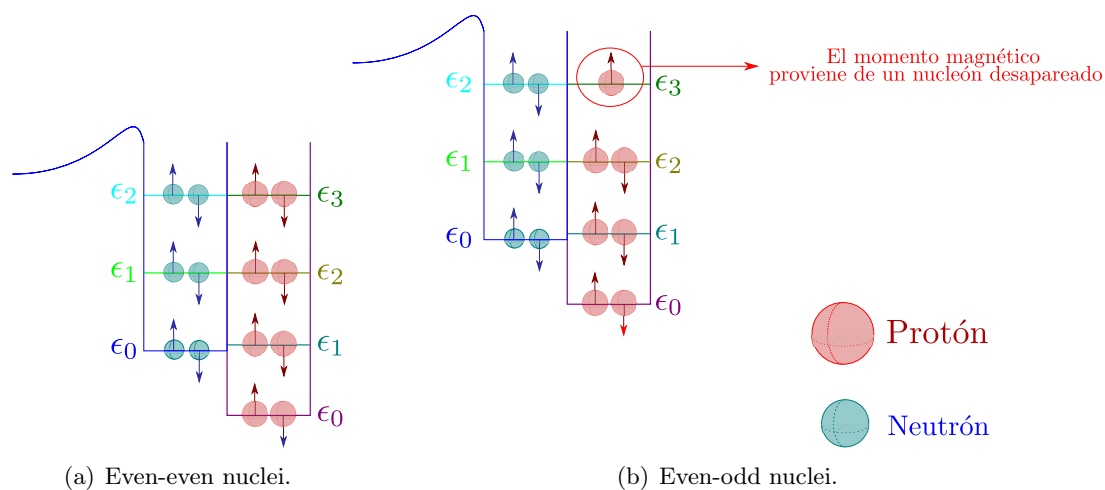


Figure B.1: *Graphic representation of level energy occupation of even-even and odd-even nuclei.*

The even-even nuclei are characterized by having all their nucleons paired, therefore the nuclear spin of this type of nucleus is  $I = 0$  and  $\mu = 0$  in its ground state, because the contribution to

the nuclear spin comes from the nucleons that are not paired. In their states excited with  $I \neq 0$  their magnetic moment values are different from zero and the measurement of these moments in excited states is the topic of interest of this work.

By using (A.10) and (A.13) with different spin values, the Schmidt lines are obtained (Figure B.2). These curves represent the prediction of the nuclear magnetic moment value for different nuclear spin states for the independent particle model.

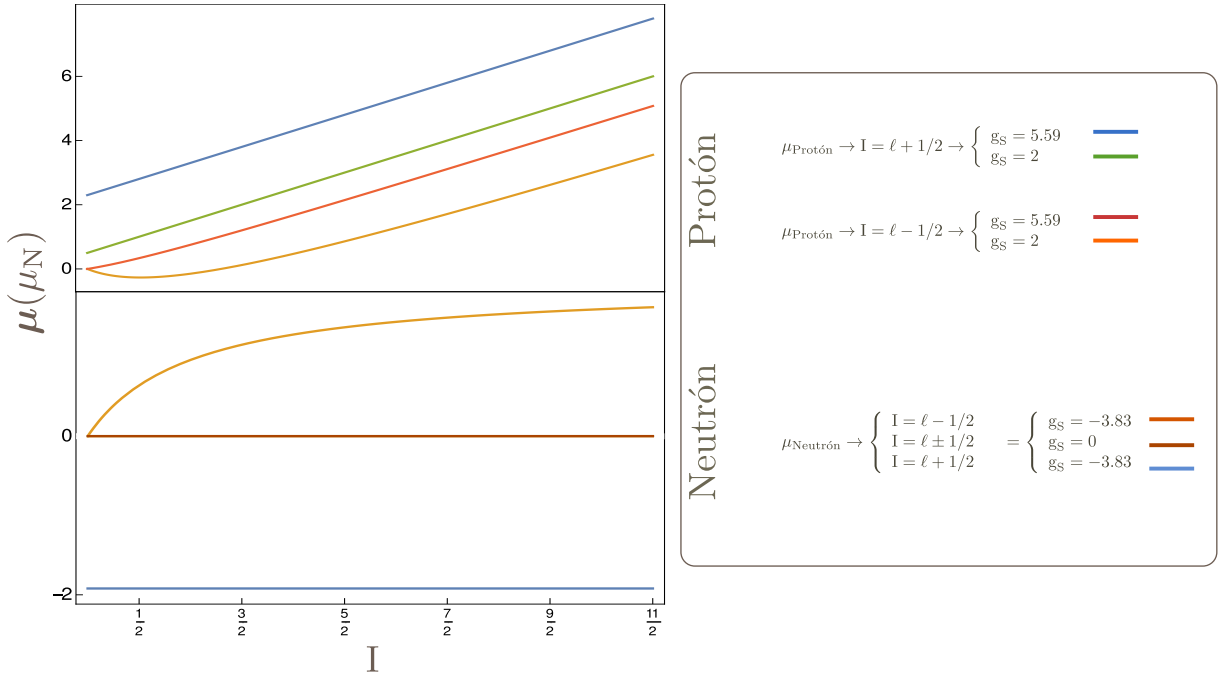


Figure B.2: *Schmidt lines with different spin values.*

Although the prediction of the Schmidt lines for the value of the nuclear magnetic moment in different states of nuclear spin approximates the experimental data of the magnetic moment of some nuclei, this prediction is not completely satisfactory. Figure B.3 illustrates the superposition of different experimental magnetic moment measurements for different nuclei.

The divergence between the experimental lines and the prediction of the independent particle model is attributed to a possible polarization of the rest of the nucleus, to a variation between the magnetic moment of the protons and neutrons inside the nucleus and the nucleons as free particles, to an exchange of meson streams, among others [33]. A good approximation of the

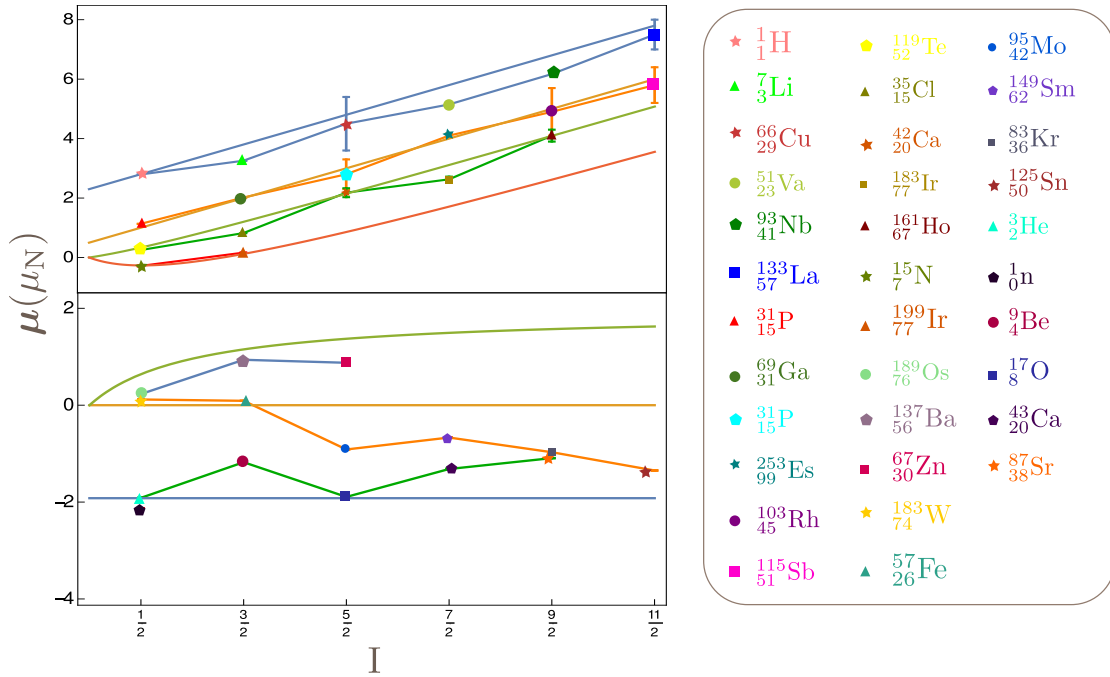


Figure B.3: Superposition of the Schmidt lines and the experimental measurements of nuclear magnetic moment of some nuclei. The experimental measurements were taken from the reference [4].

magnetic moment measurements is obtained when the spin part of the factor  $g$ , is reduced to an effective  $g_S^{\text{eff}} \approx 0.7g_S^{\text{free}}$ .



## Appendix **C**

### Larmor Theorem

---

*For a system of charged particles, all with the same charge-mass ratio, the movement of the particles subjected to a central force field and a uniform magnetic induction  $\mathbf{B}$  due to a magnetic field, will be exactly equal to movement described in the absence of  $\mathbf{B}$ , except for the superposition of a common precession of angular velocity equal to the Larmor frequency.*

#### ***Proof***

*Hypothesis: The only force that disturbs the movement of the charged particle system is the central type force.*

Consider the motion of a particle of mass  $m$  and charge  $q$  under the influence of a central-type force  $f(r)\mathbf{r}$  and the Lorentz force due to a static magnetic field  $\mathbf{B}$ .

$$\mathbf{F} = f(r)\mathbf{r} + q\mathbf{v} \times \mathbf{B}. \quad (\text{C.1})$$

If the particle is observed from an inertial frame of reference with coordinates  $\mathbf{r}$  and from a frame of reference that is rotating with a velocity  $\boldsymbol{\omega}$  with respect to the frame of inertial reference, with rotated coordinates  $\mathbf{r}'$ , the equation (C.1), seen from the inertial frame would be;

---


$$\mathbf{F}_{\text{inerc}} = f(r)\mathbf{r} + q\mathbf{v}_{\text{inerc}} \times \mathbf{B}. \quad (\text{C.2})$$

Bearing in mind that for a rotating reference system the speed, seen from an inertial frame of reference, is given by:

$$\dot{\mathbf{r}} = \dot{\mathbf{r}}' + \boldsymbol{\omega} \times \mathbf{r}, \quad (\text{C.3})$$

where  $\mathbf{v}_{\text{inerc}} = \dot{\mathbf{r}}$  and  $\mathbf{v}_{\text{rot}} = \dot{\mathbf{r}}'$ ; acceleration is given by:

$$\ddot{\mathbf{r}} = \frac{d\mathbf{v}_{\text{rot}}}{dt} + \boldsymbol{\omega} \times \dot{\mathbf{r}}. \quad (\text{C.4})$$

Recalling  $\frac{d\mathbf{v}_{\text{rot}}}{dt} = \ddot{\mathbf{r}}' + \boldsymbol{\omega} \times \mathbf{v}_{\text{rot}}$  and  $\boldsymbol{\omega} \times \dot{\mathbf{r}} = \boldsymbol{\omega} \times \mathbf{v}_{\text{rot}} + \boldsymbol{\omega} \times (\boldsymbol{\omega} \times \mathbf{r})$  substituting  $\mathbf{a}_{\text{inerc}} = \ddot{\mathbf{r}}$  y  $\mathbf{a}_{\text{rot}} = \ddot{\mathbf{r}}'$ , (C.4) becomes in:

$$\mathbf{a}_{\text{inerc}} = \mathbf{a}_{\text{rot}} + 2\boldsymbol{\omega} \times \mathbf{v}_{\text{rot}} + \boldsymbol{\omega} \times (\boldsymbol{\omega} \times \mathbf{r}). \quad (\text{C.5})$$

Multiplying by the mass of the particle on both sides of (C.5)

$$\mathbf{F}_{\text{inerc}} = \mathbf{F}_{\text{rot}} + 2m\boldsymbol{\omega} \times \mathbf{v}_{\text{rot}} + m\boldsymbol{\omega} \times (\boldsymbol{\omega} \times \mathbf{r}). \quad (\text{C.6})$$

according with anti-commutative property of the vector product, the second term of (C.6) becomes;

$$\mathbf{F}_{\text{inerc}} = \mathbf{F}_{\text{rot}} - 2m\mathbf{v}_{\text{rot}} \times \boldsymbol{\omega} + m\boldsymbol{\omega} \times (\boldsymbol{\omega} \times \mathbf{r}). \quad (\text{C.7})$$

Equating (C.2) y (C.7), it haves:



$$\mathbf{F}_{\text{rot}} - 2m\mathbf{v}_{\text{rot}} \times \boldsymbol{\omega} + m\boldsymbol{\omega} \times (\boldsymbol{\omega} \times \mathbf{r}) = f(r)\mathbf{r} + q\mathbf{v}_{\text{inerc}} \times \mathbf{B}. \quad (\text{C.8})$$

Using (C.3), second term from right side of (C.8) is now:

$$\mathbf{F}_{\text{rot}} - 2m\mathbf{v}_{\text{rot}} \times \boldsymbol{\omega} + m\boldsymbol{\omega} \times (\boldsymbol{\omega} \times \mathbf{r}) = f(r)\mathbf{r} + q\mathbf{v}_{\text{rot}} \times \mathbf{B} + q(\boldsymbol{\omega} \times \mathbf{r}) \times \mathbf{B}. \quad (\text{C.9})$$

grouping similar terms in (C.9)

$$\mathbf{F}_{\text{rot}} - \mathbf{v}_{\text{rot}} \times (2m\boldsymbol{\omega} \times + q\mathbf{B}) + (q\mathbf{B} + m\boldsymbol{\omega})(\boldsymbol{\omega} \times \mathbf{r}) = f(r)\mathbf{r}. \quad (\text{C.10})$$

Larmor's theorem will be assumed to be true to prove the hypothesis by affirmation. Therefore if  $\boldsymbol{\omega} = -\frac{q}{2m}\mathbf{B}$  (C.10) becomes:

$$\begin{aligned} \mathbf{F}_{\text{rot}} - \mathbf{v}_{\text{rot}} \times \left( \cancel{-q\mathbf{B} \times +q\mathbf{B}} \right) - \frac{q^2}{4m} [\mathbf{B} \times (\mathbf{B} \times \mathbf{r})] &= f(r)\mathbf{r} \\ \therefore \mathbf{F}_{\text{rot}} &= f(r)\mathbf{r} + \frac{q^2}{4m} [\mathbf{B} \times (\mathbf{B} \times \mathbf{r})] \end{aligned} \quad (\text{C.11})$$

Assuming that the magnetic field involved is a weak field, the second term on the right side of (C.11) will become zero, therefore the hypothesis is affirmed that the central type force is the only one acting on the system of charged particles.



## Appendix **D**

### São Paulo Proposal

---

In the next page is attached the experimental proposal presented to the Laboratório Aberto de Física Nuclear in São Paulo, Brazil. This proposal was presented in 2018 and accepted the same year, it is scheduled to be performed in 2019.

**Research Project**

**Program to Study Reaction Mechanism and Population of excited  
nuclear states Using Alpha Transfer Reactions at the Laboratório  
Aberto de Física Nuclear, Universidad de São Paulo, Brazil**

Diego Alejandro Torres Galindo,\* Fitzgerald Ramírez Moreno, Fernando  
Cristancho Mejía, Edna Carolina Pinilla, and Ana Maria Gomez Londoño  
*Universidad Nacional de Colombia, Bogotá, Colombia.*

José Roberto Brandão de Oliveira, Nilberto Medina, V. Kurman, V.A.P. Aguiar, S.  
Alberton, J.A. Alcántara-Núñez, P.R.P. Allegro, R. Escudeiro, R. V. Ribas, and A. Souza  
*Instituto de Física da USP - Departamento de Física Nuclear, São Paulo, Brazil*

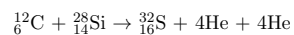
V.A.B. Zagatto  
*IFUFF, Niterói, Rio de Janeiro, Brazil*

Corina Andreoui  
*Simon Fraser University, Canada.*

## Abstract

A research program to study  $\alpha$ -transfer reactions from  $n\alpha$  nuclei-like systems, such as  $^{12}\text{C}$ ,  $^{16}\text{O}$ ,  $^{20}\text{Ca}$ ,  $^{24}\text{Mg}$ , and the subsequent population mechanism of excited states of the formed nuclei is proposed. The study will provide information of the stellar nucleo-synthesis processes and nuclear structure information. The experimental tools will involve the use of particle- $\gamma$  coincidences using high-efficiency scintillator detectors LYSO(Ce), coupled to silicon photo-multipliers (SiPM), for  $\gamma$ -ray detection and to an array of  $\Delta E - E$  photoswich type (Plastic Scintillators). The Tandem Pelletron accelerator at University of Sao Paulo, Brazil, will be utilized to accelerate the nuclei of interest at energies around the coulomb barrier. Theoretically, the use of the Sao Paulo potential in conjunction with recent developed tools will be utilized to describe and test the results.

The initial proposed experiment is:



With a range of energies between 0.7 to 1.3 the Coulomb barrier, thus between 9.31 MeV to 17.3 MeV beam energy. A total of five days of beam time is requested plus two days for the preparing of the experimental setup.

Keywords: alpha transfer, Sao Paulo potential

---

\* datorresg@unal.edu.co

## A. Introduction

The nuclear structure information is closely related to the reaction mechanism [8], it is expected that due to its high binding energy the transfer of an  $\alpha$  cluster from a projectile or from a target will yield information on the structure of the residual nuclei. Research around  $\alpha$  transfer has two focal and related points:

1. the reaction mechanism of the process.
2. the nuclear structure information, such as  $\alpha$  widths, spectroscopic factors, and wave functions as the ultimate goal.

In recent years the use of  $\alpha$ -transfer reactions near and even below the coulomb barrier to populate excited states in radioactive nuclei has allowed the study of magnetic and electric moments using stable beams [6, 15–18, 24–26, 30]. The produced nuclei are created with enough yields to allow the use of experimental techniques such as the Transient Field and the Doppler Shift Attenuation Method, to study the main components of the nuclear wave function in states near to the ground state. Many of the produced nuclei cannot be produced with enough intensity in the present reaction beam facilities, and it is worth to mention that the understanding of  $\alpha$ -transfer reactions will also provide information to use in future experiments using radioactive beams, this will open the possibility to have more available and clean radioactive beams.

Magnetic moments measurements that make use of  $\alpha$ -transfer reactions have a lack of precision due to the poor nuclear-spin alignment of the reaction. Compared with coulomb excitation reactions, with errors of the order of 5%, the  $\alpha$ -transfer provides values of around 40%. The understanding of the reaction process and the population mechanism is pivotal to re-evaluate the obtained values, and to propose future experiments to measure magnetic and electric moments in radioactive species.

The study of  $\alpha$ -transfer reactions has been subject of study for several decades, and most of those agree that the reaction mechanism is complex and the main focus has been in the explanation of  $\alpha$ -particle clustering in nuclei. The use of particle- $\gamma$  correlations, using high-efficiency setups, gives a powerful tool to extract detailed information in the reaction mechanism and the structure of the states, in conjunction with theoretical tools such as:

- Distorted Wave Born Approximation (DWBA) in conjunction with optical potential,

as the Sao Paulo potential for example, to explain the reaction mechanism [3, 11, 19, 27]. Also, algebraic scattering theory has been utilized to understand the angular distribution in certain systems [28].

- For the structure part three main models are worth to be mentioned [9]:
  1.  $J - J$  shell model.
  2. the SU(3) model.
  3. The pairing vibrational model.

To date, there is a lack of information in the reaction mechanism and the population of the states of the residual nuclei for reactions around the coulomb barrier. The use of particle- $\gamma$  coincidence provides one of the most outstanding experimental tools to study this type of reaction.

In this document, a experimental campaign to study the  $\alpha$ -transfer mechanism for energies around and bellow the Coulomb barrier will be proposed. The use of a  $\gamma$ -ray array of LYSO(Ce) detectors and Ge detectors, in conjunction with telescopes SiPM for the detection of residual nuclei will be utilized [13]. The Pelletron at Sao Paulo University will be used to accelerate the ion of interest. The experimental results will be analyzed with the use of the Sao Paulo potential.

## B. Alpha transfer reactions

During the 60's and the 70's the study of  $\alpha$ -transfer reactions was an active area of study, leaded by the existence of new available beams of lithium, oxygen, nitrogen, flourine and neon. The theoretical description used the DWBA formalism, and bellow the coulomb barrier probably a direct tunneling mechanism is dominating the reaction. Experimentally, transfer bellow the coulomb barrier has been observed recently in several experiments, and a clear explanation for this process, including the effects of deformation and/or diffuseness of the barrier, is needed.

The relationship between the reaction mechanism and the structure is alto to be investigated. An overview of some experimental and theoretical tool in  $\alpha$  transfer reactions is presented in the Table below.

Nuclear Model	Studied Reaction	Reference
Anomalous large-angle alpha scattering, optical model and Regge pole calculation		[10]
Distorted Wave Born Approximation using the Gobbi and Vandenbosch potentials		[3]
Three-Body Model and continuum-discretized coupled-channels method (CDCC)		[20]
The j-j coupled Shell Model, The SU(3) model, The pairing Vibration Model		[9]
Optical model and closed formalism parameters		[27]
The alpha particle model for $^{16}\text{O}$ and $^{12}\text{C}$		[21]
Modified DWBA model considering the reaction take place at the nuclear surface. It has useful to consider the introduction of interference and recoil effects which are not considered by DWBA model. The alternative is the use of phenomenological calculations considering the plane wave approximation		[8]
Intranuclear cascade model	$\alpha+^{27}\text{Al}$	[23]
Single folding optical model	$\alpha+^{24,28,32,40}\text{Mg,Si,S,Ca}$	[2]
semimicroscopic single folding potentials	$^4\text{He}+^{12}\text{C}$ and $^4\text{He}+^{16}\text{O}$	[1]
Optical model code SPI-GENOA	$^{12}\text{C}(^{16}\text{O}, ^{12}\text{C})^{16}\text{O}$ & $^{16}\text{O}(^{12}\text{C}, ^{16}\text{O})^{12}\text{C}$	[22]
DWBA calculations in combination with extensive shell-model calculations	$^{32}\text{S}(^{16}\text{O}, ^{12}\text{C})^{36}\text{Ar}$	[5]
SU(3). Calculations of $^8\text{Be}$	$^{16}\text{O}, ^{24,26}\text{Mg}, ^{28}\text{Si}, ^{32}\text{S}, ^{40}\text{Ca}(\alpha, ^{12}\text{C})$	[4]
Microscopic and macroscopic DWBA	$^{28}\text{Si}(\alpha, \text{d})^{30}\text{P}$ & $^{32}\text{S}(\alpha, \text{d})^{34}\text{Cl}$	[12]
DWBA. $\alpha$ -transfer reaction between light nuclei.	$^{20}\text{Ne}(^{16}\text{O}, ^{20}\text{Ne})^{16}\text{O}$	[29]
Alpha transfer reaction and distorted-wave Born approximation analysis.	$^{27}\text{Al}(^6\text{Li}, ^2\text{H})^{31}\text{P}$ , $^{29}\text{Si}(^6\text{Li}, ^2\text{H})^{33}\text{S}$ $^{31}\text{P}(^6\text{Li}, ^2\text{H})^{35}\text{Cl}$	[14]



---

Alpha transfer reaction in combination with	[18],
Transient Field Technique	[16],
	[15],
	[24],
	[7],
	[31]

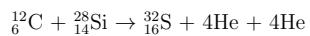
---

### C. Proposed Experiment

The use of particle- $\gamma$  correlations is the proposed experimental technique. This will allow the study of both, the reaction mechanism and the nuclear structure of the systems. Recent experiments use  $\alpha$ -transfer as a mechanism to populate excited states in radioactive nuclei. The setup is presented in Fig. 2 and results from particle- $\gamma$  coincidences are presented in Fig. 1.

The obtaining of a detailed particle- $\gamma$  angular correlation is one experimental challenge of the proposal. To do this a highly efficient setup will be utilized, composed by  $\gamma$ -ray LYSO scintillator detectors, see Fig. 3, working in coincidence with 16  $\Delta E$ - $E$  telescopes.

The proposed experiment will be



At beam energies between 9.31 MeV to 17.3 MeV, the Coulomb barrier is estimated to be at  $V_c = 13.13$  MeV.

A minimum of 5 measures should be taken along this range. With a cross section of around 150 mb and a current of 1 pnA, and a efficiency detection of around 2% for the system working in coincidence, it is estimated that a day of data taking per energy will be required. This gives a total of five days of experiment.

A deep understanding of the  $\alpha$ -transfer mechanism from  $n\alpha$  nuclei is expected to be

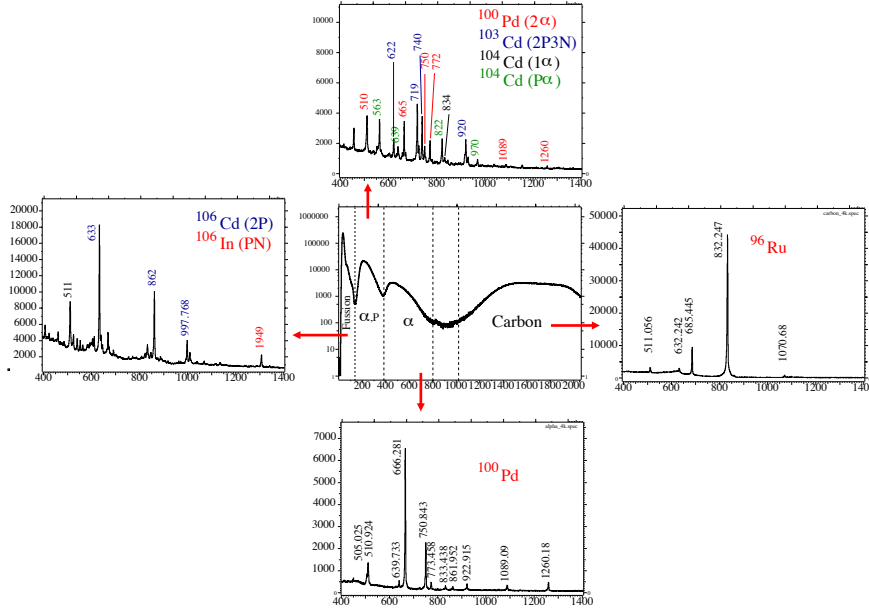


FIG. 1. Results from the  $^{96}\text{Ru}+^{12}\text{C}$  reaction at 350 MeV [15], the coulomb barrier is estimated at  $\sim 335$  MeV, the energy at the middle of the target is around the Coulomb barrier. The experimental setup is presented at figure 2. The central figure corresponds to the signals from the particle detector, silicon PIPs. Outside figures correspond to the  $\gamma$ -ray signals from the Ge-Clover detectors in coincidence with the different particle regions. The signals from the particle detector are very clean, and allows a clear identification of the residual nuclei.

obtained as a result of this project.

- 
- [1] A.H. Al-Ghamdi, A.A. Ibraheem, and M.E.-A. Farid. An investigation of  $^4\text{He}+^{12}\text{C}$  and  $^4\text{He}+^{16}\text{O}$  reactions using the cluster model. *Communications in Theoretical Physics*, 58(1):135–140, 2012.

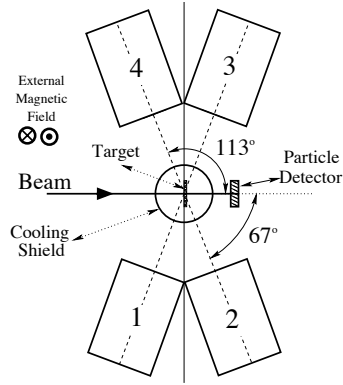


FIG. 2. The experimental setup utilized in experiments reported in Ref. [15, 24] to study magnetic moments using  $\alpha$ -transfer reactions from a carbon target in inverse kinematic reactions. Gamma-ray Ge-Clover detectors 2 and 3 were placed at  $\pm 67^\circ$  with respect to the beam, while clovers 1 and 4 were placed at  $\pm 113^\circ$ . A silicon PIPs particle detector was positioned behind the target to detect the  ${}^8\text{Be}=2\alpha$  particles. A heavy-ion beam impact a multilayered target with carbon as the first layer. For inverse kinematic reactions the  ${}^{12}\text{C}$  layer provides the environment for both  $\alpha$ -transfer and Coulomb-excitation reactions, producing highly forward-focused  ${}^{12}\text{C}$  ions and  $\alpha$  particles from the decay of  ${}^8\text{Be}$ , with distinct energies for each reaction. Figure 1 presents results from one of the experiments.

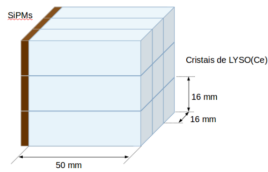


FIG. 3. Scintillator  $\gamma$ -ray detector LYSO(Ce). LYSO crystal is an ideal generation scintillator crystal. LYSO (Cerium-doped Lutetium Yttrium Orthosilicate.) LYSO crystal has the advantages of high light output and density, quick decay time, adequate energy resolution and low cost.

- [2] A.H. Al-Ghamdi, A.A. Ibraheem, and M.E.-A. Farid. Comparative study of alpha + nucleus elastic scattering using different models. *International Journal of Modern Physics E*, 24(1), 2015.
- [3] A.I. Assad and H.S. Ashour. Analysis of alpha transfer reactions using different optical potentials. *Journal of Applied Sciences*, 7(7):1001–1004, 2007.
- [4] F.D. Becchetti, K.T. Hecht, J. Jänecke, D. Overway, and G. Kekelis.  $^{16}\text{O}$ ,  $^{24,26}\text{Mg}$ ,  $^{28}\text{Si}$ ,  $^{32}\text{S}$ ,  $^{40}\text{Ca}(\alpha, ^{12}\text{C})$  and multi- $\alpha$ -cluster transfer reactions. *Nuclear Physics, Section A*, 339(1):132–156, 1980.
- [5] A. Becker, C. Alderliesten, E.A. Bakkum, C.P.M. Van Engelen, and R. Kamermans. Four-nucleon transfer with the  $^{32}\text{S}(^{16}\text{O}, ^{12}\text{C})^{36}\text{Ar}$  reaction. *Nuclear Physics, Section A*, 412(1):159–188, 1984.
- [6] N. Benczer-Koller, G. J. Kumbartzki, K.-H. Speidel, D. A. Torres, S. J. Q. Robinson, Y. Y. Sharon, J. M. Allmond, P. Fallon, I. Abramovic, L. A. Bernstein, J. E. Bevens, H. L. Crawford, Z. E. Guevara, A. M. Hurst, L. Kirsch, T. A. Laplace, A. Lo, E. F. Matthews, I. Mayers, L. W. Phair, F. Ramirez, and A. Wiens. Magnetic moment and lifetime measurements of coulomb-excited states in  $^{106}\text{Cd}$ . *Phys. Rev. C*, 94:034303, Sep 2016.
- [7] N. Benczer-Koller, G. J. Kumbartzki, K.-H. Speidel, D. A. Torres, S. J. Q. Robinson, Y. Y. Sharon, J. M. Allmond, P. Fallon, I. Abramovic, L. A. Bernstein, J. E. Bevens, H. L. Crawford, Z. E. Guevara, A. M. Hurst, L. Kirsch, T. A. Laplace, A. Lo, E. F. Matthews, I. Mayers, L. W. Phair, F. Ramirez, and A. Wiens. Magnetic moment and lifetime measurements of coulomb-excited states in  $^{106}\text{Cd}$ . *Phys. Rev. C*, 94:034303, Sep 2016.
- [8] K Bethge. Alpha-particle transfer reactions. *Annual Review of Nuclear Science*, 20(1):255–288, 1970.
- [9] R.R. Betts. Alpha-transfer reactions. *International Workshop on Nuclear Structure*, 1981.
- [10] P. Braun-Munzinger and J. Barrette. Dynamical aspects of large angle heavy-ion scattering. *Physics Reports*, 87(5):209 – 258, 1982.
- [11] L. F. Canto, R. Donangelo, M. S. Hussein, and A. Lépine-Szily. Multistep  $\alpha$ -particle-transfer description of anomalous heavy-ion elastic scattering. *Phys. Rev. Lett.*, 51:95–98, Jul 1983.
- [12] R.J. De Meijer, L.W. Put, J.J. Akkerman, J.C. Vermeulen, and C.R. Bingham. Microscopic and macroscopic dwba analysis of the reactions  $^{28}\text{Si}(\alpha, d)^{30}\text{P}$ ,  $^{32}\text{S}(d, \alpha)^{30}\text{P}$  and  $^{32}\text{S}(\alpha, d)^{34}\text{Cl}$  studied at  $e_\alpha = 50$  mev and  $e_d = 40$  mev. *Nuclear Physics, Section A*, 386(2):200–244, 1982.

- [13] Prof. Dr. Jose Roberto Brandao de Oliveira. Projeto de pesquisa nucleos fracamente ligados e mecanismos de quebra com e sem transferencias. Unpublished project, internal communication, 2017.
- [14] M.A. Eswaran, H.E. Gove, R. Cook, and B. Sikora. The  $\alpha$ -transfer reactions  $^{27}\text{Al}(^6\text{Li}, d)^{31}\text{P}$ ,  $^{29}\text{Si}(^6\text{Li}, d)^{33}\text{S}$  and  $^{31}\text{P}(^6\text{Li}, d)^{35}\text{Cl}$  at 36 mev. *Nuclear Physics, Section A*, 325(1):269–282, 1979.
- [15] D.A. Torres et al. First  $g$ -factor measurements of the  $2_1^+$  and the  $4_1^+$  states of radioactive  $^{100}\text{Pd}$ . *Phys. Rev. C*, 84:044327, Oct 2011.
- [16] G.J. Kumbartzki et al. Structure of the Sr-Zr isotopes near and at the magic  $N = 50$  shell from  $g$ -factor and lifetime measurements in  $^{88}_{40}\text{Zr}$  and  $^{84,86,88}_{38}\text{Sr}$ . *Phys. Rev. C*, 85:044322, Apr 2012.
- [17] K.-H. Speidel et al. Experimental  $g$  factors and  $B(E2)$  values in Ar isotopes: Crossing the  $N=20$  semi-magic divide. *Physics Letters B*, 632(2-3):207 – 211, 2006.
- [18] S. Schielke et al. First measurement and shell model interpretation of the  $g$  factor of the  $2_1^+$  state in self-conjugate radioactive  $^{44}\text{Ti}$ . *Physics Letters B*, 567(3-4):153 – 158, 2003.
- [19] R. Lichtenthaler Filho, A. Lepine-Szily, A. C. C. Villari, and O. Portezan Filho. Effect of  $\alpha$ -transfer polarization potential in the  $^{24}\text{Mg}+^{16}\text{O}$  system. *Phys. Rev. C*, 39:884–890, Mar 1989.
- [20] Tokuro Fukui, Kazuyuki Ogata, and Masanobu Yahiro. Three-body model analysis of sub-barrier alpha transfer reaction. *Prog.Theor.Phys*, 125:1193–1204, 2011.
- [21] Goran Faldt and Lars Gislen. Fragmentation of relativistic nuclei in the  $\alpha$ -particle model. *Nuclear Physics A*, 254(2):341 – 348, 1975.
- [22] S. Hamada, N. Burtbayev, K.A. Gridnev, and N. Amangeldi. Analysis of alpha-cluster transfer in  $^{16}\text{o}+^{12}\text{c}$  and  $^{12}\text{c}+^{16}\text{o}$  at energies near coulomb barrier. *Nuclear Physics A*, 859(1):29–38, 2011.
- [23] M.J. Kobra, G. Watanabe, Y. Yamaguchi, Y. Uozumi, and M. Nakano. An intranuclear cascade model for inelastic scattering and breakup reactions involving deuterons and alpha particles. *Journal of Nuclear Science and Technology*, 55(2):209–216, 2018.
- [24] G. J. Kumbartzki, N. Benczer-Koller, K.-H. Speidel, D. A. Torres, J. M. Allmond, P. Fallon, I. Abramovic, L. A. Bernstein, J. E. Bevins, H. L. Crawford, Z. E. Guevara, G. Gurdal, A. M. Hurst, L. Kirsch, T. A. Laplace, A. Lo, E. F. Matthews, I. Mayers, L. W. Phair, F. Ramirez,

- S. J. Q. Robinson, Y. Y. Sharon, and A. Wiens.  $z = 50$  core stability in  $^{110}\text{Sn}$  from magnetic-moment and lifetime measurements. *Phys. Rev. C*, 93:044316, Apr 2016.
- [25] G.J. Kumbartzki. Transition from collectivity to single-particle degrees of freedom from magnetic moment measurements on  $^{82}_{38}\text{Sr}_{44}$  and  $^{90}_{38}\text{Sr}_{52}$ . *Phys. Rev. C*, 89:064305, Jun 2014.
- [26] J. Leske, K.-H. Speidel, S. Schielke, O. Kenn, J. Gerber, P. Maier-Komor, S. J. Q. Robinson, A. Escuderos, Y. Y. Sharon, and L. Zamick. Nuclear structure of the first  $2+$  state in radioactive  $^{68}\text{Ge}$  based on  $g$  factor and lifetime measurements. *Phys. Rev. C*, 71(4):044316, Apr 2005.
- [27] R. Lichtenthaler, A. Lépine-Szily, A. C. C. Villari, W. Mittig, V. J. G. Porto, and C. V. Acquadro. Effect of the  $\alpha$ -transfer reaction on the elastic scattering of  $^{12}\text{C}+^{24}\text{Mg}$ . *Phys. Rev. C*, 26:2487–2495, Dec 1982.
- [28] A. Lépine-Szily, M.M. Obuti, R. Lichtenthaler Filho, J.M. Oliveira, and A.C.C. Villari. Back-angle anomaly and coupling between seven reaction channels of  $^{12}\text{c} + ^{24}\text{Mg}$  using algebraic scattering theory. *Physics Letters B*, 243(1):23 – 28, 1990.
- [29] T. Motobayashi, I. Kohno, T. Ooi, and S. Nakajima. alpha-transfer reactions between light nuclei. *Nuclear Physics, Section A*, 331(1):193–212, 1979.
- [30] K.-H. Speidel, J. Leske, S. Schielke, S.C. Bedi, O. Zell, P. Maier-Komor, S.J.Q. Robinson, Y. Y. Sharon, and L. Zamick. Low-level structure of  $^{52}\text{Ti}$  based on  $g$  factor and lifetime measurements. *Physics Letters B*, 633(2-3):219 – 224, 2006.
- [31] DA Torres and F Ramfrez. Populating low-spin states in radioactive nuclei to measure magnetic moments using the transient field technique. *Acta Physica Polonica*, 47:405, 2016.

## Appendix **E**

### TRIUMF possible experiments list

---

The following table shows all possible Alpha-Transfer reactions that can be obtained from shooting all beams available at TRIUMF lab to  $^{12}\text{C}$ -layer as a target. The column labeled as  $\tau$  contains the time-life values of the resulting nuclei.

Table E.1: *Table of Alpha-Transfer reactions with available beams (parent) at TRIUMF [7]. All lifetimes corresponds to ground state of the daughter nuclei.  $\tau$  values were taken from [8].*

Parent	Daughter	$\tau$
$^6\text{He}$	$^{10}\text{Be}$	$1.5 \times 10^6$ ( $4 \times 10^6$ ) y
$^8\text{He}$	$^{12}\text{Be}$	21.47(4) ms
$^6\text{Li}$	$^{10}\text{B}$	stable
$^7\text{Li}$	$^{11}\text{B}$	stable
$^8\text{Li}$	$^{12}\text{B}$	20.26(2) ms
$^9\text{Li}$	$^{13}\text{B}$	17.33(17) ms
$^{11}\text{Li}$	$^{15}\text{B}$	10.18(3) ms

Continued on next column

---

Continued from previous column

Parent	Daughter	$\tau$
$^7\text{Be}$	$^{11}\text{C}$	20.364(14) m
$^9\text{Be}$	$^{13}\text{C}$	stable
$^{10}\text{Be}$	$^{14}\text{C}$	5700(30) y
$^{11}\text{Be}$	$^{15}\text{C}$	2.449(5) s
$^{12}\text{Be}$	$^{16}\text{C}$	0.747(8) s
$^9\text{C}$	$^{13}\text{O}$	8.58(5) ms
$^{10}\text{C}$	$^{14}\text{O}$	70.62(15) s
$^{11}\text{C}$	$^{15}\text{O}$	122.24(16) s
$^{15}\text{C}$	$^{19}\text{O}$	26.88(5) s
$^{16}\text{C}$	$^{20}\text{O}$	13.51(5) s
$^{13}\text{N}$	$^{17}\text{F}$	64.49(16) s
$^{14}\text{O}$	$^{18}\text{Ne}$	1.66(17) s
$^{15}\text{O}$	$^{19}\text{Ne}$	17.22(2) s
$^{19}\text{O}$	$^{23}\text{Ne}$	37.24(12) s
$^{20}\text{O}$	$^{24}\text{Ne}$	3.38(2) m
$^{21}\text{O}$	$^{25}\text{Ne}$	602(8) ms
$^{17}\text{F}$	$^{21}\text{Na}$	22.49(4) s

Continued on next column

---

Continued from previous column

Parent	Daughter	$\tau$
$^{18}\text{F}$	$^{22}\text{Na}$	2.6018(22) y
$^{20}\text{F}$	$^{24}\text{Na}$	14.997(12) y
$^{21}\text{F}$	$^{25}\text{Na}$	59.1(6) s
$^{22}\text{F}$	$^{26}\text{Na}$	1.07128(25) s
$^{23}\text{F}$	$^{27}\text{Na}$	301(6) ms
$^{17}\text{Ne}$	$^{21}\text{Mg}$	122(33) ms
$^{18}\text{Ne}$	$^{22}\text{Mg}$	3.8755(1) s
$^{19}\text{Ne}$	$^{23}\text{Mg}$	11.317(11) s
$^{23}\text{Ne}$	$^{27}\text{Mg}$	9.458(12) m
$^{24}\text{Ne}$	$^{28}\text{Mg}$	20.915(9) h
$^{25}\text{Ne}$	$^{29}\text{Mg}$	1.3(12) s
$^{20}\text{Na}$	$^{24}\text{Al}$	20.053(4) s
$^{21}\text{Na}$	$^{25}\text{Al}$	7.183(12) s
$^{22}\text{Na}$	$^{26}\text{Al}$	$7.17 \times 10^5 (24 \times 10^5)$ y
$^{23}\text{Na}$	$^{27}\text{Al}$	stable
$^{24}\text{Na}$	$^{28}\text{Al}$	2.245(2) m
$^{25}\text{Na}$	$^{29}\text{Al}$	6.56(6) m
$^{26}\text{Na}$	$^{30}\text{Al}$	3.62(6) s
$^{27}\text{Na}$	$^{31}\text{Al}$	644(25) ms
$^{28}\text{Na}$	$^{32}\text{Al}$	31.9(8) ms
$^{29}\text{Na}$	$^{33}\text{Al}$	41.7(2) ms
$^{30}\text{Na}$	$^{34}\text{Al}$	56.3(6) ms
$^{31}\text{Na}$	$^{35}\text{Al}$	37.6(14) ms
$^{32}\text{Na}$	$^{36}\text{Al}$	94(37) ms

Continued on next column

Continued from previous column

Parent	Daughter	$\tau$
$^{20}\text{Mg}$	$^{24}\text{Si}$	140.5(15) ms
$^{21}\text{Mg}$	$^{25}\text{Si}$	220(3) ms
$^{22}\text{Mg}$	$^{26}\text{Si}$	2.2453(7) s
$^{23}\text{Mg}$	$^{27}\text{Si}$	4.15(4) s
$^{24}\text{Mg}$	$^{28}\text{Si}$	stable
$^{25}\text{Mg}$	$^{29}\text{Si}$	stable
$^{26}\text{Mg}$	$^{30}\text{Si}$	stable
$^{27}\text{Mg}$	$^{31}\text{Si}$	157.36(6) m
$^{28}\text{Mg}$	$^{32}\text{Si}$	153(19) y
$^{29}\text{Mg}$	$^{33}\text{Si}$	6.11(21) s
$^{30}\text{Mg}$	$^{34}\text{Si}$	2.77(20) s
$^{31}\text{Mg}$	$^{35}\text{Si}$	780(120) ms
$^{32}\text{Mg}$	$^{36}\text{Si}$	450(60) ms
$^{33}\text{Mg}$	$^{37}\text{Si}$	90(60) ms
$^{34}\text{Mg}$	$^{38}\text{Si}$	95(10) ms
$^{35}\text{Mg}$	$^{39}\text{Si}$	47.5(20) ms
$^{23}\text{Al}$	$^{27}\text{P}$	260(80) ms
$^{24}\text{Al}$	$^{28}\text{P}$	270.3(5) ms
$^{25}\text{Al}$	$^{29}\text{P}$	4.142(15) s
$^{26}\text{Al}$	$^{30}\text{P}$	2.498(4) m
$^{28}\text{Al}$	$^{32}\text{P}$	14.268(5) d
$^{29}\text{Al}$	$^{33}\text{P}$	25.35(11) d
$^{30}\text{Al}$	$^{34}\text{P}$	12.43(10) s
$^{33}\text{Cl}$	$^{37}\text{K}$	1.226(7) s

Continued on next column



Continued from previous column

Parent	Daughter	$\tau$
$^{34}\text{Cl}$	$^{38}\text{K}$	7.636(18) m
$^{38}\text{Cl}$	$^{42}\text{K}$	12.355(7) h
$^{39}\text{Cl}$	$^{43}\text{K}$	22.3(1) h
$^{40}\text{Cl}$	$^{44}\text{K}$	22.13(19) m
$^{41}\text{Cl}$	$^{45}\text{K}$	17.81(61) m
$^{33}\text{Ar}$	$^{37}\text{Ca}$	181.1(10) ms
$^{34}\text{Ar}$	$^{38}\text{Ca}$	440(12) ms
$^{35}\text{Ar}$	$^{39}\text{Ca}$	859.6(14) ms
$^{36}\text{Ar}$	$^{40}\text{Ca}$	$> 3.0 \times 10^{21}$ y
$^{41}\text{Ar}$	$^{45}\text{Ca}$	162.61(9) d
$^{43}\text{Ar}$	$^{47}\text{Ca}$	4.536(3) d
$^{44}\text{Ar}$	$^{48}\text{Ca}$	$> 5.8 \times 10^{22}$ y
$^{45}\text{Ar}$	$^{49}\text{Ca}$	8.178(6) m
$^{46}\text{Ar}$	$^{50}\text{Ca}$	31.9(6) s
$^{35}\text{K}$	$^{39}\text{Sc}$	300 ns
$^{36}\text{K}$	$^{40}\text{Sc}$	182.3(7) ms
$^{37}\text{K}$	$^{41}\text{Sc}$	596.3(17) ms
$^{38}\text{K}$	$^{42}\text{Sc}$	680.79(28) ms
$^{42}\text{K}$	$^{46}\text{Sc}$	83.79(4) d
$^{43}\text{K}$	$^{47}\text{Sc}$	3.3492(6) d
$^{44}\text{K}$	$^{48}\text{Sc}$	43.67(9) h
$^{45}\text{K}$	$^{49}\text{Sc}$	57.18(13) m
$^{46}\text{K}$	$^{50}\text{Sc}$	102.5(5) s
$^{47}\text{K}$	$^{51}\text{Sc}$	12.4(1) s

Continued on next column

Continued from previous column

Parent	Daughter	$\tau$
$^{48}\text{K}$	$^{52}\text{Sc}$	8.2(2) s
$^{49}\text{K}$	$^{53}\text{Sc}$	2.6(4) s
$^{50}\text{K}$	$^{54}\text{Sc}$	526(15) ms
$^{51}\text{K}$	$^{55}\text{Sc}$	105(6) ms
$^{52}\text{K}$	$^{56}\text{Sc}$	26(6) ms
$^{38}\text{Ca}$	$^{42}\text{Ti}$	208.65(8) ms
$^{39}\text{Ca}$	$^{43}\text{Ti}$	509(5) ms
$^{47}\text{Ca}$	$^{51}\text{Ti}$	5.76(1) m
$^{49}\text{Ca}$	$^{53}\text{Ti}$	32.7(9) s
$^{50}\text{Ca}$	$^{54}\text{Ti}$	2.1(10) s
$^{51}\text{Ca}$	$^{55}\text{Ti}$	1.3(1) s
$^{52}\text{Ca}$	$^{56}\text{Ti}$	0.2(5) s
$^{50}\text{Sc}$	$^{54}\text{V}$	49.8(5) s
$^{51}\text{Sc}$	$^{55}\text{V}$	6.54(15) s
$^{52}\text{Sc}$	$^{56}\text{V}$	0.216(4) s
$^{46}\text{Ti}$	$^{50}\text{Cr}$	$1.3 \times 10^{18}$ y
$^{47}\text{Ti}$	$^{51}\text{Cr}$	27.704(4) d
$^{48}\text{Ti}$	$^{52}\text{Cr}$	stable
$^{49}\text{Ti}$	$^{53}\text{Cr}$	stable
$^{50}\text{Ti}$	$^{54}\text{Cr}$	stable
$^{51}\text{Ti}$	$^{55}\text{Cr}$	3.4976(3) m
$^{52}\text{Ti}$	$^{56}\text{Cr}$	5.94(10) m
$^{53}\text{Ti}$	$^{57}\text{Cr}$	21.1(10) s
$^{54}\text{V}$	$^{58}\text{Mn}$	3(1) s

Continued on next column

## Continued from previous column

Parent	Daughter	$\tau$
$^{51}\text{Cr}$	$^{55}\text{Fe}$	2.744(9) y
$^{56}\text{Cr}$	$^{60}\text{Fe}$	$2.6 \times 10^6(4 \times 10^6)$ y
$^{49}\text{Mn}$	$^{53}\text{Co}$	240(9) ms
$^{50}\text{Mn}$	$^{54}\text{Co}$	193.28(7) ms
$^{51}\text{Mn}$	$^{55}\text{Co}$	17.53(3) h
$^{52}\text{Mn}$	$^{56}\text{Co}$	77.236(23) d
$^{53}\text{Mn}$	$^{57}\text{Co}$	271.74(6) d
$^{54}\text{Mn}$	$^{58}\text{Co}$	70.86(6) d
$^{55}\text{Mn}$	$^{59}\text{Co}$	stable
$^{56}\text{Mn}$	$^{60}\text{Co}$	1925.28(14) d
$^{57}\text{Mn}$	$^{61}\text{Co}$	1.649(5) h
$^{58}\text{Mn}$	$^{62}\text{Co}$	1.54(10) m
$^{59}\text{Mn}$	$^{63}\text{Co}$	27.4(5) s
$^{60}\text{Mn}$	$^{64}\text{Co}$	0.3(3) s
$^{61}\text{Mn}$	$^{65}\text{Co}$	1.16(3) s
$^{62}\text{Mn}$	$^{66}\text{Co}$	0.2(2) s
$^{63}\text{Mn}$	$^{67}\text{Co}$	0.425(20) s
$^{64}\text{Mn}$	$^{68}\text{Co}$	0.2(2) s
$^{65}\text{Mn}$	$^{69}\text{Co}$	227(11) ms
$^{66}\text{Mn}$	$^{70}\text{Co}$	112(7) ms
$^{67}\text{Mn}$	$^{71}\text{Co}$	80(3) ms
$^{68}\text{Mn}$	$^{72}\text{Co}$	59.9(17) ms
$^{57}\text{Ni}$	$^{61}\text{Zn}$	89.1(2) s
$^{57}\text{Cu}$	$^{61}\text{Ga}$	167(3) ms

Continued on next column

## Continued from previous column

Parent	Daughter	$\tau$
$^{58}\text{Cu}$	$^{62}\text{Ga}$	116.121(21) ms
$^{59}\text{Cu}$	$^{63}\text{Ga}$	32.4(5) s
$^{60}\text{Cu}$	$^{64}\text{Ga}$	2.627(12) m
$^{61}\text{Cu}$	$^{65}\text{Ga}$	15.2(2) m
$^{62}\text{Cu}$	$^{66}\text{Ga}$	9.49(3) h
$^{63}\text{Cu}$	$^{67}\text{Ga}$	3.2617(5) d
$^{64}\text{Cu}$	$^{68}\text{Ga}$	67.71(8) m
$^{65}\text{Cu}$	$^{69}\text{Ga}$	stable
$^{66}\text{Cu}$	$^{70}\text{Ga}$	21.14(5) m
$^{67}\text{Cu}$	$^{71}\text{Ga}$	stable
$^{68}\text{Cu}$	$^{72}\text{Ga}$	14.1(2) h
$^{69}\text{Cu}$	$^{73}\text{Ga}$	4.86(3) h
$^{70}\text{Cu}$	$^{74}\text{Ga}$	8.12(12) m
$^{71}\text{Cu}$	$^{75}\text{Ga}$	126(2) s
$^{72}\text{Cu}$	$^{76}\text{Ga}$	32.6(6) s
$^{73}\text{Cu}$	$^{77}\text{Ga}$	13.2(2) s
$^{74}\text{Cu}$	$^{78}\text{Ga}$	5.09(5) s
$^{59}\text{Zn}$	$^{63}\text{Ge}$	150(9) ms
$^{60}\text{Zn}$	$^{64}\text{Ge}$	63.75(25) s
$^{61}\text{Zn}$	$^{65}\text{Ge}$	30.9(5) s
$^{62}\text{Zn}$	$^{66}\text{Ge}$	2.26(5) h
$^{63}\text{Zn}$	$^{67}\text{Ge}$	18.9(3) m
$^{64}\text{Zn}$	$^{68}\text{Ge}$	270.93(13) d
$^{65}\text{Zn}$	$^{69}\text{Ge}$	39.05(10) h

Continued on next column

Continued from previous column

Parent	Daughter	$\tau$
$^{66}\text{Zn}$	$^{70}\text{Ge}$	stable
$^{67}\text{Zn}$	$^{71}\text{Ge}$	11.43(3) d
$^{69}\text{Zn}$	$^{73}\text{Ge}$	stable
$^{70}\text{Zn}$	$^{74}\text{Ge}$	stable
$^{71}\text{Zn}$	$^{75}\text{Ge}$	82.78(4) m
$^{72}\text{Zn}$	$^{76}\text{Ge}$	stable
$^{73}\text{Zn}$	$^{77}\text{Ge}$	11.211(3) h
$^{74}\text{Zn}$	$^{78}\text{Ge}$	88(10) m
$^{75}\text{Zn}$	$^{79}\text{Ge}$	18.98(3) s
$^{76}\text{Zn}$	$^{80}\text{Ge}$	29.5(4) s
$^{77}\text{Zn}$	$^{81}\text{Ge}$	7.6(6) s
$^{78}\text{Zn}$	$^{82}\text{Ge}$	4.56(26) s
$^{79}\text{Zn}$	$^{83}\text{Ge}$	1.85(6) s
$^{61}\text{Ga}$	$^{65}\text{As}$	128(16) ms
$^{62}\text{Ga}$	$^{66}\text{As}$	95.77(23) ms
$^{63}\text{Ga}$	$^{67}\text{As}$	42.5(12) s
$^{64}\text{Ga}$	$^{68}\text{As}$	151.6(8) s
$^{65}\text{Ga}$	$^{69}\text{As}$	15.2(2) m
$^{66}\text{Ga}$	$^{70}\text{As}$	52.6(3) m
$^{67}\text{Ga}$	$^{71}\text{As}$	65.3(7) h
$^{68}\text{Ga}$	$^{72}\text{As}$	26(1) h
$^{69}\text{Ga}$	$^{73}\text{As}$	80.3(6) d
$^{70}\text{Ga}$	$^{74}\text{As}$	17.77(2) d
$^{71}\text{Ga}$	$^{75}\text{As}$	stable

Continued on next column

Continued from previous column

Parent	Daughter	$\tau$
$^{72}\text{Ga}$	$^{76}\text{As}$	26.24(9) h
$^{73}\text{Ga}$	$^{77}\text{As}$	38.79(5) h
$^{74}\text{Ga}$	$^{78}\text{As}$	90.7(2) m
$^{75}\text{Ga}$	$^{79}\text{As}$	9.01(15) m
$^{76}\text{Ga}$	$^{80}\text{As}$	15.2(2) s
$^{77}\text{Ga}$	$^{81}\text{As}$	33.3(8) s
$^{78}\text{Ga}$	$^{82}\text{As}$	19.1(5) s
$^{79}\text{Ga}$	$^{83}\text{As}$	13.4(3) s
$^{80}\text{Ga}$	$^{84}\text{As}$	4.2(5) s
$^{81}\text{Ga}$	$^{85}\text{As}$	2.021(12) s
$^{82}\text{Ga}$	$^{86}\text{As}$	0.945(8) s
$^{83}\text{Ga}$	$^{87}\text{As}$	484(40) ms
$^{84}\text{Ga}$	$^{88}\text{As}$	0.2(s)
$^{64}\text{Ge}$	$^{68}\text{Se}$	35.5(7) s
$^{65}\text{Ge}$	$^{69}\text{Se}$	27.4(2) s
$^{66}\text{Ge}$	$^{70}\text{Se}$	41.1(3) m
$^{67}\text{Ge}$	$^{71}\text{Se}$	4.74(5) m
$^{69}\text{Ge}$	$^{73}\text{Se}$	7.15(8) h
$^{71}\text{Ge}$	$^{75}\text{Se}$	119.7(5) d
$^{76}\text{Ge}$	$^{80}\text{Se}$	stable
$^{80}\text{Ge}$	$^{84}\text{Se}$	3.26(10) m
$^{71}\text{Se}$	$^{75}\text{Kr}$	4.6(7) m
$^{72}\text{Se}$	$^{76}\text{Kr}$	14.8(1) h
$^{73}\text{Se}$	$^{77}\text{Kr}$	74.4(6) m

Continued on next column

Continued from previous column

Parent	Daughter	$\tau$
$^{71}\text{Br}$	$^{75}\text{Rb}$	19(12) s
$^{72}\text{Br}$	$^{76}\text{Rb}$	36.5(6) s
$^{73}\text{Br}$	$^{77}\text{Rb}$	3.78(4) m
$^{74}\text{Br}$	$^{78}\text{Rb}$	17.66(3) m
$^{75}\text{Br}$	$^{79}\text{Rb}$	22.9(5) m
$^{84}\text{Br}$	$^{88}\text{Rb}$	17.773(18) m
$^{85}\text{Br}$	$^{89}\text{Rb}$	15.32(10) m
$^{86}\text{Br}$	$^{90}\text{Rb}$	158(5) s
$^{87}\text{Br}$	$^{91}\text{Rb}$	58.3(2) s
$^{88}\text{Br}$	$^{92}\text{Rb}$	4.48(3) s
$^{89}\text{Br}$	$^{93}\text{Rb}$	5.84(2) s
$^{72}\text{Kr}$	$^{76}\text{Sr}$	7.89(7) s
$^{73}\text{Kr}$	$^{77}\text{Sr}$	9(2) s
$^{74}\text{Kr}$	$^{78}\text{Sr}$	160(8) s
$^{75}\text{Kr}$	$^{79}\text{Sr}$	2.25(10) m
$^{76}\text{Kr}$	$^{80}\text{Sr}$	106.3(15) m
$^{77}\text{Kr}$	$^{81}\text{Sr}$	22.3(4) m
$^{79}\text{Kr}$	$^{83}\text{Sr}$	25.35(3) d
$^{87}\text{Kr}$	$^{91}\text{Sr}$	9.65(6) h
$^{88}\text{Kr}$	$^{92}\text{Sr}$	2.611(17) h
$^{89}\text{Kr}$	$^{93}\text{Sr}$	7.43(3) m
$^{90}\text{Kr}$	$^{94}\text{Sr}$	75.3(2) s
$^{91}\text{Kr}$	$^{95}\text{Sr}$	23.9(14) s
$^{92}\text{Kr}$	$^{96}\text{Sr}$	1.07(1) s

Continued on next column

Continued from previous column

Parent	Daughter	$\tau$
$^{93}\text{Kr}$	$^{97}\text{Sr}$	429(5) ms
$^{94}\text{Kr}$	$^{98}\text{Sr}$	0.653(2) s
$^{95}\text{Kr}$	$^{99}\text{Sr}$	0.269(1) s
$^{96}\text{Kr}$	$^{100}\text{Sr}$	202(3) ms
$^{97}\text{Kr}$	$^{101}\text{Sr}$	118(3) ms
$^{74}\text{Rb}$	$^{78}\text{Y}$	53(8) ms
$^{75}\text{Rb}$	$^{79}\text{Y}$	14.8(6) s
$^{76}\text{Rb}$	$^{80}\text{Y}$	30.1(5) s
$^{77}\text{Rb}$	$^{81}\text{Y}$	70.4(1) s
$^{78}\text{Rb}$	$^{82}\text{Y}$	8.3(20) s
$^{79}\text{Rb}$	$^{83}\text{Y}$	7.08(8) ms
$^{80}\text{Rb}$	$^{84}\text{Y}$	39.5(8) m
$^{81}\text{Rb}$	$^{85}\text{Y}$	2.68(5) h
$^{82}\text{Rb}$	$^{86}\text{Y}$	14.74(2) h
$^{83}\text{Rb}$	$^{87}\text{Y}$	79.8(3) h
$^{84}\text{Rb}$	$^{88}\text{Y}$	106.626(21) d
$^{86}\text{Rb}$	$^{90}\text{Y}$	64(21) h
$^{88}\text{Rb}$	$^{92}\text{Y}$	3.54(1) h
$^{89}\text{Rb}$	$^{93}\text{Y}$	10.18(8) h
$^{90}\text{Rb}$	$^{94}\text{Y}$	18.7(1) m
$^{91}\text{Rb}$	$^{95}\text{Y}$	10.3(1) m
$^{92}\text{Rb}$	$^{96}\text{Y}$	5.34(5) s
$^{93}\text{Rb}$	$^{97}\text{Y}$	3.75(3) s
$^{94}\text{Rb}$	$^{98}\text{Y}$	0.548(2) s

Continued on next column

Continued from previous column

Parent	Daughter	$\tau$
$^{95}\text{Rb}$	$^{99}\text{Y}$	1.484(7) s
$^{96}\text{Rb}$	$^{100}\text{Y}$	735(7) ms
$^{97}\text{Rb}$	$^{101}\text{Y}$	0.45(2) s
$^{98}\text{Rb}$	$^{102}\text{Y}$	0.36(4) s
$^{99}\text{Rb}$	$^{103}\text{Y}$	0.23(2) s
$^{100}\text{Rb}$	$^{104}\text{Y}$	197(4) ms
$^{101}\text{Rb}$	$^{105}\text{Y}$	95(9) ms
$^{76}\text{Sr}$	$^{80}\text{Zr}$	4.6(6) s
$^{78}\text{Sr}$	$^{82}\text{Zr}$	37(5) s
$^{79}\text{Sr}$	$^{83}\text{Zr}$	42(2) s
$^{80}\text{Sr}$	$^{84}\text{Zr}$	25.8(5) m
$^{81}\text{Sr}$	$^{85}\text{Zr}$	7.86(4) m
$^{83}\text{Sr}$	$^{87}\text{Zr}$	1.68(1) h
$^{85}\text{Sr}$	$^{89}\text{Zr}$	78.41(12) h
$^{87}\text{Sr}$	$^{91}\text{Zr}$	stable
$^{91}\text{Sr}$	$^{95}\text{Zr}$	64.032(6) d
$^{92}\text{Sr}$	$^{96}\text{Zr}$	$2.0 \times 10^{19} (4 \times 10^{19})$ y
$^{93}\text{Sr}$	$^{97}\text{Zr}$	16.749(8) h
$^{94}\text{Sr}$	$^{98}\text{Zr}$	30.7(4) s
$^{95}\text{Sr}$	$^{99}\text{Zr}$	21.1(1) s
$^{96}\text{Sr}$	$^{100}\text{Zr}$	7.1(4) s
$^{97}\text{Sr}$	$^{101}\text{Zr}$	2.3(1) s
$^{98}\text{Sr}$	$^{102}\text{Zr}$	2.9(2) s
$^{99}\text{Sr}$	$^{103}\text{Zr}$	1.3(1) s

Continued on next column

Continued from previous column

Parent	Daughter	$\tau$
$^{100}\text{Sr}$	$^{104}\text{Zr}$	1.2(3) s
$^{101}\text{Sr}$	$^{105}\text{Zr}$	670(28) ms
$^{102}\text{Sr}$	$^{106}\text{Zr}$	180(9) ms
$^{83}\text{Y}$	$^{87}\text{Nb}$	3.7(1) m
$^{84}\text{Y}$	$^{88}\text{Nb}$	14.5(11) m
$^{86}\text{Y}$	$^{90}\text{Nb}$	14.6(5) h
$^{87}\text{Y}$	$^{91}\text{Nb}$	$6.8 \times 10^2 (13 \times 10^2)$ y
$^{88}\text{Y}$	$^{92}\text{Nb}$	$3.47 \times 10^7 (24 \times 10^7)$ y
$^{89}\text{Y}$	$^{93}\text{Nb}$	stable
$^{90}\text{Y}$	$^{94}\text{Nb}$	$2.034 \times 10^4 (16 \times 10^4)$ y
$^{91}\text{Y}$	$^{95}\text{Nb}$	34.991(6) d
$^{94}\text{Y}$	$^{98}\text{Nb}$	2.86(6) s
$^{95}\text{Y}$	$^{99}\text{Nb}$	15(2) s
$^{96}\text{Y}$	$^{100}\text{Nb}$	1.5(2) s
$^{97}\text{Y}$	$^{101}\text{Nb}$	7.1(3) s
$^{98}\text{Y}$	$^{102}\text{Nb}$	4.3(4) s
$^{99}\text{Y}$	$^{103}\text{Nb}$	1.5(2) S
$^{99}\text{Tc}$	$^{103}\text{Rh}$	stable
$^{98}\text{Ag}$	$^{102}\text{In}$	23.3(1) s
$^{99}\text{Ag}$	$^{103}\text{In}$	65 (7) s
$^{100}\text{Ag}$	$^{104}\text{In}$	1.80(3) m
$^{101}\text{Ag}$	$^{105}\text{In}$	5.07(7) m
$^{102}\text{Ag}$	$^{106}\text{In}$	6.2(1) m
$^{103}\text{Ag}$	$^{107}\text{In}$	32.4(3) m

Continued on next column

Continued from previous column

Parent	Daughter	$\tau$
$^{104}\text{Ag}$	$^{108}\text{In}$	58.0(12) m
$^{105}\text{Ag}$	$^{109}\text{In}$	4.159(10) h
$^{107}\text{Ag}$	$^{111}\text{In}$	2.8047(4) d
$^{109}\text{Ag}$	$^{113}\text{In}$	stable
$^{110}\text{Ag}$	$^{114}\text{In}$	71.9(1) s
$^{111}\text{Ag}$	$^{115}\text{In}$	$4.41 \times 10^{14} (25 \times 10^{14})$ y
$^{112}\text{Ag}$	$^{116}\text{In}$	14.10(3) s
$^{113}\text{Ag}$	$^{117}\text{In}$	43.2(3) m
$^{115}\text{Ag}$	$^{119}\text{In}$	2.4(1) m
$^{116}\text{Ag}$	$^{120}\text{In}$	3.08(8) s
$^{117}\text{Ag}$	$^{121}\text{In}$	23.1(6) s
$^{118}\text{Ag}$	$^{122}\text{In}$	1.5(3) s
$^{119}\text{Ag}$	$^{123}\text{In}$	6.17(5) s
$^{120}\text{Ag}$	$^{124}\text{In}$	3.12(9) s
$^{117}\text{Cd}$	$^{121}\text{Sr}$	27.03(4) h
$^{119}\text{Cd}$	$^{123}\text{Sr}$	129.2(4) d
$^{121}\text{Cd}$	$^{125}\text{Sr}$	9.64(33) d
$^{123}\text{Cd}$	$^{127}\text{Sr}$	2.10(4) h
$^{124}\text{Cd}$	$^{128}\text{Sr}$	59.07(14) m
$^{125}\text{Cd}$	$^{129}\text{Sr}$	2.23(4) m
$^{126}\text{Cd}$	$^{130}\text{Sr}$	3.72(7)m
$^{127}\text{Cd}$	$^{131}\text{Sr}$	56.0(5) s
$^{129}\text{Cd}$	$^{133}\text{Sr}$	1.46(3) s
$^{130}\text{Cd}$	$^{134}\text{Sr}$	1.050(11) s

Continued on next column

Continued from previous column

Parent	Daughter	$\tau$
$^{104}\text{In}$	$^{108}\text{Sb}$	7.4(3) s
$^{105}\text{In}$	$^{109}\text{Sb}$	17.2(5) s
$^{106}\text{In}$	$^{110}\text{Sb}$	23.6(3) s
$^{107}\text{In}$	$^{111}\text{Sb}$	75(1) s
$^{108}\text{In}$	$^{112}\text{Sb}$	53.5(6) s
$^{109}\text{In}$	$^{113}\text{Sb}$	6.67(7) m
$^{110}\text{In}$	$^{114}\text{Sb}$	3.49(3) m
$^{111}\text{In}$	$^{115}\text{Sb}$	32.1(3) m
$^{112}\text{In}$	$^{116}\text{Sb}$	15.8(8) m
$^{116}\text{In}$	$^{120}\text{Sb}$	15.89(4) m
$^{118}\text{In}$	$^{122}\text{Sb}$	2.72348(2) d
$^{119}\text{In}$	$^{123}\text{Sb}$	stable
$^{120}\text{In}$	$^{124}\text{Sb}$	60.20(3) d
$^{121}\text{In}$	$^{125}\text{Sb}$	2.75856(25) y
$^{122}\text{In}$	$^{126}\text{Sb}$	12.35(6) d
$^{123}\text{In}$	$^{127}\text{Sb}$	3.85(5) d
$^{124}\text{In}$	$^{128}\text{Sb}$	9.05 (4) h
$^{125}\text{In}$	$^{129}\text{Sb}$	4.366 (26) h
$^{126}\text{In}$	$^{130}\text{Sb}$	39.5 (8) m
$^{127}\text{In}$	$^{131}\text{Sb}$	23.03 (4) m
$^{128}\text{In}$	$^{132}\text{Sb}$	2.79 (7) m
$^{129}\text{In}$	$^{133}\text{Sb}$	2.34 (5) m
$^{130}\text{In}$	$^{134}\text{Sb}$	0.78 (6) s
$^{131}\text{In}$	$^{135}\text{Sb}$	1.679 (15) s

Continued on next column

Continued from previous column

Parent	Daughter	$\tau$
$^{132}\text{In}$	$^{136}\text{Sb}$	0.923 (14) s
$^{133}\text{In}$	$^{137}\text{Sb}$	450 (50) ms
$^{104}\text{Sn}$	$^{108}\text{Te}$	2.1(1) s
$^{105}\text{Sn}$	$^{109}\text{Te}$	4.4(2) s
$^{106}\text{Sn}$	$^{110}\text{Te}$	18.6(8) s
$^{107}\text{Sn}$	$^{111}\text{Te}$	19.3(4) s
$^{108}\text{Sn}$	$^{112}\text{Te}$	2(2) m
$^{109}\text{Sn}$	$^{113}\text{Te}$	1.7(2) m
$^{110}\text{Sn}$	$^{114}\text{Te}$	15.2(7) m
$^{111}\text{Sn}$	$^{115}\text{Te}$	5.8(2) m
$^{112}\text{Sn}$	$^{116}\text{Te}$	2.49(4) h
$^{113}\text{Sn}$	$^{117}\text{Te}$	62(2) m
$^{114}\text{Sn}$	$^{118}\text{Te}$	6(2) d
$^{115}\text{Sn}$	$^{119}\text{Te}$	16.05(5) h
$^{116}\text{Sn}$	$^{120}\text{Te}$	stable
$^{117}\text{Sn}$	$^{121}\text{Te}$	19.17(4) d
$^{118}\text{Sn}$	$^{122}\text{Te}$	stable
$^{119}\text{Sn}$	$^{123}\text{Te}$	$9.2 \times 10^{16}$ y
$^{120}\text{Sn}$	$^{124}\text{Te}$	stable
$^{121}\text{Sn}$	$^{125}\text{Te}$	stable
$^{122}\text{Sn}$	$^{126}\text{Te}$	stable
$^{124}\text{Sn}$	$^{128}\text{Te}$	$7.7 \times 10^{24} (4 \times 10^{24})$ y
$^{108}\text{Sb}$	$^{112}\text{I}$	3.34(8) s
$^{109}\text{Sb}$	$^{113}\text{I}$	6.6(2) s

Continued on next column

Continued from previous column

Parent	Daughter	$\tau$
$^{110}\text{Sb}$	$^{114}\text{I}$	2.1(2) s
$^{111}\text{Sb}$	$^{115}\text{I}$	1.3(2) m
$^{112}\text{Sb}$	$^{116}\text{I}$	2.91(15) s
$^{113}\text{Sb}$	$^{117}\text{I}$	2.22(4) m
$^{114}\text{Sb}$	$^{118}\text{I}$	13.7(5) m
$^{115}\text{Sb}$	$^{119}\text{I}$	19.1(4) m
$^{116}\text{Sb}$	$^{120}\text{I}$	81.6(2) m
$^{117}\text{Sb}$	$^{121}\text{I}$	2.12(1) h
$^{118}\text{Sb}$	$^{122}\text{I}$	3.63(6) m
$^{119}\text{Sb}$	$^{123}\text{I}$	13.2235(19) h
$^{120}\text{Sb}$	$^{124}\text{I}$	4.176(3) d
$^{130}\text{Sb}$	$^{134}\text{I}$	52.5(2) m
$^{121}\text{I}$	$^{125}\text{Cs}$	46.7(1) m
$^{122}\text{I}$	$^{126}\text{Cs}$	1.64(2) m
$^{123}\text{I}$	$^{127}\text{Cs}$	6.25(10) h
$^{124}\text{I}$	$^{128}\text{Cs}$	3.64(14) m
$^{130}\text{I}$	$^{134}\text{Cs}$	2.0652(4) y
$^{138}\text{I}$	$^{142}\text{Cs}$	1.684(14) s
$^{123}\text{Xe}$	$^{127}\text{Ba}$	12.7(4) m
$^{125}\text{Xe}$	$^{129}\text{Ba}$	2.23(11) h
$^{127}\text{Xe}$	$^{131}\text{Ba}$	11.5(6) d
$^{138}\text{Xe}$	$^{142}\text{Ba}$	10.6(2) m
$^{139}\text{Xe}$	$^{143}\text{Ba}$	14.5(3) s
$^{140}\text{Xe}$	$^{144}\text{Ba}$	11.5(2) s

Continued on next column

Continued from previous column

Parent	Daughter	$\tau$
$^{141}\text{Xe}$	$^{145}\text{Ba}$	4.31(16) s
$^{142}\text{Xe}$	$^{146}\text{Ba}$	2.21(6) s
$^{143}\text{Xe}$	$^{147}\text{Ba}$	0.894(10) s
$^{117}\text{Cs}$	$^{121}\text{La}$	5.3(2) s
$^{118}\text{Cs}$	$^{122}\text{La}$	8.6(5) s
$^{119}\text{Cs}$	$^{123}\text{La}$	17(3) s
$^{120}\text{Cs}$	$^{124}\text{La}$	21(4) s
$^{121}\text{Cs}$	$^{125}\text{La}$	64.8(12) s
$^{122}\text{Cs}$	$^{126}\text{La}$	54(2) s
$^{123}\text{Cs}$	$^{127}\text{La}$	5.1(1) m
$^{124}\text{Cs}$	$^{128}\text{La}$	5.18(14) m
$^{125}\text{Cs}$	$^{129}\text{La}$	11.6(2) m
$^{126}\text{Cs}$	$^{130}\text{La}$	8.7(1) m
$^{127}\text{Cs}$	$^{131}\text{La}$	59(2) m
$^{128}\text{Cs}$	$^{132}\text{La}$	4.8(2) h
$^{129}\text{Cs}$	$^{133}\text{La}$	3.912(8) h
$^{130}\text{Cs}$	$^{134}\text{La}$	6.45(16) m
$^{132}\text{Cs}$	$^{136}\text{La}$	9.87(3) m
$^{138}\text{Cs}$	$^{142}\text{La}$	91.1(5) m
$^{139}\text{Cs}$	$^{143}\text{La}$	14.2(1) m
$^{140}\text{Cs}$	$^{144}\text{La}$	40.8(4) s
$^{141}\text{Cs}$	$^{145}\text{La}$	3.01(6) m
$^{142}\text{Cs}$	$^{146}\text{La}$	13.49(16) m
$^{143}\text{Cs}$	$^{147}\text{La}$	4.06(4) s

Continued on next column

Continued from previous column

Parent	Daughter	$\tau$
$^{144}\text{Cs}$	$^{148}\text{La}$	1.26(8) s
$^{125}\text{Ba}$	$^{129}\text{Ce}$	3.5(3) m
$^{129}\text{Ba}$	$^{133}\text{Ce}$	97(4) m
$^{137}\text{Ba}$	$^{141}\text{Ce}$	32.511(13) d
$^{139}\text{Ba}$	$^{143}\text{Ce}$	33.039(6) h
$^{140}\text{Ba}$	$^{144}\text{Ce}$	284.91(5) d
$^{141}\text{Ba}$	$^{145}\text{Ce}$	3.01(6) m
$^{142}\text{Ba}$	$^{146}\text{Ce}$	13.49(16) m
$^{143}\text{Ba}$	$^{147}\text{Ce}$	56.4(10) s
$^{147}\text{Ba}$	$^{151}\text{Ce}$	1.76(6) s
$^{128}\text{La}$	$^{132}\text{Pr}$	1.6(3) m
$^{129}\text{La}$	$^{133}\text{Pr}$	6.5(3) m
$^{130}\text{La}$	$^{134}\text{Pr}$	17(2) m
$^{131}\text{La}$	$^{135}\text{Pr}$	24(1) m
$^{132}\text{La}$	$^{136}\text{Pr}$	13.1(1) m
$^{142}\text{La}$	$^{146}\text{Pr}$	24.09(10) m
$^{146}\text{La}$	$^{150}\text{Pr}$	6.19(16) s
$^{131}\text{Ce}$	$^{135}\text{Nd}$	12.4(6) m
$^{132}\text{Ce}$	$^{136}\text{Nd}$	50.65(33) m
$^{135}\text{Ce}$	$^{139}\text{Nd}$	29.7(5) m
$^{146}\text{Ce}$	$^{150}\text{Nd}$	$0.91 \times 10^{19} (7 \times 10^{19})$ y
$^{130}\text{Pr}$	$^{136}\text{Pm}$	47(2) s
$^{131}\text{Pr}$	$^{137}\text{Pm}$	2.4(1) m
$^{132}\text{Pr}$	$^{138}\text{Pm}$	10(2) s

Continued on next column



Continued from previous column

Parent	Daughter	$\tau$
$^{133}\text{Pr}$	$^{139}\text{Pm}$	4.15(5) m
$^{134}\text{Pr}$	$^{140}\text{Pm}$	9.2(2) s
$^{135}\text{Pr}$	$^{141}\text{Pm}$	20.9(5) m
$^{136}\text{Pr}$	$^{142}\text{Pm}$	40.5(5) s
$^{146}\text{Pr}$	$^{152}\text{Pm}$	4.12(8) m
$^{129}\text{Nd}$	$^{133}\text{Sm}$	2.89(16)
$^{133}\text{Nd}$	$^{137}\text{Sm}$	45(1) s
$^{136}\text{Nd}$	$^{140}\text{Sm}$	14.82(12) m
$^{137}\text{Nd}$	$^{141}\text{Sm}$	10.2(2) m
$^{141}\text{Nd}$	$^{145}\text{Sm}$	140(3) d
$^{134}\text{Pm}$	$^{138}\text{Eu}$	12.1(6) s
$^{135}\text{Pm}$	$^{139}\text{Eu}$	17.9(6) s
$^{136}\text{Pm}$	$^{140}\text{Eu}$	1.51(2) s
$^{137}\text{Pm}$	$^{141}\text{Eu}$	40.7(7) s
$^{138}\text{Pm}$	$^{142}\text{Eu}$	2.34(12) s
$^{141}\text{Pm}$	$^{145}\text{Eu}$	5.93(4) d
$^{142}\text{Pm}$	$^{146}\text{Eu}$	4.61(3) d
$^{136}\text{Sm}$	$^{140}\text{Gd}$	43327(4) s
$^{137}\text{Sm}$	$^{141}\text{Gd}$	14(4) s
$^{139}\text{Sm}$	$^{143}\text{Gd}$	39(2) s
$^{140}\text{Sm}$	$^{144}\text{Gd}$	4.47(6) m
$^{141}\text{Sm}$	$^{145}\text{Gd}$	23(4) m
$^{143}\text{Sm}$	$^{147}\text{Gd}$	38.06(12) h
$^{138}\text{Eu}$	$^{142}\text{Tb}$	597(17) ms

Continued on next column

Continued from previous column

Parent	Daughter	$\tau$
$^{141}\text{Eu}$	$^{145}\text{Tb}$	
$^{142}\text{Eu}$	$^{146}\text{Tb}$	8(4) s
$^{143}\text{Eu}$	$^{147}\text{Tb}$	1.64(3) h
$^{144}\text{Eu}$	$^{148}\text{Tb}$	60(1) m
$^{145}\text{Eu}$	$^{149}\text{Tb}$	4.118(25) h
$^{146}\text{Eu}$	$^{150}\text{Tb}$	3.48(16) h
$^{158}\text{Eu}$	$^{162}\text{Tb}$	7.6(15) m
$^{159}\text{Eu}$	$^{163}\text{Tb}$	19.5(3) m
$^{160}\text{Eu}$	$^{164}\text{Tb}$	3(1) m
$^{161}\text{Eu}$	$^{165}\text{Tb}$	2.11(10) m
$^{162}\text{Eu}$	$^{166}\text{Tb}$	25.1(21) s
$^{163}\text{Eu}$	$^{167}\text{Tb}$	19.4(27) s
$^{164}\text{Eu}$	$^{168}\text{Tb}$	8.2(13) s
$^{143}\text{Gd}$	$^{147}\text{Dy}$	67(7) s
$^{144}\text{Gd}$	$^{148}\text{Dy}$	3.3(2) m
$^{145}\text{Gd}$	$^{149}\text{Dy}$	4.2(14) m
$^{146}\text{Gd}$	$^{150}\text{Dy}$	7.17(5) m
$^{147}\text{Gd}$	$^{151}\text{Dy}$	17.9(3) m
$^{148}\text{Gd}$	$^{152}\text{Dy}$	2.38(2) h
$^{149}\text{Gd}$	$^{153}\text{Dy}$	6.4(0.1) h
$^{150}\text{Gd}$	$^{154}\text{Dy}$	$3.0 \times 10^{16} (15 \times 10^{16})$ y
$^{151}\text{Gd}$	$^{155}\text{Dy}$	9.9(2) h
$^{152}\text{Gd}$	$^{156}\text{Dy}$	stable
$^{153}\text{Gd}$	$^{157}\text{Dy}$	8.14(4) h

Continued on next column

Continued from previous column

Parent	Daughter	$\tau$
$^{154}\text{Gd}$	$^{158}\text{Dy}$	stable
$^{145}\text{Tb}$	$^{149}\text{Ho}$	21.1(2) s
$^{146}\text{Tb}$	$^{150}\text{Ho}$	72(4) s
$^{147}\text{Tb}$	$^{151}\text{Ho}$	35.2(1) s
$^{148}\text{Tb}$	$^{152}\text{Ho}$	161.8(3) s
$^{149}\text{Tb}$	$^{153}\text{Ho}$	2.01(3) m
$^{150}\text{Tb}$	$^{154}\text{Ho}$	11.76(19) m
$^{151}\text{Tb}$	$^{155}\text{Ho}$	48(1) m
$^{152}\text{Tb}$	$^{156}\text{Ho}$	56(1) m
$^{153}\text{Tb}$	$^{157}\text{Ho}$	12.6(2) m
$^{154}\text{Tb}$	$^{158}\text{Ho}$	11.3(4) m
$^{155}\text{Tb}$	$^{159}\text{Ho}$	33.05(11) m
$^{147}\text{Dy}$	$^{151}\text{Er}$	23.5(2) s
$^{148}\text{Dy}$	$^{152}\text{Er}$	10.3(1) s
$^{149}\text{Dy}$	$^{153}\text{Er}$	37.1(2) s
$^{150}\text{Dy}$	$^{154}\text{Er}$	3.73(9) m
$^{151}\text{Dy}$	$^{155}\text{Er}$	5.3(3) m
$^{152}\text{Dy}$	$^{156}\text{Er}$	19.5(10) m
$^{153}\text{Dy}$	$^{157}\text{Er}$	18.65(10) m
$^{157}\text{Dy}$	$^{161}\text{Er}$	3.21(3) h
$^{146}\text{Ho}$	$^{150}\text{Tm}$	2.2(6) s
$^{147}\text{Ho}$	$^{151}\text{Tm}$	4.17(11) s
$^{148}\text{Ho}$	$^{152}\text{Tm}$	8(1) s
$^{149}\text{Ho}$	$^{153}\text{Tm}$	1.48(1) s

Continued on next column

Continued from previous column

Parent	Daughter	$\tau$
$^{150}\text{Ho}$	$^{154}\text{Tm}$	8.1(3) s
$^{151}\text{Ho}$	$^{155}\text{Tm}$	21.6(2) s
$^{152}\text{Ho}$	$^{156}\text{Tm}$	83.8(18) s
$^{153}\text{Ho}$	$^{157}\text{Tm}$	3.63(9) m
$^{154}\text{Ho}$	$^{158}\text{Tm}$	3.98(6) m
$^{155}\text{Ho}$	$^{159}\text{Tm}$	9.13(16) m
$^{156}\text{Ho}$	$^{160}\text{Tm}$	9.4(3) m
$^{157}\text{Ho}$	$^{161}\text{Tm}$	30.2(8) m
$^{158}\text{Ho}$	$^{162}\text{Tm}$	21.7(19) m
$^{159}\text{Ho}$	$^{163}\text{Tm}$	1.81(5) h
$^{160}\text{Ho}$	$^{164}\text{Tm}$	2(1) m
$^{161}\text{Ho}$	$^{165}\text{Tm}$	30.06(3) h
$^{162}\text{Ho}$	$^{166}\text{Tm}$	7.7(3) h
$^{163}\text{Ho}$	$^{167}\text{Tm}$	9.25(2) d
$^{164}\text{Ho}$	$^{168}\text{Tm}$	93.1(2) d
$^{165}\text{Ho}$	$^{169}\text{Tm}$	stable
$^{149}\text{Er}$	$^{153}\text{Yb}$	4.2(2) s
$^{151}\text{Er}$	$^{155}\text{Yb}$	1.793(19) s
$^{152}\text{Er}$	$^{156}\text{Yb}$	26.1(7) s
$^{153}\text{Er}$	$^{157}\text{Yb}$	38.6(10) s
$^{154}\text{Er}$	$^{158}\text{Yb}$	1.49(13) m
$^{155}\text{Er}$	$^{159}\text{Yb}$	1.67(9) m
$^{156}\text{Er}$	$^{160}\text{Yb}$	4.8(2) m
$^{157}\text{Er}$	$^{161}\text{Yb}$	4.2(2) m

Continued on next column

Continued from previous column

Parent	Daughter	$\tau$
$^{158}\text{Er}$	$^{162}\text{Yb}$	18.87(19) m
$^{159}\text{Er}$	$^{163}\text{Yb}$	11.05(35) m
$^{160}\text{Er}$	$^{164}\text{Yb}$	75.8(17) m
$^{161}\text{Er}$	$^{165}\text{Yb}$	9.9(3) m
$^{163}\text{Er}$	$^{167}\text{Yb}$	17.5(2) m
$^{164}\text{Er}$	$^{168}\text{Yb}$	stable
$^{167}\text{Er}$	$^{171}\text{Yb}$	stable
$^{153}\text{Tm}$	$^{157}\text{Lu}$	6.8(18) s
$^{155}\text{Tm}$	$^{159}\text{Lu}$	12.1(10) s
$^{156}\text{Tm}$	$^{160}\text{Lu}$	36.1(3) s
$^{157}\text{Tm}$	$^{161}\text{Lu}$	77(2) s
$^{158}\text{Tm}$	$^{162}\text{Lu}$	1.37(2) m
$^{159}\text{Tm}$	$^{163}\text{Lu}$	3.97(13) m
$^{160}\text{Tm}$	$^{164}\text{Lu}$	3.14(3) m
$^{161}\text{Tm}$	$^{165}\text{Lu}$	10.74(10) m
$^{162}\text{Tm}$	$^{166}\text{Lu}$	2.65(10) m
$^{163}\text{Tm}$	$^{167}\text{Lu}$	51.5(10) m
$^{164}\text{Tm}$	$^{168}\text{Lu}$	5.5(1) m
$^{165}\text{Tm}$	$^{169}\text{Lu}$	34.06(5) h
$^{166}\text{Tm}$	$^{170}\text{Lu}$	2.012(20) d
$^{172}\text{Tm}$	$^{176}\text{Lu}$	$3.76 \times 10^{10} (7 \times 10^{10})$ y
$^{173}\text{Tm}$	$^{177}\text{Lu}$	6.647(4) d
$^{174}\text{Tm}$	$^{178}\text{Lu}$	28.4(2) m
$^{175}\text{Tm}$	$^{179}\text{Lu}$	4.59(6) h

Continued on next column

Continued from previous column

Parent	Daughter	$\tau$
$^{176}\text{Tm}$	$^{180}\text{Lu}$	5.7(1) m
$^{153}\text{Yb}$	$^{157}\text{Hf}$	115(1) ms
$^{154}\text{Yb}$	$^{158}\text{Hf}$	2.85(7) s
$^{155}\text{Yb}$	$^{159}\text{Hf}$	5.6(4) s
$^{156}\text{Yb}$	$^{160}\text{Hf}$	13.6(2) s
$^{157}\text{Yb}$	$^{161}\text{Hf}$	18.4(4) s
$^{158}\text{Yb}$	$^{162}\text{Hf}$	39.4(9) s
$^{159}\text{Yb}$	$^{163}\text{Hf}$	40(6) s
$^{160}\text{Yb}$	$^{164}\text{Hf}$	111(8) s
$^{162}\text{Yb}$	$^{166}\text{Hf}$	6.77(30) m
$^{163}\text{Yb}$	$^{167}\text{Hf}$	2.05(5) m
$^{164}\text{Yb}$	$^{168}\text{Hf}$	25.95(20) m
$^{165}\text{Yb}$	$^{169}\text{Hf}$	3.24(4) m
$^{166}\text{Yb}$	$^{170}\text{Hf}$	16.01(13) h
$^{167}\text{Yb}$	$^{171}\text{Hf}$	12.1(4) h
$^{168}\text{Yb}$	$^{172}\text{Hf}$	1.87(3) y
$^{169}\text{Yb}$	$^{173}\text{Hf}$	23.6(1) h
$^{170}\text{Yb}$	$^{174}\text{Hf}$	$2.0 \times 10^{15} (4 \times 10^{15})$ y
$^{171}\text{Yb}$	$^{175}\text{Hf}$	70(2) d
$^{172}\text{Yb}$	$^{176}\text{Hf}$	stable
$^{174}\text{Yb}$	$^{178}\text{Hf}$	stable
$^{175}\text{Yb}$	$^{179}\text{Hf}$	stable
$^{176}\text{Yb}$	$^{180}\text{Hf}$	stable
$^{177}\text{Yb}$	$^{181}\text{Hf}$	42.39(6) d

Continued on next column

Continued from previous column

Parent	Daughter	$\tau$
$^{178}\text{Yb}$	$^{182}\text{Hf}$	$8.90 \times 10^6 (9 \times 10^6) \text{ y}$
$^{156}\text{Lu}$	$^{160}\text{Ta}$	155(4) s
$^{158}\text{Lu}$	$^{162}\text{Ta}$	3.357(12) s
$^{159}\text{Lu}$	$^{163}\text{Ta}$	10.6(18) s
$^{160}\text{Lu}$	$^{164}\text{Ta}$	14.2(3) s
$^{162}\text{Lu}$	$^{166}\text{Ta}$	34.4(5) s
$^{163}\text{Lu}$	$^{167}\text{Ta}$	80(4) s
$^{164}\text{Lu}$	$^{168}\text{Ta}$	2(1) m
$^{165}\text{Lu}$	$^{169}\text{Ta}$	4.9(4) m
$^{166}\text{Lu}$	$^{170}\text{Ta}$	6.76(6) m
$^{167}\text{Lu}$	$^{171}\text{Ta}$	23.3(3) m
$^{168}\text{Lu}$	$^{172}\text{Ta}$	36.8(3) m
$^{169}\text{Lu}$	$^{173}\text{Ta}$	3.14(13) h
$^{170}\text{Lu}$	$^{174}\text{Ta}$	1.14(8) h
$^{171}\text{Lu}$	$^{175}\text{Ta}$	10.5(2) h
$^{172}\text{Lu}$	$^{176}\text{Ta}$	8.09(5) h
$^{174}\text{Lu}$	$^{178}\text{Ta}$	2.36(8) h
$^{176}\text{Lu}$	$^{180}\text{Ta}$	8.154(6) h
$^{177}\text{Lu}$	$^{181}\text{Ta}$	stable
$^{178}\text{Lu}$	$^{182}\text{Ta}$	114.74(12) d
$^{179}\text{Lu}$	$^{183}\text{Ta}$	5.1(1) d
$^{180}\text{Lu}$	$^{184}\text{Ta}$	8.7(1) h
$^{190}\text{Au}$	$^{194}\text{Tl}$	33(5) m
$^{190}\text{Hg}$	$^{194}\text{Pb}$	10.7(6) m

Continued on next column

Continued from previous column

Parent	Daughter	$\tau$
$^{191}\text{Hg}$	$^{195}\text{Pb}$	15 m
$^{192}\text{Hg}$	$^{196}\text{Pb}$	37(3) m
$^{207}\text{Hg}$	$^{211}\text{Pb}$	36.1(2) m
$^{190}\text{Tl}$	$^{194}\text{Bi}$	95(3) s
$^{191}\text{Tl}$	$^{195}\text{Bi}$	183(4) s
$^{192}\text{Tl}$	$^{196}\text{Bi}$	308(12) s
$^{193}\text{Tl}$	$^{197}\text{Bi}$	9.33(50) m
$^{194}\text{Tl}$	$^{198}\text{Bi}$	10.3(3) m
$^{195}\text{Tl}$	$^{199}\text{Bi}$	27(1) m
$^{196}\text{Tl}$	$^{200}\text{Bi}$	36.4(5) m
$^{197}\text{Tl}$	$^{201}\text{Bi}$	103(3) m
$^{198}\text{Tl}$	$^{202}\text{Bi}$	1.71(4) h
$^{200}\text{Tl}$	$^{204}\text{Bi}$	11.22(10) h
$^{208}\text{Tl}$	$^{212}\text{Bi}$	60.55(6) m
$^{190}\text{Pb}$	$^{194}\text{Po}$	0.392(4) s
$^{191}\text{Pb}$	$^{195}\text{Po}$	4.64(9) s
$^{192}\text{Pb}$	$^{196}\text{Po}$	5.8(2) s
$^{193}\text{Pb}$	$^{197}\text{Po}$	84(16) s
$^{195}\text{Pb}$	$^{199}\text{Po}$	5.47(15) m
$^{196}\text{Pb}$	$^{200}\text{Po}$	11.51(8) m
$^{198}\text{Pb}$	$^{202}\text{Po}$	44.6(4) m
$^{199}\text{Pb}$	$^{203}\text{Po}$	36.7(5) m
$^{211}\text{Pb}$	$^{215}\text{Po}$	1.781(5) ms
$^{192}\text{Bi}$	$^{196}\text{At}$	0.388(7) s

Continued on next column

Continued from previous column

Parent	Daughter	$\tau$
$^{193}\text{Bi}$	$^{197}\text{At}$	0.388(6) s
$^{195}\text{Bi}$	$^{199}\text{At}$	7.03(15) s
$^{196}\text{Bi}$	$^{200}\text{At}$	43(1) s
$^{197}\text{Bi}$	$^{201}\text{At}$	85.2(16) s
$^{198}\text{Bi}$	$^{202}\text{At}$	184(1) s
$^{199}\text{Bi}$	$^{203}\text{At}$	7.4(2) m
$^{200}\text{Bi}$	$^{204}\text{At}$	9.12(11) m
$^{201}\text{Bi}$	$^{205}\text{At}$	26.9(8) m
$^{202}\text{Bi}$	$^{206}\text{At}$	30.6(8) m
$^{204}\text{Bi}$	$^{208}\text{At}$	1.63(3) h
$^{211}\text{Bi}$	$^{215}\text{At}$	0.1(2) ms
$^{212}\text{Bi}$	$^{216}\text{At}$	0.3(3) ms
$^{213}\text{Bi}$	$^{217}\text{At}$	32.3(4) ms
$^{195}\text{Po}$	$^{199}\text{Rn}$	0.59(3) s
$^{196}\text{Po}$	$^{200}\text{Rn}$	1.03( $20^{-11}$ ) s
$^{197}\text{Po}$	$^{201}\text{Rn}$	7(4) s
$^{198}\text{Po}$	$^{202}\text{Rn}$	9.7(1) s
$^{199}\text{Po}$	$^{203}\text{Rn}$	44(2) s
$^{200}\text{Po}$	$^{204}\text{Rn}$	74.5(14) s
$^{201}\text{Po}$	$^{205}\text{Rn}$	170(4) s
$^{202}\text{Po}$	$^{206}\text{Rn}$	5.67(17) m
$^{203}\text{Po}$	$^{207}\text{Rn}$	9.25(17) m
$^{204}\text{Po}$	$^{208}\text{Rn}$	24.35(14) m
$^{205}\text{Po}$	$^{209}\text{Rn}$	28.8(10) m

Continued on next column

Continued from previous column

Parent	Daughter	$\tau$
$^{206}\text{Po}$	$^{210}\text{Rn}$	2.4(1) h
$^{207}\text{Po}$	$^{211}\text{Rn}$	14.6(2) h
$^{208}\text{Po}$	$^{212}\text{Rn}$	23.9(12) m
$^{210}\text{Po}$	$^{214}\text{Rn}$	0.27(2) $\mu\text{s}$
$^{211}\text{Po}$	$^{215}\text{Rn}$	2.3(10) $\mu\text{s}$
$^{195}\text{At}$	$^{199}\text{Fr}$	12( $10^{-4}$ ) ms
$^{196}\text{At}$	$^{200}\text{Fr}$	49(4) ms
$^{197}\text{At}$	$^{201}\text{Fr}$	62(5) ms
$^{198}\text{At}$	$^{202}\text{Fr}$	0.3(5) s
$^{199}\text{At}$	$^{203}\text{Fr}$	0.55(1) s
$^{200}\text{At}$	$^{204}\text{Fr}$	1.8(3) s
$^{201}\text{At}$	$^{205}\text{Fr}$	3.92(4) s
$^{202}\text{At}$	$^{206}\text{Fr}$	16 s
$^{203}\text{At}$	$^{207}\text{Fr}$	14.8(1) s
$^{204}\text{At}$	$^{208}\text{Fr}$	59.1(3) s
$^{205}\text{At}$	$^{209}\text{Fr}$	50.5(7) s
$^{206}\text{At}$	$^{210}\text{Fr}$	3.18(6) m
$^{207}\text{At}$	$^{211}\text{Fr}$	3.1(2) m
$^{208}\text{At}$	$^{212}\text{Fr}$	20(6) m
$^{209}\text{At}$	$^{213}\text{Fr}$	34.82(14) s
$^{210}\text{At}$	$^{214}\text{Fr}$	5(2) ms
$^{211}\text{At}$	$^{215}\text{Fr}$	86(5) ns
$^{212}\text{At}$	$^{216}\text{Fr}$	0.7(2) $\mu\text{s}$
$^{217}\text{At}$	$^{221}\text{Fr}$	4.9(2) m

Continued on next column

Continued from previous column

Parent	Daughter	$\tau$
$^{218}\text{At}$	$^{222}\text{Fr}$	14.2(3) m
$^{219}\text{At}$	$^{223}\text{Fr}$	22(7) m
$^{201}\text{Rn}$	$^{205}\text{Ra}$	210(+60-40) ms
$^{202}\text{Rn}$	$^{206}\text{Ra}$	0.24(2) s
$^{203}\text{Rn}$	$^{207}\text{Ra}$	1.35(+22-13) s
$^{204}\text{Rn}$	$^{208}\text{Ra}$	1.3(2) s
$^{205}\text{Rn}$	$^{209}\text{Ra}$	4.8(2) s
$^{206}\text{Rn}$	$^{210}\text{Ra}$	3.7(2) s
$^{207}\text{Rn}$	$^{211}\text{Ra}$	13(2) s
$^{208}\text{Rn}$	$^{212}\text{Ra}$	13(2) s
$^{209}\text{Rn}$	$^{213}\text{Ra}$	2.73(5) m
$^{210}\text{Rn}$	$^{214}\text{Ra}$	2.46(3) s
$^{211}\text{Rn}$	$^{215}\text{Ra}$	1.66(2) ms
$^{212}\text{Rn}$	$^{216}\text{Ra}$	182(10) ns
$^{213}\text{Rn}$	$^{217}\text{Ra}$	1.6(2) $\mu$ s
$^{218}\text{Rn}$	$^{222}\text{Ra}$	38(5) s
$^{219}\text{Rn}$	$^{223}\text{Ra}$	11.43(5) d
$^{220}\text{Rn}$	$^{224}\text{Ra}$	3.6319(2) d
$^{221}\text{Rn}$	$^{225}\text{Ra}$	14.9(2) d
$^{222}\text{Rn}$	$^{226}\text{Ra}$	1600(7) y
$^{223}\text{Rn}$	$^{227}\text{Ra}$	42.2(5) m
$^{201}\text{Fr}$	$^{205}\text{Ac}$	20(+99 - 7) ms
$^{202}\text{Fr}$	$^{206}\text{Ac}$	22(+9-5) ms
$^{203}\text{Fr}$	$^{207}\text{Ac}$	27(+11-6) ms

Continued on next column

Continued from previous column

Parent	Daughter	$\tau$
$^{204}\text{Fr}$	$^{208}\text{Ac}$	95(+24-16) ms
$^{205}\text{Fr}$	$^{209}\text{Ac}$	0.087(+12-9) s
$^{206}\text{Fr}$	$^{210}\text{Ac}$	0.35(5) s
$^{207}\text{Fr}$	$^{211}\text{Ac}$	0.21(3) s
$^{208}\text{Fr}$	$^{212}\text{Ac}$	0.93(5) s
$^{209}\text{Fr}$	$^{213}\text{Ac}$	738(16) ms
$^{210}\text{Fr}$	$^{214}\text{Ac}$	8.2(2) s
$^{211}\text{Fr}$	$^{215}\text{Ac}$	0.17(1) s
$^{212}\text{Fr}$	$^{216}\text{Ac}$	440(16) $\mu$ s
$^{213}\text{Fr}$	$^{217}\text{Ac}$	69(4) ns
$^{214}\text{Fr}$	$^{218}\text{Ac}$	1.08(9) $\mu$ s
$^{218}\text{Fr}$	$^{222}\text{Ac}$	5(5) s
$^{219}\text{Fr}$	$^{223}\text{Ac}$	2.1(5) ms
$^{220}\text{Fr}$	$^{224}\text{Ac}$	2.78(16) h
$^{221}\text{Fr}$	$^{225}\text{Ac}$	9.9203(3) d
$^{222}\text{Fr}$	$^{226}\text{Ac}$	29.37(12) h
$^{223}\text{Fr}$	$^{227}\text{Ac}$	21.772(3) y
$^{224}\text{Fr}$	$^{228}\text{Ac}$	6.15(2) h
$^{225}\text{Fr}$	$^{229}\text{Ac}$	62.7(5) h
$^{227}\text{Fr}$	$^{231}\text{Ac}$	7.5(1) m
$^{228}\text{Fr}$	$^{232}\text{Ac}$	119(5) s
$^{229}\text{Fr}$	$^{233}\text{Ac}$	145(10) s
$^{230}\text{Fr}$	$^{234}\text{Ac}$	44(7) s
$^{231}\text{Fr}$	$^{235}\text{Ac}$	62(4) s

Continued on next column

Continued from previous column

Parent	Daughter	$\tau$
$^{207}\text{Ra}$	$^{211}\text{Th}$	37(+28-11) ms
$^{208}\text{Ra}$	$^{212}\text{Th}$	31.7(13) ms
$^{209}\text{Ra}$	$^{213}\text{Th}$	144(21) ms
$^{210}\text{Ra}$	$^{214}\text{Th}$	87(10) ms
$^{211}\text{Ra}$	$^{215}\text{Th}$	1.2(2) s
$^{212}\text{Ra}$	$^{216}\text{Th}$	26(2) ms
$^{213}\text{Ra}$	$^{217}\text{Th}$	0.241(5) ms
$^{214}\text{Ra}$	$^{218}\text{Th}$	117(9) ns
$^{220}\text{Ra}$	$^{224}\text{Th}$	1.04(2) s
$^{221}\text{Ra}$	$^{225}\text{Th}$	8.75(4) m
$^{222}\text{Ra}$	$^{226}\text{Th}$	30.57(10) m
$^{223}\text{Ra}$	$^{227}\text{Th}$	18.697(7) d
$^{224}\text{Ra}$	$^{228}\text{Th}$	1.9116(16) y
$^{225}\text{Ra}$	$^{229}\text{Th}$	7880(120) y
$^{226}\text{Ra}$	$^{230}\text{Th}$	$7.54 \times 10^4 (3 \times 10^4)$ y
$^{227}\text{Ra}$	$^{231}\text{Th}$	25.52(1) h
$^{229}\text{Ra}$	$^{233}\text{Th}$	21.83(4) m
$^{230}\text{Ra}$	$^{234}\text{Th}$	24.1(3) d
$^{231}\text{Ra}$	$^{235}\text{Th}$	7.2(1) m
$^{233}\text{Ra}$	$^{237}\text{Th}$	4.8(5) m
$^{222}\text{Ac}$	$^{226}\text{Pa}$	1.8(2) m
$^{223}\text{Ac}$	$^{227}\text{Pa}$	38.3(3) m
$^{225}\text{Ac}$	$^{229}\text{Pa}$	1.5(5) d
$^{226}\text{Ac}$	$^{230}\text{Pa}$	17.4(5) d

Continued on next column

Continued from previous column

Parent	Daughter	$\tau$
$^{228}\text{Ac}$	$^{232}\text{Pa}$	1.32(2) d
$^{229}\text{Ac}$	$^{233}\text{Pa}$	26.975(13) d
$^{230}\text{Ac}$	$^{234}\text{Pa}$	6.7(5) h
$^{231}\text{Ac}$	$^{235}\text{Pa}$	24.4(2) m
$^{232}\text{Ac}$	$^{236}\text{Pa}$	9.1(1) m
$^{233}\text{Ac}$	$^{237}\text{Pa}$	8.7(2) m
$^{239}\text{Pu}$	$^{241}\text{Cm}$	29.1(1) y

Concluded





## Acknowledgements

---

I would like to deeply thank all the people who somehow contributed to the realization of this work but I especially want to thank:

- My thesis advisor Diego Alejandro Torres Galindo for his academic advice and support of this project.
- The scholarship program "Beca Auxiliar Docente" and Colciencias for partially funding this work.
- My boyfriend Janis Danebergs and the Swedish state for partially funding this work.
- All my relatives, friends and classmates, in especial my mother and my grandma, Gloria Amparo Londoño and María Díaz de Gómez for their emotional and economical support.
- The GFNUN, in special professor Edna Carolina Pinilla Beltran for her academic advice and emotional support and professor Fernando Cristancho for his academic advice.

Bogotá, 2019

*Ana María Gómez Londoño*



## Bibliography

---

- [1] D. A. Torres, G. J. Kumbartzki, Y. Y. Sharon, L. Zamick, B. Manning, N. Benczer-Koller, G. Gürdal, K.-H. Speidel, M. Hjorth-Jensen, P. Maier-Komor, S. J. Q. Robinson, T. Ahn, V. Anagnostatou, M. Elvers, P. Goddard, A. Heinz, G. Ilie, D. Radeck, D. Savran, and V. Werner, “First  $g$ -factor measurements of the  $2_1^+$  and the  $4_1^+$  states of radioactive  $^{100}\text{Pd}$ ,” *Phys. Rev. C*, vol. 84, p. 044327, Oct 2011. [Online]. Available: <https://link.aps.org/doi/10.1103/PhysRevC.84.044327>
- [2] F. D. Becchetti, L. T. Chua, J. Jänecke, and A. M. VanderMolen, “Systematics of the ( $d$ ,  $^6\text{Li}$ ) reaction and  $\alpha$  clustering in heavy nuclei,” *Phys. Rev. Lett.*, vol. 34, pp. 225–227, Jan 1975. [Online]. Available: <https://link.aps.org/doi/10.1103/PhysRevLett.34.225>
- [3] R. Horstman, J. Eberhardt, H. Doubt, C. Otten, and G. V. Middelkoop, “Recoil-distance measurements of  $g$ -factors for  $^{24}\text{Mg}(21^+)$  and  $^{20}\text{Ne}(21^+)$ ,” *Nuclear Physics A*, vol. 248, no. 2, pp. 291 – 316, 1975. [Online]. Available: <http://www.sciencedirect.com/science/article/pii/0375947475901670>
- [4] N. Stone, “Table of nuclear magnetic dipole and electric quadrupole moments,” *Atomic Data and Nuclear Data Tables*, vol. 90, no. 1, pp. 75 – 176, 2005. [Online]. Available: <http://www.sciencedirect.com/science/article/pii/S0092640X05000239>
- [5] K. Nakai, B. Herskind, J. Blomqvist, A. Filevich, K.-G. Rensfelt, J. Sztarkier, I. Bergström, and S. Nagamiya, “The  $g$ -factor of the  $12^+$  isomeric state in  $^{206}\text{Pb}$  and the effective orbital  $g$ -factor of the neutron,” *Nuclear Physics A*, vol. 189, no. 3, pp. 526 – 538, 1972. [Online]. Available: <http://www.sciencedirect.com/science/article/pii/0375947472903119>

- [6] D. Radeck, A. Blazhev, M. Albers, C. Bernards, A. Dewald, C. Fransen, M. Heidemann, J. Jolie, B. Melon, D. Mücher, T. Pissulla, W. Rother, K. O. Zell, and O. Möller, “First measurement of lifetimes in the yrast band of  $^{100}\text{Pd}$ ,” *Phys. Rev. C*, vol. 80, p. 044331, Oct 2009. [Online]. Available: <https://link.aps.org/doi/10.1103/PhysRevC.80.044331>
- [7] “ISAC Yield Data Base,” <https://mis.triumf.ca/science/planning/yield/beam>, [Online; accessed 21-July-2018].
- [8] “Table of nuclides,” <https://www-nds.iaea.org/relnsd/vcharthtml/VChartHTML.html>, [Online; accessed 21-July-2018].
- [9] Z. Sosin, J. Błocki, J. Kallunkathariyil, J. Łukasik, and P. Pawłowski, “Alpha-cluster model of atomic nuclei,” *The European Physical Journal A*, vol. 52, no. 5, p. 120, May 2016. [Online]. Available: <https://doi.org/10.1140/epja/i2016-16120-4>
- [10] S. Micheletti and J. Mead, “Direct interaction mechanism in  $(d, \alpha)$  reactions,” *Nuclear Physics*, vol. 37, pp. 201 – 214, 1962. [Online]. Available: <http://www.sciencedirect.com/science/article/pii/0029558262902584>
- [11] L.-H. Xia, C.-Q. Gao, P.-Z. Ning, and G.-Z. He, “Alpha transfer mechanism in heavy-ion reactions,” *Phys. Rev. C*, vol. 31, pp. 2128–2132, Jun 1985. [Online]. Available: <https://link.aps.org/doi/10.1103/PhysRevC.31.2128>
- [12] H. Fröhlich, T. Shimoda, M. Ishihara, K. Nagatani, T. Udagawa, and T. Tamura, “Alpha-transfer reactions with large energy transfers,” *Phys. Rev. Lett.*, vol. 42, pp. 1518–1520, Jun 1979. [Online]. Available: <https://link.aps.org/doi/10.1103/PhysRevLett.42.1518>
- [13] K. Bethge, “Alpha-particle transfer reactions,” *Annual Review of Nuclear Science*, vol. 20, no. 1, pp. 255–288, 1970. [Online]. Available: <https://doi.org/10.1146/annurev.ns.20.120170.001351>
- [14] K.-H. Speidel, S. Schielke, J. Leske, J. Gerber, P. Maier-Komor, S. Robinson, Y. Sharon, and L. Zamick, “Experimental  $g$  factors and  $b(e2)$  values in  $ar$  isotopes: Crossing the

- n=20 semi-magic divide,” *Physics Letters B*, vol. 632, no. 2, pp. 207 – 211, 2006. [Online]. Available: <http://www.sciencedirect.com/science/article/pii/S0370269305015418>
- [15] S. Schielke, K.-H. Speidel, O. Kenn, J. Leske, N. Gemein, M. Offer, Y. Sharon, L. Zamick, J. Gerber, and P. Maier-Komor, “First measurement and shell model interpretation of the g factor of the 21+ state in self-conjugate radioactive 44ti,” *Physics Letters B*, vol. 567, no. 3, pp. 153 – 158, 2003. [Online]. Available: <http://www.sciencedirect.com/science/article/pii/S0370269303009171>
- [16] K.-H. Speidel, J. Leske, S. Schielke, S. Bedi, O. Zell, P. Maier-Komor, S. Robinson, Y. Sharon, and L. Zamick, “Low-level structure of 52ti based on g factor and lifetime measurements,” *Physics Letters B*, vol. 633, no. 2, pp. 219 – 224, 2006. [Online]. Available: <http://www.sciencedirect.com/science/article/pii/S0370269305017582>
- [17] J. Leske, K.-H. Speidel, S. Schielke, O. Kenn, J. Gerber, P. Maier-Komor, S. J. Q. Robinson, A. Escuderos, Y. Y. Sharon, and L. Zamick, “Nuclear structure of the first 2+ state in radioactive 68Ge based on g factor and lifetime measurements,” *Phys. Rev. C*, vol. 71, p. 044316, Apr 2005. [Online]. Available: <https://link.aps.org/doi/10.1103/PhysRevC.71.044316>
- [18] N. Benczer-Koller and G. J. Kumbartzki, “Exploration of nuclear structure beyond the limits of stability via magnetic moment measurements: 82 sr and 90 sr,” *Journal of Physics: Conference Series*, vol. 580, no. 1, p. 012013, 2015. [Online]. Available: <http://stacks.iop.org/1742-6596/580/i=1/a=012013>
- [19] G. J. Kumbartzki, K.-H. Speidel, N. Benczer-Koller, D. A. Torres, Y. Y. Sharon, L. Zamick, S. J. Q. Robinson, P. Maier-Komor, T. Ahn, V. Anagnostatou, C. Bernards, M. Elvers, P. Goddard, A. Heinz, G. Ilie, D. Radeck, D. Savran, V. Werner, and E. Williams, “Structure of the sr-zr isotopes near and at the magic  $n = 50$  shell from  $g$ -factor and lifetime measurements in  ${}^{88}_{40}\text{Zr}$  and  ${}^{84,86}_{38}\text{Sr}$ ,” *Phys. Rev. C*, vol. 85, p. 044322, Apr 2012. [Online]. Available: <https://link.aps.org/doi/10.1103/PhysRevC.85.044322>

- [20] D. A. Torres, G. J. Kumbartzki, Y. Y. Sharon, L. Zamick, B. Manning, N. Benczer-Koller, G. Gürdal, K.-H. Speidel, M. Hjorth-Jensen, P. Maier-Komor, S. J. Q. Robinson, T. Ahn, V. Anagnostatou, M. Elvers, P. Goddard, A. Heinz, G. Ilie, D. Radeck, D. Savran, and V. Werner, “First  $g$ -factor measurements of the  $2_1^+$  and the  $4_1^+$  states of radioactive  $^{100}\text{Pd}$ ,” *Phys. Rev. C*, vol. 84, p. 044327, Oct 2011. [Online]. Available: <https://link.aps.org/doi/10.1103/PhysRevC.84.044327>
- [21] G. J. Kumbartzki, N. Benczer-Koller, K.-H. Speidel, D. A. Torres, J. M. Allmond, P. Fallon, I. Abramovic, L. A. Bernstein, J. E. Bevins, H. L. Crawford, Z. E. Guevara, G. Gürdal, A. M. Hurst, L. Kirsch, T. A. Laplace, A. Lo, E. F. Matthews, I. Mayers, L. W. Phair, F. Ramirez, S. J. Q. Robinson, Y. Y. Sharon, and A. Wiens, “ $z = 50$ ,” *Phys. Rev. C*, vol. 93, p. 044316, Apr 2016. [Online]. Available: <https://link.aps.org/doi/10.1103/PhysRevC.93.044316>
- [22] D. J. Pisano and P. D. Parker, “Alpha-transfer reactions in light nuclei. ii. ( $^3\text{He}$ ,  $^7\text{Be}$ ) pickup reactions,” *Phys. Rev. C*, vol. 14, pp. 475–490, Aug 1976. [Online]. Available: <https://link.aps.org/doi/10.1103/PhysRevC.14.475>
- [23] P. Forum, “<https://www.physicsforums.com/threads/velocities-of-nucleons.505461/>.” [Online]. Available: <https://www.physicsforums.com/threads/velocities-of-nucleons.505461/>
- [24] D. A. T. Galindo and F. Ramirez, “Nuclear structure aspects via  $g$ -factor measurements: pushing the frontiers,” *PoS*, vol. XLASNPA, p. 021, 2014.
- [25] M. G. Mayer, “On closed shells in nuclei. ii,” *Phys. Rev.*, vol. 75, pp. 1969–1970, Jun 1949. [Online]. Available: <https://link.aps.org/doi/10.1103/PhysRev.75.1969>
- [26] A. G. W. Cameron, “A revised semiempirical atomic mass formula,” *Canadian Journal of Physics*, vol. 35, no. 9, pp. 1021–1032, 1957. [Online]. Available: <https://doi.org/10.1139/p57-114>
- [27] H. Reiss, “Theory of the liquid drop model.” *Industrial & Engineering Chemistry*, vol. 44, no. 6, pp. 1284–1288, 1952. [Online]. Available: <https://doi.org/10.1021/ie50510a029>

- [28] —, “Theory of the liquid drop model.” *Industrial & Engineering Chemistry*, vol. 44, no. 6, pp. 1284–1288, 1952. [Online]. Available: <https://doi.org/10.1021/ie50510a029>
- [29] C. Cohen-Tannoudji, B. Diu, and F. Laloë, *Quantum mechanics*, ser. Quantum Mechanics. Wiley, 1977. [Online]. Available: <https://books.google.com.co/books?id=rr0PAQAAMAAJ>
- [30] A. Koning and J. Delaroche, “Local and global nucleon optical models from 1 keV to 200 MeV,” *Nuclear Physics A*, vol. 713, no. 3, pp. 231 – 310, 2003. [Online]. Available: <http://www.sciencedirect.com/science/article/pii/S0375947402013210>
- [31] L. Chamon, “The São Paulo potential,” *Nuclear Physics A*, vol. 787, no. 1, pp. 198 – 205, 2007, proceedings of the Ninth International Conference on Nucleus-Nucleus Collisions. [Online]. Available: <http://www.sciencedirect.com/science/article/pii/S037594740601013X>
- [32] Oliveira, J.R.B., Zagatto, V., Pereira, D., Lubian, J., Allegro, P.R.P., Chamon, L.C., Cybulska, E.W., Linares, R., Medina, N.H., Ribas, R.V., Rossi Jr, E.S., Seale, W.A., Silva, C.P., Toufen, D.L., Silveira, M.A.G., Zahn, G.S., Genezini, F.A., Gasques, L., and Shorto, J.M.B., “Exploring the potential of the São Paulo potential,” *EPJ Web of Conferences*, vol. 2, p. 02002, 2010. [Online]. Available: <https://doi.org/10.1051/epjconf/20100202002>
- [33] F. C. Mejía, “Notas de clase: Espectroscopia nuclear.”
- [34] A. G. Smith, R. Orlandi, D. Patel, G. S. Simpson, R. M. Wall, J. F. Smith, O. J. Onakanmi, I. Ahmad, J. P. Greene, M. P. Carpenter, T. Lauritsen, C. J. Lister, R. V. F. Janssens, F. G. Kondev, D. Seweryniak, B. J. P. Gall, O. Dorvaux, and B. Roux, “The magnetic properties of collective states in a 100 fission fragments,” *Journal of Physics G: Nuclear and Particle Physics*, vol. 31, no. 10, p. S1433, 2005. [Online]. Available: <http://stacks.iop.org/0954-3899/31/i=10/a=009>
- [35] L. Brillouin, “A theorem of Larmor and its importance for electrons in magnetic fields,” *Phys. Rev.*, vol. 67, pp. 260–266, Apr 1945. [Online]. Available: <http://link.aps.org/doi/10.1103/PhysRev.67.260>

- 
- [36] G. Kumbartzki, *Nuclear Magnetic Moments*, [http : //www.physics.rutgers.edu/ ~ kum/tfbook.pdf](http://www.physics.rutgers.edu/~kum/tfbook.pdf).
- [37] J. Eberhardt, G. V. Middelkoop, R. Horstman, and H. Doubt, “Anomalously large transient field through polarized electron capture,” *Physics Letters B*, vol. 56, no. 4, pp. 329 – 331, 1975. [Online]. Available: <http://www.sciencedirect.com/science/article/pii/0370269375903111>
- [38] N. Benczer-Koller, M. Hass, and J. Sak, “Transient magnetic fields at swift ions traversing ferromagnetic media and application to measurements of nuclear moments,” *Annual Review of Nuclear and Particle Science*, vol. 30, no. 1, pp. 53–84, 1980. [Online]. Available: <http://dx.doi.org/10.1146/annurev.ns.30.120180.000413>
- [39] A. M. Gómez and D. A. Torres, “About the parametrizations utilized to perform magnetic moments measurements using the transient field technique,” *AIP Conference Proceedings*, vol. 1753, no. 1, p. 030005, 2016. [Online]. Available: <https://aip.scitation.org/doi/abs/10.1063/1.4955346>
- [40] P. Jones, L. Wei, F. Beck, P. Butler, T. Byrski, G. Duchêne, G. de France, F. Hannachi, G. Jones, and B. Kharraja, “Calibration of the new composite “clover” detector as a compton polarimeter for the eurogam array,” *Nuclear Instruments and Methods in Physics Research Section A: Accelerators, Spectrometers, Detectors and Associated Equipment*, vol. 362, no. 2, pp. 556 – 560, 1995. [Online]. Available: <http://www.sciencedirect.com/science/article/pii/0168900295002464>
- [41] H. J. Rose and D. M. Brink, “Angular distributions of gamma rays in terms of phase-defined reduced matrix elements,” *Rev. Mod. Phys.*, vol. 39, pp. 306–347, Apr 1967. [Online]. Available: <http://link.aps.org/doi/10.1103/RevModPhys.39.306>
- [42] N. Benczer-Koller and G. J. Kumbartzki, “Magnetic moments of short-lived excited nuclear states: measurements and challenges,” *Journal of Physics G: Nuclear and Particle Physics*, vol. 34, no. 9, p. R321, 2007. [Online]. Available: <http://stacks.iop.org/0954-3899/34/i=9/a=R01>



- [43] J. R. MacDonald, “Doppler shift measurements of nuclear lifetimes,” *Science*, vol. 167, no. 3923, pp. 1339–1347, 1970. [Online]. Available: <http://www.jstor.org/stable/1728868>
- [44] H. W. Fulbright, “Alpha transfer reactions in light nuclei,” *Annual Review of Nuclear and Particle Science*, vol. 29, no. 1, pp. 161–202, 1979. [Online]. Available: <https://doi.org/10.1146/annurev.ns.29.120179.001113>
- [45] R. H. Stuewer, *Gamow’s Theory of Alpha-Decay*. Dordrecht: Springer Netherlands, 1986, pp. 147–186. [Online]. Available: [https://doi.org/10.1007/978-94-009-5496-0\\_14](https://doi.org/10.1007/978-94-009-5496-0_14)
- [46] B. Buck, A. C. Merchant, M. J. Horner, and S. M. Perez, “Choosing cluster and core in cluster models of nuclei,” *Phys. Rev. C*, vol. 61, p. 024314, Jan 2000. [Online]. Available: <https://link.aps.org/doi/10.1103/PhysRevC.61.024314>
- [47] R. Guardiola, I. Moliner, and M. Nagarajan, “Alpha-cluster model for 8be and 12c with correlated alpha particles,” *Nuclear Physics A*, vol. 679, no. 3, pp. 393 – 409, 2001. [Online]. Available: <http://www.sciencedirect.com/science/article/pii/S0375947400003663>
- [48] “Mass defect curve and nuclear constitution,” *Proceedings of the Royal Society of London A: Mathematical, Physical and Engineering Sciences*, vol. 126, no. 803, pp. 632–644, 1930. [Online]. Available: <http://rspa.royalsocietypublishing.org/content/126/803/632>
- [49] L. R. Hafstad and E. Teller, “The alpha-particle model of the nucleus,” *Phys. Rev.*, vol. 54, pp. 681–692, Nov 1938. [Online]. Available: <https://link.aps.org/doi/10.1103/PhysRev.54.681>
- [50] H. Bradlow, W. Rae, P. Fisher, N. Godwin, G. Proudfoot, and D. Sinclair, “A dwba analysis of heavy ion  $\alpha$ -transfer reactions on 16o,” *Nuclear Physics A*, vol. 314, pp. 171–206, 01 1979.
- [51] Y. Yoshida, Y. Kanada-En’yo, and F. Kobayashi, “ $\alpha$ -cluster excited states in 32S,” *Progress of Theoretical and Experimental Physics*, vol. 2016, no. 4, 04 2016. [Online]. Available: <https://dx.doi.org/10.1093/ptep/ptw016>
- [52] NNDC. (2000) NNDC chart of nuclides. [Online]. Available: <http://web.archive.org/web/20080207010024/http://www.808multimedia.com/winnt/kernel.htm>

- [53] Y. Gangrsky, K. Marinova, S. Zemlyanoi, M. Avgoulea, J. Billowes, P. Campbell, B. Cheal, B. Tordoff, M. Bissell, D. H. Forest, M. Gardner, G. Tungate, J. Huikari, H. Penttilä, and J. Äystö, “Nuclear charge radii and electromagnetic moments of scandium isotopes and isomers in the  $f7/2$  shell,” *Hyperfine Interactions*, vol. 171, no. 1, pp. 209–215, 2006, .
- [54] A. Chevallier, J. Chevallier, J. L. Gross, B. Haas, N. Schulz, J. Styczen, and M. Toulemonde, “Lifetime and  $g$ -factor measurements in  $^{44}\text{Sc}$ ,” *Zeitschrift für Physik A Atoms and Nuclei*, vol. 275, no. 1, pp. 51–53, 1975. [Online]. Available: <http://dx.doi.org/10.1007/BF01409499>
- [55] M. E. Barclay, L. Cleemann, A. V. Ramayya, J. H. Hamilton, C. F. Maguire, W. C. Ma, R. Soundranayagam, K. Zhao, A. Balanda, J. D. Cole, R. B. Piercey, A. Faessler, and S. Kuyucak, “ $g$ -factor measurements in  $^{68}\text{Ge}$  and evidence for higher multipole forces,” *Journal of Physics G: Nuclear Physics*, vol. 12, no. 12, p. L295, 1986. [Online]. Available: <http://stacks.iop.org/0305-4616/12/i=12/a=006>
- [56] G. J. Kumbartzki, K.-H. Speidel, N. Benczer-Koller, D. A. Torres, Y. Y. Sharon, L. Zamick, S. J. Q. Robinson, P. Maier-Komor, T. Ahn, V. Anagnostatou, C. Bernards, M. Elvers, P. Goddard, A. Heinz, G. Ilie, D. Radeck, D. Savran, V. Werner, and E. Williams, “Structure of the  $\text{Sr-Zr}$  isotopes near and at the magic  $n = 50$  shell from  $g$ -factor and lifetime measurements in  $^{88}_{40}\text{Zr}$  and  $^{84,86}_{38}\text{Sr}$ ,” *Phys. Rev. C*, vol. 85, p. 044322, Apr 2012. [Online]. Available: <https://link.aps.org/doi/10.1103/PhysRevC.85.044322>
- [57] E. Browne, “Nuclear data sheets for  $a = 90$ ,” *Nuclear Data Sheets*, vol. 82, no. 3, pp. 379 – 546, 1997. [Online]. Available: <http://www.sciencedirect.com/science/article/pii/S0090375297900211>
- [58] G. J. Kumbartzki, N. Benczer-Koller, S. Burcher, A. Ratkiewicz, S. L. Rice, Y. Y. Sharon, L. Zamick, K.-H. Speidel, D. A. Torres, K. Sieja, M. McCleskey, A. Cudd, M. Henry, A. Saastamoinen, M. Slater, A. Spiridon, S. Y. Torilov, V. I. Zhrebchevsky, G. Gürdal, S. J. Q. Robinson, S. D. Pain, and J. T. Burke, “Transition from collectivity to single-particle degrees of freedom from magnetic moment measurements

- on  $^{82}_{38}\text{Sr}_{44}$  and  $^{90}_{38}\text{Sr}_{52}$ ,” *Phys. Rev. C*, vol. 89, p. 064305, Jun 2014. [Online]. Available: <https://link.aps.org/doi/10.1103/PhysRevC.89.064305>
- [59] B. Singh, “Nuclear data sheets for  $a = 172$ ,” *Nuclear Data Sheets*, vol. 75, no. 2, pp. 199 – 376, 1995. [Online]. Available: <http://www.sciencedirect.com/science/article/pii/S0090375285710253>
- [60] Z. Berant, E. Oster, R. J. Casperson, A. Wolf, V. Werner, A. Heinz, R. F. Casten, G. Gurdal, E. A. McCutchan, D. S. Brenner, J. R. Terry, R. Winkler, E. Williams, J. Qian, A. Schmidt, M. K. Smith, T. Ahn, C. W. Beausang, P. H. Regan, T. Ross, M. Bunce, B. Darakchieva, D. A. Meyer, J. LeBlanc, K. Dudziak, C. Bauer, and G. Henning, “ $g$ ,” *Phys. Rev. C*, vol. 80, p. 057303, Nov 2009. [Online]. Available: <https://link.aps.org/doi/10.1103/PhysRevC.80.057303>
- [61] P. Walker, D. Ward, O. Häusser, H. Andrews, and T. Faestermann, “ $g$ -factors for 172, 173, 174, 178hf  $k$ -isomers,” *Nuclear Physics A*, vol. 349, no. 1, pp. 1 – 9, 1980. [Online]. Available: <http://www.sciencedirect.com/science/article/pii/037594748090439X>
- [62] H. Hübel, C. Günther, E. Schoeters, R. Silverans, and L. Vanneste, “Nuclear orientation measurements on  $^{183}\text{re}$  and  $^{184}\text{re}$ ,” *Nuclear Physics A*, vol. 210, no. 2, pp. 317 – 328, 1973. [Online]. Available: <http://www.sciencedirect.com/science/article/pii/0375947473903059>
- [63] K. S. Krane, C. E. Olsen, and W. A. Steyert, “Parity mixing and the nuclear structure of  $^{183,184}\text{W}$  and nuclear spin-lattice relaxation following the decays of oriented  $^{183,184g,184m}\text{Re}$ ,” *Phys. Rev. C*, vol. 7, pp. 263–275, Jan 1973. [Online]. Available: <https://link.aps.org/doi/10.1103/PhysRevC.7.263>
- [64] R. Kroth, S. Bhattacharjee, C. Günther, M. Guttormsen, K. Hardt, H. Hübel, and A. Kleinrahm, “ $g$ -factors of high-spin isomers in  $^{194}\text{hg}$  and  $^{196}\text{hg}$ ,” *Physics Letters B*, vol. 97, no. 2, pp. 197 – 199, 1980. [Online]. Available: <http://www.sciencedirect.com/science/article/pii/037026938090581X>
- [65] B. Fant, T. Weckström, H. Jain, L. Norlin, K.-G. Rensfelt, P. Carle, and

- U. Rosengård, “Investigation of the high-spin structure of 200,202pb,” *Nuclear Physics A*, vol. 475, no. 2, pp. 338 – 360, 1987. [Online]. Available: <http://www.sciencedirect.com/science/article/pii/0375947487901709>
- [66] W. Thomas, K. Kroth, and H. R. Zilligen, “Measurement of the  $g$ -factor of the  $4\ 1\ +$  -state of 202pb,” *Zeitschrift für Physik A Atoms and Nuclei*, vol. 280, no. 4, pp. 371–375, 1977. [Online]. Available: <http://dx.doi.org/10.1007/BF01435446>
- [67] K. Hardt, R. Kroth, G. Mikus, C. Günther, M. Guttormsen, H. Hübel, J. Recht, and R. Tischler, “Spin precession of po in ni detected by in-beam conversion electrons and the magnetic moment of the 15 isomer in 204po,” *Zeitschrift für Physik A Atoms and Nuclei*, vol. 305, no. 1, pp. 1–7, 1982. [Online]. Available: <http://dx.doi.org/10.1007/BF01415071>
- [68] O. Häusser, T. Alexander, J. Beene, E. Earle, A. McDonald, F. Khanna, and I. Towner, “Magnetic moments and half-lives of isomeric states in polonium isotopes,” *Nuclear Physics A*, vol. 273, no. 1, pp. 253 – 268, 1976. [Online]. Available: <http://www.sciencedirect.com/science/article/pii/0375947476903122>
- [69] A. Kusoglu, A. E Stuchbery, G. Georgiev, A. Goasduff, L. Atanasova, D. Balabanski, M. Bostan, M. Danchev, P. Detistov, K. Gladnishki, J. Ljungvall, I. Matea, D. Radeck, C. Sotty, I. Stefan, D. Verney, and D. T Yordanov, “Nuclear  $g$  -factor measurement with time-dependent recoil in vacuum in radioactive-beam geometry,” *Journal of Physics: Conference Series*, vol. 590, p. 012041, 04 2015.
- [70] N. Benczer-Koller, “The role of magnetic moments in the determination of nuclear wave functions of short-lived excited states,” *Journal of Physics: Conference Series*, vol. 20, no. 1, p. 51, 2005. [Online]. Available: <http://stacks.iop.org/1742-6596/20/i=1/a=009>
- [71] L. F. Canto, R. Donangelo, M. S. Hussein, and A. Lépine-Szily, “Multistep  $\alpha$ -particle-transfer description of anomalous heavy-ion elastic scattering,” *Phys. Rev. Lett.*, vol. 51, pp. 95–98, Jul 1983. [Online]. Available: <https://link.aps.org/doi/10.1103/PhysRevLett.51.95>
- [72] A. Lépine-Szily, M. Obuti, R. L. Filho, J. Oliveira, and A. Villari, “Back-angle anomaly

- and coupling between seven reaction channels of  $^{12}\text{C} + ^{24}\text{Mg}$  using algebraic scattering theory,” *Physics Letters B*, vol. 243, no. 1, pp. 23 – 28, 1990. [Online]. Available: <http://www.sciencedirect.com/science/article/pii/0370269390909497>
- [73] A. Lépine-Szily, R. Lichtenthäler Filho, M. M. Obuti, J. M. de Oliveira, O. Portezan Filho, W. Sciani, and A. C. C. Villari, “Structures in the excitation function of  $^{24}\text{Mg} (^{16}\text{O}, ^{20}\text{Ne})^{20}\text{Ne}$  and a nonresonant description of these structures,” *Phys. Rev. C*, vol. 40, pp. 681–684, Aug 1989. [Online]. Available: <https://link.aps.org/doi/10.1103/PhysRevC.40.681>
- [74] J. M. Oliveira, A. Lépine-Szily, A. C. C. Villari, R. Lichtenthäler, L. C. Gomes, W. Sciani, P. Fachini, G. L. Lima, A. C. G. Martins, V. Chiste, J. M. Casandjian, A. J. Pacheco, J. E. Testoni, D. Abriola, A. O. Macchiavelli, F. Hasenbalg, O. A. Capurro, D. Tomasi, J. F. Niello, and D. Brandizzi, “Orbiting features in the strongly damped binary decay of the  $^{28}\text{Si} + ^{16}\text{O}$  system,” *Phys. Rev. C*, vol. 53, pp. 2926–2932, Jun 1996. [Online]. Available: <https://link.aps.org/doi/10.1103/PhysRevC.53.2926>
- [75] Ian Thompson. Coupled reaction channels calculations. [Online]. Available: [www.fresco.org.uk](http://www.fresco.org.uk)



## Abbreviations

---

NMM	Nuclear Magnetic Moment
TF	Transient Field
ATR	Alpha Transfer Reaction
RIV	Recoil Into Vacuum
DSAM	Doppler Shift Attenuation Method
NMM	Nuclear Magnetic Moment
TDRIV	Time Differential Recoil Into Vacuum
DWBA	Distorted Wave Born Approximation
TDPAD	Time Differential Perturbed Angular distribution
PAC	Perturbed Angular Correlation
NMR	Nuclear Magnetic Resonance
SPP	São Paulo Potential
HP-Ge	High-Purity Germanium
NEC	National Electrostatic Corporation
LAFN	Laboratorio Aberto de Fisica Nuclear
MC-SNICS	Multicathode Source of Negative Ions by Cesium Sputtering
SiPM	Silicon Photomultiplier
LYSO(Ce)	Cerium-doped Lutetium Yttrium Orthosilicate
PIPS	Passivated Implanted Planar Silicon







